Tesi di dottorato in Ingegneria Biomedica, di Antonino Salerno,
discussa presso l'Università Campus Bio-Medico di Roma in data 20/03/2012.
La disseminazione e la riproduzione di questo documento sono consentite per scopi di didattica e ricerca,
a condizione che ne venga citata la fonte

Università Campus Bio-Medico di Roma
School of Engineering
PhD Course in Biomedical Engineering
(XXIV - 2009/2011)

Design and Development of Robot Control Systems for Biomedical Applications

Antonino Salerno

PhD Program Coordinator
Prof. Giulio Iannello

Supervisor
Prof. Eugenio Guglielmelli

Co-Supervisor
Dr. Loredana Zollo

March 2012

Tesi di dottorato in Ingegneria Biomedica, di Antonino Salerno,
discussa presso l'Università Campus Bio-Medico di Roma in data 20/03/2012.
La disseminazione e la riproduzione di questo documento sono consentite per scopi di didattica e ricerca,
a condizione che ne venga citata la fonte

Design and Development of Robot Control Systems for Biomedical Applications

A thesis presented by

Antonino Salerno

in partial fulfillment of the requirements for the degree of

Doctor of Philosophy

in Biomedical Engineering

Università Campus Bio-Medico di Roma

School of Engineering

PhD Program Coordinator
Prof. Giulio Iannello

Supervisor
Prof. Eugenio Guglielmelli

Co-Supervisor
Dr. Loredana Zollo

March 2012

Tesi di dottorato in Ingegneria Biomedica, di Antonino Salerno,
discussa presso l'Università Campus Bio-Medico di Roma in data 20/03/2012.
La disseminazione e la riproduzione di questo documento sono consentite per scopi di didattica e ricerca,
a condizione che ne venga citata la fonte

Committee:

Prof. Giulio Iannello (Università Campus Bio-Medico di Roma)
Prof. Riccardo Pietrabissa (Politecnico di Milano)
Prof. Salvatore Andrea Sciuto (Università degli studi ROMA TRE)

Reviewer:

Prof. Nicolas García Aracil (Universidad Miguel Hernandez)

Tesi di dottorato in Ingegneria Biomedica, di Antonino Salerno,
discussa presso l'Università Campus Bio-Medico di Roma in data 20/03/2012.
La disseminazione e la riproduzione di questo documento sono consentite per scopi di didattica e ricerca,
a condizione che ne venga citata la fonte

To my family

Tesi di dottorato in Ingegneria Biomedica, di Antonino Salerno,
discussa presso l'Università Campus Bio-Medico di Roma in data 20/03/2012.
La disseminazione e la riproduzione di questo documento sono consentite per scopi di didattica e ricerca,
a condizione che ne venga citata la fonte

Tesi di dottorato in Ingegneria Biomedica, di Antonino Salerno,
discussa presso l'Università Campus Bio-Medico di Roma in data 20/03/2012.
La disseminazione e la riproduzione di questo documento sono consentite per scopi di didattica e ricerca,
a condizione che ne venga citata la fonte

Contents

Tesi di dottorato in Ingegneria Biomedica, di Antonino Salerno,
discussa presso l'Università Campus Bio-Medico di Roma in data 20/03/2012.
La disseminazione e la riproduzione di questo documento sono consentite per scopi di didattica e ricerca,
a condizione che ne venga citata la fonte

Tesi di dottorato in Ingegneria Biomedica, di Antonino Salerno,
discussa presso l'Università Campus Bio-Medico di Roma in data 20/03/2012.
La disseminazione e la riproduzione di questo documento sono consentite per scopi di didattica e ricerca,
a condizione che ne venga citata la fonte

Tesi di dottorato in Ingegneria Biomedica, di Antonino Salerno,
discussa presso l'Università Campus Bio-Medico di Roma in data 20/03/2012.
La disseminazione e la riproduzione di questo documento sono consentite per scopi di didattica e ricerca,
a condizione che ne venga citata la fonte

Tesi di dottorato in Ingegneria Biomedica, di Antonino Salerno,
discussa presso l'Università Campus Bio-Medico di Roma in data 20/03/2012.
La disseminazione e la riproduzione di questo documento sono consentite per scopi di didattica e ricerca,
a condizione che ne venga citata la fonte

Chapter 1

Introduction on Upper-limb Rehabilitation and Assistive Robotics

According to the World Health Organization, by 2050, the number of persons over 65 years old will increase by 73 percent in the industrialized countries and by 207 percent worldwide. This segment of population is particularly prone to suffer a cerebrovascular accident or stroke, since the relative incidence of stroke doubles every decade after age 55.

Stroke is a growing social problem in the most industrialized countries all over the world and cause of serious long-term disability.

For example in Canada, stroke is the third leading cause of death, since six percent of all deaths in Canada are due to stroke [1].

Tesi di dottorato in Ingegneria Biomedica, di Antonino Salerno,
discussa presso l'Università Campus Bio-Medico di Roma in data 20/03/2012.
La disseminazione e la riproduzione di questo documento sono consentite per scopi di didattica e ricerca,
a condizione che ne venga citata la fonte

There are over 50,000 strokes in Canada each year. Of every 100 people who have a stroke:

- 15 die (15%)
- 10 recover completely (10%)
- 25 recover with a minor impairment or disability (25%)
- 40 are left with a moderate to severe impairment (40%)
- 10 are so severely disabled they require long-term care (10%)

Stroke costs the Canadian economy $3.6 billion a year in physician services, hospital costs, lost wages, and decreased productivity (2000 statistic) [2].

In [3] is estimated that 7 000 000 people ≥ 20 years of age have had a stroke in the United States only. Each year, around 795 000 people experience a new or recurrent stroke. Approximately 610 000 of these are first attacks, and 185 000 are recurrent attacks (Greater Cincinnati/Northern Kentucky Stroke Study, National Institutes of Neurological Disorders and Stroke (**GCNKSS**), National Heart, Lung, and Blood Institute (**NHLBI**) and National Institutes of Neurological Disorders and Stroke (**NINDS**); GCNKSS and NINDS data for 1999 provided July 9, 2008; estimates compiled by NHLBI). Projections show that by 2030, an additional 4 million people will have had a stroke, a 24.9% increase in prevalence from 2010.

As declared by National Stroke Association, a total of 6,400,000 stroke survivors live in the Unites States, accounting for 2,9% of the population more than 20 years old.

In the NHLBI's FHS (Framingham Heart Study), among ischemic stroke survivors who were ≥65 years of age, these disabilities were observed at 6 months after stroke [4]:

- 50% had some hemiparesis
- 30% were unable to walk without some assistance

Tesi di dottorato in Ingegneria Biomedica, di Antonino Salerno,
discussa presso l'Università Campus Bio-Medico di Roma in data 20/03/2012.
La disseminazione e la riproduzione di questo documento sono consentite per scopi di didattica e ricerca,
a condizione che ne venga citata la fonte

- 26% were dependent in activities of daily living
- 19% had aphasia
- 35% had depressive symptoms
- 26% were institutionalized in a nursing home

The social-economic impact is enormous: the estimated direct and indirect social cost of stroke amounts to 73.7 billion for 2010 only for US.

To summarize, meanly about 80 percent of stroke survivors have a disturbed sensory feedback or motor control of the upper limb on the paretic side [3]. Sensory distortion expresses itself through a reduction of tactile or afferent feedback, or as the opposite, through hypersensitivity. The loss of motor control is seen in typical neurological impairments, listed in following:

- *Muscle weakness*: upper-limb weakness after stroke is common and results in substantial disability since the cortex activation decreases and consequently the muscular recruitment [5]. Therefore the peak force exercisable by subject after stroke is limited with respect to before stroke.
- *Hyperactive reflexes* manifest as increased muscle tone, joint resistance [6] and spasticity [7].
- *Abnormal muscle synergies*: a loss of independent joint control, where involuntary co-activation of muscles occurs over multiple joints [8].

After a long period without training, this can result in muscle atrophy and increased joint stiffness. These permanent disabilities need to be treated and evaluated in objective way together to patient improvements. Based on traditional approach, the levels of motor impairment are roughly classified as:

- Severe, with almost no useful muscle activation or limb movements.
- Moderate, with operational but clearly affected limb movements.
- Mild, with close to full functional control of arm, hand and fingers.

Tesi di dottorato in Ingegneria Biomedica, di Antonino Salerno,
discussa presso l'Università Campus Bio-Medico di Roma in data 20/03/2012.
La disseminazione e la riproduzione di questo documento sono consentite per scopi di didattica e ricerca,
a condizione che ne venga citata la fonte

With reference to upper limb impairments, the main scales used to quantify motor and functional impairment are:

- Barthel Index (BI): measures independent functioning and mobility in daily life.
- Functional Independence Measure (FIM): measures sensitivity and comprehensiveness in daily life.
- Chedoke-McMaster Stroke Assessment (CMSA): measures impairment and activities of daily life.
- Motor Activity Log (MAL): measures arm usage.
- Modified Ashworth Scale (MAS): measures muscle tone of 14 muscular group of the upper limb.
- Tone Assessment Scale (TAS): measures muscle tone in response to passive movements.
- Modified Tardieu Scale (MTS): determines the passive range of movement at different movement velocities, with the relative difference between a slow and a fast velocity passive stretch determining the dynamic component of the muscle contracture.
- Motor Assessment Scale (MAS): assesses performance of functional tasks (i.e. activities of daily living) rather than isolated patterns of movement.
- Fugl-Meyer Assessment (FMA): measures motor and joint function and sensation.
- Action Research Arm Test (ARAT): measures ability to handle different objects.
- Nine Hole Peg Test (NHPT): measures fine manual dexterity.
- Wolf Motor Function Test (WMFT): is a time-based method to evaluate upper extremity performance while providing insight into joint-specific and total limb movements.
- Motor Power (MP): force measurement of shoulder and elbow.

Tesi di dottorato in Ingegneria Biomedica, di Antonino Salerno,
discussa presso l'Università Campus Bio-Medico di Roma in data 20/03/2012.
La disseminazione e la riproduzione di questo documento sono consentite per scopi di didattica e ricerca,
a condizione che ne venga citata la fonte

As declared by the International Bobath Instructors Training Association (IBITA), the traditional therapy consists of individual sessions with a therapist that administers repetitive motor exercises (depending on motor impairments) assisting the patient. The patient improvements are monitored exploiting the assessment scale above mentioned. Generally these scales are administered by a therapist at the admission and discharge of the patients. A drawback of cited method is that the scales are operator-dependent. In other words, the same scale administered to the same patient by two different therapists can often provide scores on the patient state.

Another feature of the traditional therapy is that repetitive and active movements seems to promote a key aspect in the recovery after stroke: the neuroplasticity [9].

Neuroplasticity is the ability of the brain and nervous system to change structurally and functionally as a result of input from the environment. Plasticity occurs on a variety of levels, ranging from cellular changes involved in learning, to large-scale changes involved in cortical remapping in response to injury. The most widely recognized forms of plasticity are learning, memory, and recovery from brain damage with therapeutic treatment [10].

During most of the 20th century, the general consensus among neuroscientists was that brain structure is relatively immutable after a developmental period during early childhood. This belief has been challenged by new findings, revealing that many aspects of the brain remain plastic even into adulthood as demonstrated in studies on adult primates in [11].

In order to enhance the neuroplasticity, movements of the rehabilitation therapy are founded on the interaction between the therapist and patient. This interaction can be classified into three broad categories [12]:

- Passive (or externally imposed) movement, which involves movement of the patient's joints by the therapist as the patient remains relaxed.

Tesi di dottorato in Ingegneria Biomedica, di Antonino Salerno,
discussa presso l'Università Campus Bio-Medico di Roma in data 20/03/2012.
La disseminazione e la riproduzione di questo documento sono consentite per scopi di didattica e ricerca,
a condizione che ne venga citata la fonte

- Active-assisted movement, which is used when the patient cannot complete a desired movement autonomously (shared control between patient and therapist);
- Active-resisted movement, which is mainly used by higher level patients and involves completing movements against resistance from gravity, additional weights, an elastic band, or the therapist.
- Bilateral movement; where the execution of a motor task is mirrored between the healthy and the hemiplegic arm.

The assistance level to provide to impaired limb is an open issue, but there is a general consensus that active participation of the patient can promote the neuroplasticity mechanism. In fact, a strong clinical evidence for active assistance is a study of 100 acute stroke participants that found significant decreases in arm impairment with an intervention of stereotyped active-assisted movements [13]. Moreover, functional brain imaging in patients recovering and recovered from stroke [14] - [18] showed increased blood flow in areas around the lesion. Functional recovery depends in part on the post-injury experience, and plasticity or reorganizational potential may be enhanced by activity [19].

Therefore an efficient and effective recovery process after stroke in chronic patients should stimulate the neuronal plasticity by promoting the active involment of the patient throughout repetitive movements with limited assistence. Additionally, an objective assessment of the patient during the treatment period should be guaranteed.

In the presented scenario, robot manipulators can be exploited as tools for therapists to increase productivity and quality of the care. In fact, the robot can deliver a quantifiable input and measure the patient's output objectively, monitoring the evolution of the therapy from admission to discharge of the patient. For quantifiable input is intended the robot possibility to generate high

Tesi di dottorato in Ingegneria Biomedica, di Antonino Salerno,
discussa presso l'Università Campus Bio-Medico di Roma in data 20/03/2012.
La disseminazione e la riproduzione di questo documento sono consentite per scopi di didattica e ricerca,
a condizione che ne venga citata la fonte

number of motor task repetitions with high accuracy modulating the assistance level in order to promote the neuroplasticity.

Moreover, a single therapist could manage multiple patients, each of whom is interacting with their device. Patient acceptance of the robotic devices as training machines fits into their conception of the standard rehabilitation gym that is already filled with wheel and pulley devices, and patients' general interest in the multimedia aspect of some of the devices is also compelling.

The therapist can perform an initial assessment of the patient's functional level exploiting also a robotic device and determine the movement patterns that would be beneficial to practice. The skill of the therapist is then augmented with a device that can accurately replicate the movement patterns and free the therapist from this time-consuming activity, in situations where one or more therapists should operate at the same time to deliver rehabilitation therapy to a single patient. In this context, the one to one traditional approach between patient and therapist could be overcome, thus allowing to satisfy an increasing care request from stroke incidence. A positive economic impact is also envisaged.

To conclude this topic, the potential role for robotic devices is to deliver highly repetitive, active assisted movement training. Robots provide an ideal platform for objective, reproducible, continuous measurement and control of therapy, which can be exploited to reduce the variability associated to the studies aimed at assessing the outcomes of different therapies.

Another field of increasing interest for robotics research is the assistive robotics. Assistive robotics aims at developing robotic solutions for promoting independent living of disabled and elderly people.

Assistive robots can be divided into three main categories: manipulation aids, mobility aids, and cognitive aids. Each can be subdivided as follows. Manipulation aids are commonly divided into fixed, portable, and mobile subtypes. Mobility aids are divided into electric wheelchairs with autonomous

Tesi di dottorato in Ingegneria Biomedica, di Antonino Salerno,
discussa presso l'Università Campus Bio-Medico di Roma in data 20/03/2012.
La disseminazione e la riproduzione di questo documento sono consentite per scopi di didattica e ricerca,
a condizione che ne venga citata la fonte

navigation features and smart walkers. Cognitive aids are divided into communication aids such as pet robots and autonomous caretaker robots.

In this scenario prosthetics, especially the artificial prostheses for upper limb, can be inserted in the field of manipulation aids. The robotic prostheses are aimed at substituting the functionality of a missing limb exhibiting physical and functional features as much as possible similar to the human ones.

In the United States 41.000 persons are registred who had an amputation of a hand or a complete arm. With the same frequency of occurrence (1 in 6100) there would be 1.000.000 such persons worldwide. The main factors for a loss of an upper extremity are accidents followed by general deseases and injuries from war. For the individual the loss of an upper limb results in a drastic restriction of function and cosmesis. In the last 4 decades an increasing number of handicapped persons have been provided with prosthetic hands that have the shape of a human hand and that are actuated by a DC motor with reduction gear trains [20].

Therefore the prosthetics tries to address an actual problem and could provide dexterity, natural mobility, and sense of touch to missing or paralyzed limbs. More generally, providing manipulation aids to disable people is a significant issue that assistive robotics tries to address.

1.1 Thesis overview and main contributions

This thesis is focussed on the design and development of control strategies for applications in both rehabilitation and assistive robotics. The common point for the developed control strategies in different fields is the bio-inspiration. In fact, findings retrieved by studies on humans represent a fundamental source of inspiration for the development of control architectures that feature the robust behaviour of biological systems in the presence of unstructured environments.

Tesi di dottorato in Ingegneria Biomedica, di Antonino Salerno,
discussa presso l'Università Campus Bio-Medico di Roma in data 20/03/2012.
La disseminazione e la riproduzione di questo documento sono consentite per scopi di didattica e ricerca,
a condizione che ne venga citata la fonte

Briefly, the control systems proposed in this work for robot-aided rehabilitation tries to provide assistance to the patients exploiting human motion generation mechanism. The main expected benefits are a tailored therapy on the patient and a 'physiological assistance' according to patient's need. For 'physiological assistance' is intended the robot capability to replicate the therapist interaction with the patient. To this purpose, a body of neuroscientific evidences is identified which supports the existence of discrete elementary units, called submovements, underlying continuous human movement and on this neuroscientific assumption a novel control approach for patient assistance is proposed. According to these evidences, a complex movement, such as pointing tasks can be decomposed in a sequence of discrete units of movements, which are usually denoted as submovements. The expected benefits of the control approach is to provide robotic assistance as similar as possible to human therapist. Additionally and in complementary way, in order to enhance robot dependability in human-robot interaction, highly nonlinear phenomena able to strongly degrade robot performance such as joints friction are investigated and compensated. The proposed control system relies further on measured electric currents to close the control loop, in lieu of traditionally used torque/force sensors, in addition to position feedback.

On the other hand, as regards the development of control systems for robotic and prosthetic hands, it can be noticed that the human hand can be considered as an example of high dexterity system able to guarantee gasp stability. The grasp stability can be regarded as a primary target to achieve by control systems developed for robotic and prosthetic hands. It is clear that, when developing control strategies for this target, the interest to replicate the human hand ability is increased for tasks such as just grasping, leading us to thoroughly study the bio-inspired grasping problem and implementing on a robotic hand a control approach grounded on human grasping mechanisms. In this context, the dissertation thesis

Tesi di dottorato in Ingegneria Biomedica, di Antonino Salerno,
discussa presso l'Università Campus Bio-Medico di Roma in data 20/03/2012.
La disseminazione e la riproduzione di questo documento sono consentite per scopi di didattica e ricerca,
a condizione che ne venga citata la fonte

is focused on the development of an optimization algorithm able to determine the optimal grasp configuration of a robotic hand and consequently the contact points between robotic fingers and object to be grasped by achieving grasp stability. Indeed, an optimal grasp configuration is a fundamental part of the grasp planning action performed by a robotic hand, and finding general rules able to reduce the number of active degrees of freedom strictly necessary for controlling the hand shape allows developing stable grasp configuration algorithms with reduced computational costs. The proposed algorithm has been implemented on a robotic arm-hand system. In particular a robotic hand has been chosen since robotic hands are more dexterous that prosthetic hands that are basically simple grippers with few degrees of freedom.
The application to prosthetic hands of the algorithm for the optimal grasp configuration is considered in the following as a possible prosecution of the work presented in this thesis for robotic hands.

In detail, the contents of the thesis are organized as follows:

- *Chapter 2* provides an overview of the state of the art on the machines for upper limb rehabilitation, robotic and prosthetic hands. After a description of a mechanical structures of the reviewed devices for rehabilitation robotics, attention is focused on the control strategies proposed in literature by highlighting the main weaknesses. In the field of the assistive robotics, the state of the art is mainly focused on robotic hands, being the system where the control algorithm for grasping tasks has been applied. Finally the main issues for both rehabilitation robotics and assistive robotics (involving robotic and prosthetic hands) are indentified and a series of proposed solutions are fully explained clarifying the thesis objectives.

Tesi di dottorato in Ingegneria Biomedica, di Antonino Salerno,
discussa presso l'Università Campus Bio-Medico di Roma in data 20/03/2012.
La disseminazione e la riproduzione di questo documento sono consentite per scopi di didattica e ricerca,
a condizione che ne venga citata la fonte

- *Chapter 3* describes the control paradigm for robot motion and interaction control based on submovements neuroscientific theory of the human motor control. A preliminary study on the feasibility to generate a predetermined sequence of motion units is carried out and on the basis of the shown benefits a dynamic sequence generator is implemented. The dynamic sequence generator module, in charge of on-line generating sequences of elementary motion units that are opportunely scaled in number and amplitude in accordance with task requirements, represents the core of the proposed robot control. The submovement sequence generation is grounded on the adaptive behaviour of four oscillators and two analytical relationship able to manage the submovements amplitude in accordance to the task. The control strategy has been validated in a simulated environment and by means trials on the MIT-Manus robotic system by highlighting the main differences with respect to the traditional approach.
- *Chapter 4* presents an interaction control approach for a rehabilitation machine with unnegligible friction and low performance in impedance regulation. Another key point of the approach proposed in this chapter is the reconstruction of the force applied to the robot end-effector by the patient by using the electrical motor currents of the actuators. Friction compensation and force reconstruction by electrical motor currents are the core of an impedance control based on the robot inverse dynamics. The control paradigm has been experimentally tested in conditions of free and constrained space on the CBM-Motus, a planar rehabilitation machine for the upper limb.
- *Chapter 5* presents the theoretical formulation and the experimental validation of a reach-and-grasp algorithm for determining the optimal hand position, after reaching, and the optimal finger configuration for grasping a cylindrical object with known features. The proposed algorithm is biologically inspired and is based on the minimization of an objective

Tesi di dottorato in Ingegneria Biomedica, di Antonino Salerno,
discussa presso l'Università Campus Bio-Medico di Roma in data 20/03/2012.
La disseminazione e la riproduzione di questo documento sono consentite per scopi di didattica e ricerca,
a condizione che ne venga citata la fonte

function expressed by the sum of the distances of the hand joints from the object surface. The first part of the chapter is focused on diagonal volar grasp, whereas in the second part the extension to transverse volar grasp is proposed by exploiting the results on human experimentation. Effectiveness of the algorithms for diagonal and transversal volar grasp has preliminarily been tested by means of simulation trials. Finally, experimental trials on a real arm-hand robotic system have been carried out in order to validate the approach and measure algorithm performance. Only for transverse volar grasp, the experimental results have been compared with the studies on humans carried out for the same typology of grasp. Main contribution of the candidate to this topic was the experimental validation on the robotic arm-hand system.

- *Chapter 6* formulates the conclusions of the work explained in the dissertation thesis and proposes some ideas for future research activities.

The *main contributions* of the candidate in the contents shown in this section are concerned with:

- in *chapter 2*, in-depth analysis of the state of the art on the machines for robot-aided therapy and on robotic and prosthetic hands by pointing out research issues and proposed solutions in both fields;
- in *chapter 3*, (i) software implementation and experimental protocol definition and the experimental validation for the static predetermined sequence generator of submovements; (ii),the theoretical formulation of the dynamic sequence generator, grounded on the adaptive behaviour of four oscillators, the software implementation and the experimental validation;

Tesi di dottorato in Ingegneria Biomedica, di Antonino Salerno,
discussa presso l'Università Campus Bio-Medico di Roma in data 20/03/2012.
La disseminazione e la riproduzione di questo documento sono consentite per scopi di didattica e ricerca,
a condizione che ne venga citata la fonte

- in *chapter 4*, theoretical formulation and software implementation on the CBM-Motus robotic system of the current-based impedance control (including the whole system dynamic identification);
- in *chapter 5*, the software implementation and experimental validation of transverse and diagonal volar grasp optimization algorithm, including the hardware arrangement (i.e. MIT-Manus and DLR-HIT\Hand II) for the experimental validation.

Tesi di dottorato in Ingegneria Biomedica, di Antonino Salerno,
discussa presso l'Università Campus Bio-Medico di Roma in data 20/03/2012.
La disseminazione e la riproduzione di questo documento sono consentite per scopi di didattica e ricerca,
a condizione che ne venga citata la fonte

Tesi di dottorato in Ingegneria Biomedica, di Antonino Salerno,
discussa presso l'Università Campus Bio-Medico di Roma in data 20/03/2012.
La disseminazione e la riproduzione di questo documento sono consentite per scopi di didattica e ricerca,
a condizione che ne venga citata la fonte

Chapter 2

State of the art

2.1 State of the art on robotic systems for upper limb rehabilitation

Several examples of robotic machines for upper-limb rehabilitation can be found in the literature. They can be grouped into two main categories:

- End-effector rehabilitation machines, i.e. robotic machines designed in such a way that only the motion of the robot end-effector in the operational space is equivalent to that of the natural effector of the human limb;

Tesi di dottorato in Ingegneria Biomedica, di Antonino Salerno,
discussa presso l'Università Campus Bio-Medico di Roma in data 20/03/2012.
La disseminazione e la riproduzione di questo documento sono consentite per scopi di didattica e ricerca,
a condizione che ne venga citata la fonte

- Exoskeletal rehabilitation machines, i.e. wearable robotic machines which are designed to approximate the motion of the human limb both in the joint space and in the operational space.

A further classification is based on the anatomical district to rehabilitate (as shown in Fig. 1).

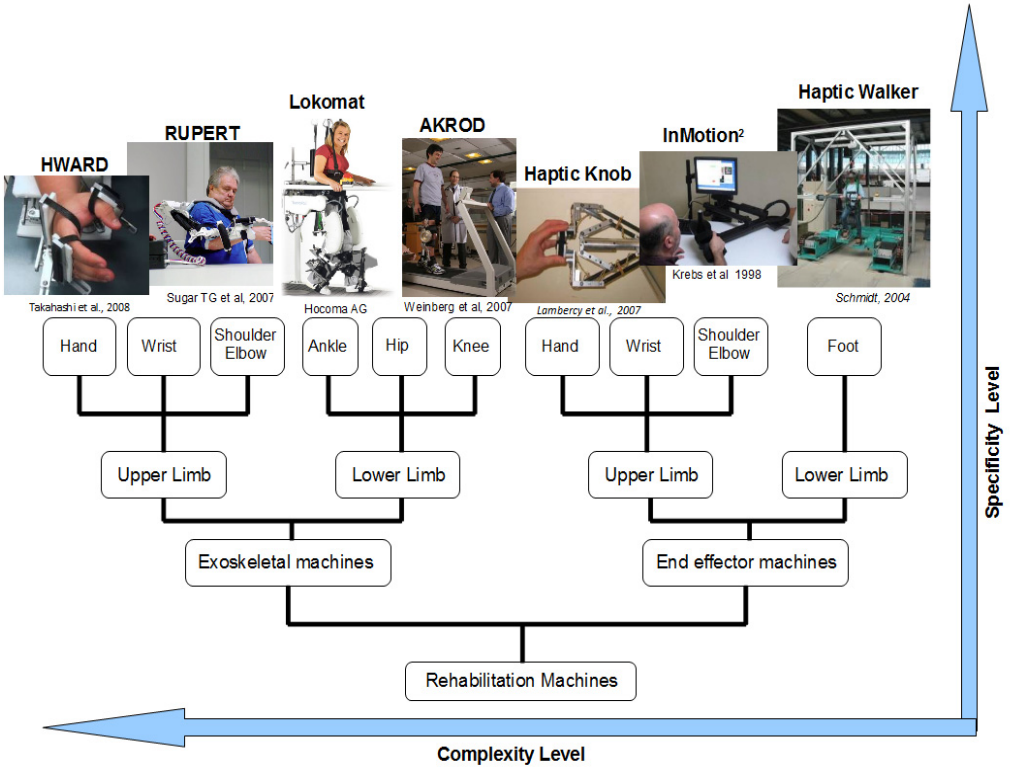

Fig. 1: Taxonomy tree of body-district specific rehabilitation robotic machines

In the following a distinction is carried out between robots for proximal upper-limb districts (i.e. shoulder and elbow), distal upper-limb districts (i.e. wrist and hand) and robots for the simultaneous training of proximal and distal upper limb districts simultaneously, i.e. arm-hand rehabilitation machines. Note that in the current literature 'arm-hand rehabilitation machine' stands for a robotic machine able to train patient arm and hand.

Tesi di dottorato in Ingegneria Biomedica, di Antonino Salerno,
discussa presso l'Università Campus Bio-Medico di Roma in data 20/03/2012.
La disseminazione e la riproduzione di questo documento sono consentite per scopi di didattica e ricerca,
a condizione che ne venga citata la fonte

2.1.1 End effector machines for proximal upper limb rehabilitation

From a historical perspective, end-effector machines were the first to appear in robot-aided rehabilitation and mainly consisted of adapting or re-configuring industrial robots for use in upper-limb rehabilitation [48], [49]. Lum and colleagues [49]-[50] have used a commercial PUMA robot augmented by improved sensors to implement the MIME (Mirror Image Movement Enabler) system, shown in Fig. 2.

Fig. 2: MIME prototype.

MIME device incorporates two commercial and sensorized mobile arm supports modified to limit arm movement to the horizontal plane, and a 6-DOF robot arm (Stäubli PUMA-260) that applies forces and torques to the paretic forearm through one of the arm supports to paretic limb (Fig. 2). Each forearm is supported by a splint attached to bilateral mobile arm that compensate the weight of the limbs. The configurations of the patient's forearms (position and orientation) placed on the splints are provided by using direct kinematics from optical encoders information. A 6-axis force/torque sensor measures the force/torque interaction between the robot and the paretic limb. System components are shown in Fig. 3.

Tesi di dottorato in Ingegneria Biomedica, di Antonino Salerno,
discussa presso l'Università Campus Bio-Medico di Roma in data 20/03/2012.
La disseminazione e la riproduzione di questo documento sono consentite per scopi di didattica e ricerca,
a condizione che ne venga citata la fonte

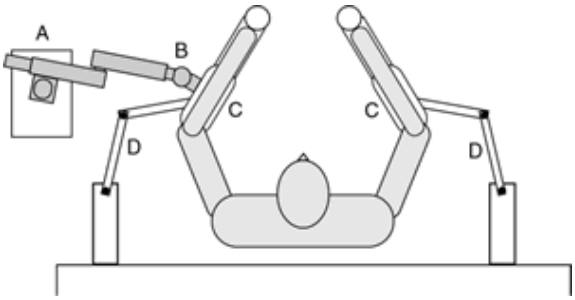

Fig. 3: Overview of MIME system. A: Puma-260 robot; B: force/torque transducer; C: forearm splints; D: arm supports.

Movements were produced in preprogrammed forearm position and orientation trajectories or by a position feedback control system that slaved the robot to the movements of the contralateral (normal) limb. In this master/slave mode, the robot continuously moved the paretic limb to the mirror-image position of the opposite limb.

Similar ideas have been implemented in [51] that used another industrial robot to move the impaired arm in the European project GENTLE [52]. The adopted industrial robot was the HapticMaster made by Fokker Control Systems. In order to compensate the patient arm weight and to connect the arm with the haptic interface, a support mechanism was developed. The system is shown in Fig. 4.

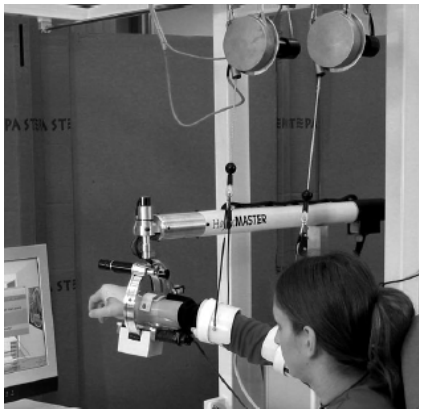

Fig. 4: The GENTLE system

Tesi di dottorato in Ingegneria Biomedica, di Antonino Salerno,
discussa presso l'Università Campus Bio-Medico di Roma in data 20/03/2012.
La disseminazione e la riproduzione di questo documento sono consentite per scopi di didattica e ricerca,
a condizione che ne venga citata la fonte

Another mechanism that adopts Haptic Master system is the Arm Coordination Training 3-D (ACT-3D) device [53].

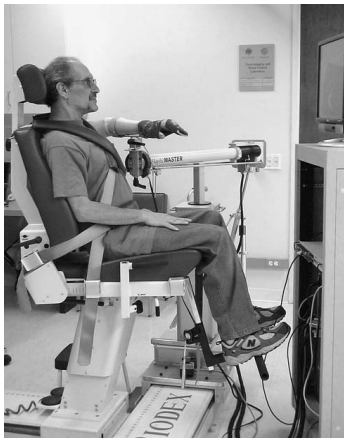

Fig. 5: ACT-3D rehabilitative robot

The ACT3D, shown in Fig. 5 consists of a modified HapticMASTER robot (Moog-FCS B.V., The Netherlands) with an instrumented end effector, integrated with a Biodex experimental chair (Biodex Medical Systems, Shirley, NY). The end effector consists of a six degree of freedom measurement device (JR3 load cell) to monitor forces and torques and an instrumented gimbal to record joint angles. The system imposes forces on the arm to either increase or decrease the amount of limb support required of the subject during the reaching task, for shoulder abduction/adduction and elbow flexion/extension. A rigid forearm-hand orthosis with Velcro straps was used to couple the arm directly to the robot. Position of the subject in relation to the robot was controlled via a common support track to which the chair and robot were both mounted.

The approach expoliting industrial robot for administering rehabilitative therapy was also employed by Toth and colleagues [54] in REHAROB design (see Fig. 6). The REHAROB Therapeutic System was the first robotic system to be built from two unmodified industrial robots working simultaneously to practice passive physiotherapy of spastic hemiparetic patients in a 3D scenario. REHAROB

Tesi di dottorato in Ingegneria Biomedica, di Antonino Salerno,
discussa presso l'Università Campus Bio-Medico di Roma in data 20/03/2012.
La disseminazione e la riproduzione di questo documento sono consentite per scopi di didattica e ricerca,
a condizione che ne venga citata la fonte

performs the exercises according to the directions of the physiotherapist. As regards shoulder and elbow motions of the 7 DoF upper limb, REHAROB was designed to include two industrial robots. The wall mounted 0.8 m reach IRB 140 industrial robot moves the upper arm, and the inverted 1.4 m reach IRB 1400H industrial robot moves the lower arm of the patient.

Fig. 6: REHAROB system for proximal upper limb rehabilitation

This approach that exploits industrial manipulators has the consequent critical drawback that low impedance comparable to that of the human arm cannot practically be obtained, being machines intrinsically position-controlled. The second design approach, that is currently predominant, consists of designing robots specifically conceived for tight human-machine interaction and for specific body district.

Many research groups have developed end-effector robotic devices for proximal upper-limb rehabilitation by using the second design approach. Take, for example, the Massachusetts Institute of Technology **(MIT)-Manus** [55]-[56].

Tesi di dottorato in Ingegneria Biomedica, di Antonino Salerno,
discussa presso l'Università Campus Bio-Medico di Roma in data 20/03/2012.
La disseminazione e la riproduzione di questo documento sono consentite per scopi di didattica e ricerca,
a condizione che ne venga citata la fonte

Fig. 7: MIT-Manus system

The machine (shown in Fig. 7) was designed to have a low intrinsic end-point impedance (i.e., be back-driveable), with a low and nearly-isotropic inertia (1±0.33 kg, maximum anisotropy 2:1) and friction (0.84±0.28 N, maximum anisotropy 2:1), and be capable of producing a predetermined range of forces (0–45 N) and impedances (0–2N/mm). The **MIT-Manus** presents a planar module that provides two translational degrees of freedom (dof) for elbow and forearm motion in the cartesian space. The planar robot is constituted by a direct-drive five bar-linkage SCARA (Selective Compliance Assembly Robot Arm) mechanism driven by brushless motors rated to 7.86 Nm of continuous stall torque with optical encoders for position and velocity measurements.

In the 2000 Reinkensmeyer and colleagues proposed the 3 degrees of freedom ARM Guide rehabilitation machine in Fig. 8. Adopting this system [57], the user is attached to a splint that slides along a linear bearing. A motor assists or resists arm movement along the linear bearing. The orientation of the linear bearing can be changed in the vertical and horizontal planes. The user receives feedback about movement and force generation of the arm on a video monitor.

Tesi di dottorato in Ingegneria Biomedica, di Antonino Salerno,
discussa presso l'Università Campus Bio-Medico di Roma in data 20/03/2012.
La disseminazione e la riproduzione di questo documento sono consentite per scopi di didattica e ricerca,
a condizione che ne venga citata la fonte

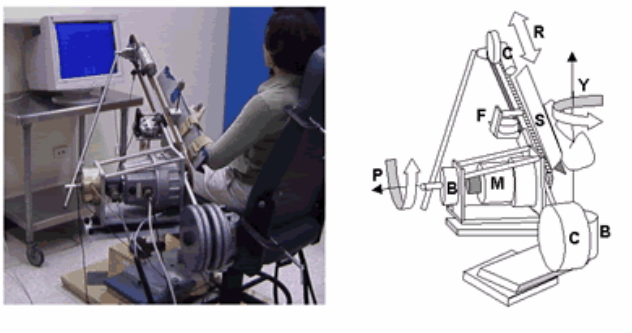

Fig. 8: Details of the ARM Guide mechanical structure. S: splint; M: motor; B: brake; F: force/torque sensor; C: counterbalance. The three degrees of freedom of the device are R: reach, Y: yaw, and P: pitch.

An alternative to serial robots for use in neurorehabilitation is provided by MACARM robot (Multi-Axis Cartesian-based Arm Rehabilitation Machine), a cable (wire) machine proposed in [58].

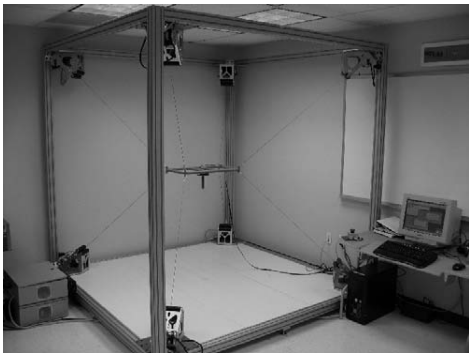

Fig. 9: MACARM system

The prototype configuration in Fig. 9 is comprised of an array of 8 motors mounted at the corners of a cubic support frame that provides, via cables, 6 degree of freedom control of a centrally located end-effector. A 6 axis load cell mounted on the end-effector provides force measurement.

Another weigh support system is Freebal [59], currently sold by Hocoma as the Armeo Boom. The Armeo Boom is based on an overhead sling suspension system with low inertia to provide an adjustable amount of arm weight support as shown in Fig. 10.

Tesi di dottorato in Ingegneria Biomedica, di Antonino Salerno,
discussa presso l'Università Campus Bio-Medico di Roma in data 20/03/2012.
La disseminazione e la riproduzione di questo documento sono consentite per scopi di didattica e ricerca,
a condizione che ne venga citata la fonte

Fig. 10: Freebal system (commercial name Armeo Boom, delivered by Hocoma)

The cable driven system is provided with a set of games for training the upper limb with 3D exercises. Further wire-based robot for neurorehabilitation is NeRebot [60]. The robot has 3 degrees of freedom and consists of a set of 3 wires indipendently driven by 3 DC motors. The wires support and move the arm of the patient in order to deliver rehabilitative therapy as depicted in Fig. 11. Extension of NeRebot was MariBot [61], where orthoses for upper limb of the patient is supported by a 5 DoF robotic arm.

Fig. 11: NeRebot

Tesi di dottorato in Ingegneria Biomedica, di Antonino Salerno,
discussa presso l'Università Campus Bio-Medico di Roma in data 20/03/2012.
La disseminazione e la riproduzione di questo documento sono consentite per scopi di didattica e ricerca,
a condizione che ne venga citata la fonte

Fig. 12: MEMOS system

MEMOS (MEchatronic system for MOtor recovery after Stroke) is a planar robot in a cartesian configuration connected to the patient at end-effector [62]. The work plane is a rectangular shape area allowing the patient's movement during the rehabilitation. Two perpendicular linear guide rails move the handle in the workspace. The actuation of the MEMOS device was achieved by using two DC motors. The overall system is shown in Fig. 12.
In 2008, also at "Università Campus Bio-Medico di Roma" a planar end-effector rehabilitation machine (namely the CBM-MOTUS) has been developed and patented [63], [64]. Further details are reported in section 4.2.

All of the reviewed robotic system have been designed for training the proximal upper limb (shoulder and elbow) of the hemiparetic arm connected to robot end-effector by enabling movement in multiple directions.

2.1.2 Exoskeletal machines for proximal upper limb rehabilitation

In this section an overview of current exoskeletal robots for proximal upper-limb districts is reported.
As exoskeletal for proximal upper limb districts, it is worth mentioning Rahman's functional upper limb orthosis [65], the Wilmington robotic exoskeleton (WREX).

Tesi di dottorato in Ingegneria Biomedica, di Antonino Salerno,
discussa presso l'Università Campus Bio-Medico di Roma in data 20/03/2012.
La disseminazione e la riproduzione di questo documento sono consentite per scopi di didattica e ricerca,
a condizione che ne venga citata la fonte

It is a passive gravity-balanced arm orthosis for patients with neuromuscular diseases. The WREX has a four-degrees-of-freedom functional orthosis and exploits elastic elements to compensate gravity of the upper limb. The exoskeletal orthosis is attached to a wheelchair, as shown in Fig. 13.

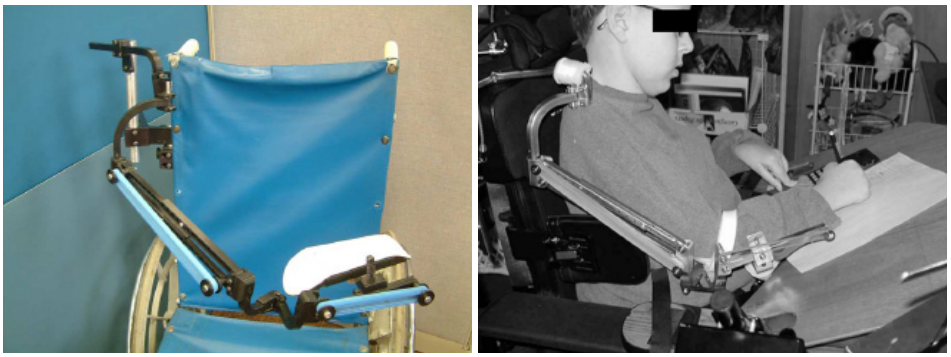

Fig. 13: WREX exoskeleton

The adult-sized version of the Wilmington Robotic Exoskeleton is the (WREX) is the Therapy WREX (T-WREX). The T-WREX is a five degrees-of-freedom mechanism that passively counterbalances the weight of the arm using elastic bands [66]. The system consists of an orthosis that assists in arm movement across a 3D workspace, a grip sensor that detects hand grip pressure, and software that simulates functional activities, as reported in Fig. 14.

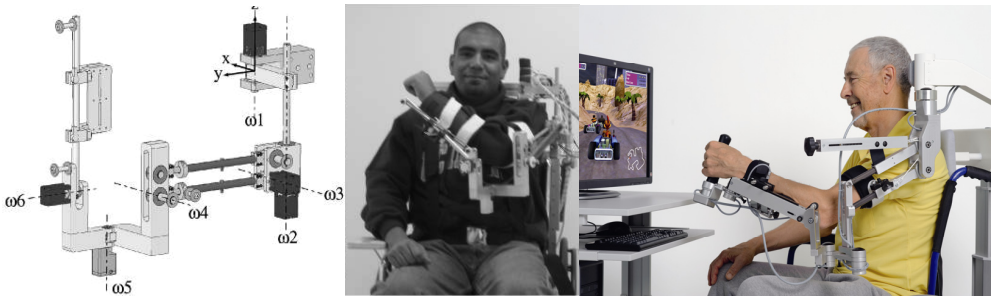

Fig. 14: from left to right the kinematic structure, the first prototype and the commercial version of the T-WREX (Hocoma Armeo Spring) respectively.

To incorporate hand grasp into therapy activities a custom-made, pressure-sensing, handgrip has been attached to the orthosis. Each joint is provided of

Tesi di dottorato in Ingegneria Biomedica, di Antonino Salerno,
discussa presso l'Università Campus Bio-Medico di Roma in data 20/03/2012.
La disseminazione e la riproduzione di questo documento sono consentite per scopi di didattica e ricerca,
a condizione che ne venga citata la fonte

absolute encoder with an accuracy of 0.3 deg. The exoskeletal machine T-WREX has been commercialized by Hocoma company with the name of Armeo Spring and is also available in pediatric version, i.e. Armeo Spring Pediatric, in the field of proximal upper limb rehabilitation.

Among the exoskeletons for the rehabilitation of the proximal district of the upper limb, it is worth mentioning the ARMin system [67][68][69]. ARMin has a semi-exoskeleton structure (the shoulder actuation is end-effector based, whereas the elbow structure is exoskeleton based) with six degrees of freedom, four active and two passive in order to enable elbow flexion/extension and spatial shoulder movements. The end-effector part compensates the weight of the robot and actuates the shoulder rotation in the horizontal plane.

This end-effector-type kinematics for the shoulder joint has been selected as exoskeleton mechanics would make it difficult to get the robot axes in alignment with the anatomical axes of the human, and misalignments would mechanically overstress and potentially harm the shoulder.

The exoskeletal part drives the internal/external rotation of the upper arm and the elbow joint, whereas horizontal and vertical shoulder rotation is actuated by an end-effector based part connecting the upper arm with the wall-mounted axes 1 and 2 in Fig. 15.

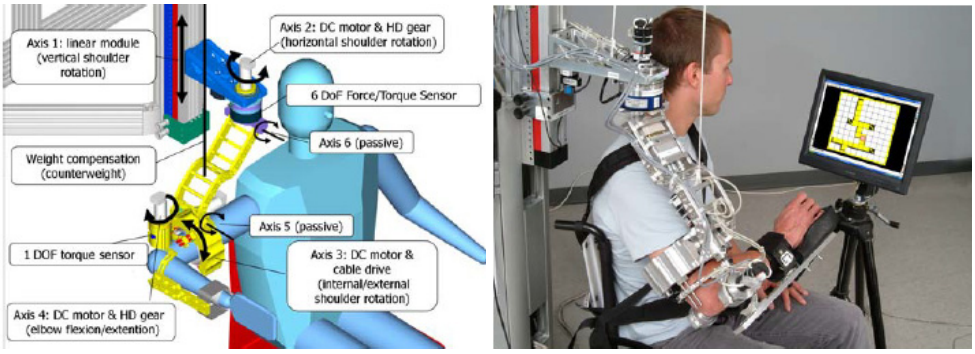

Fig. 15: ARMin system

Tesi di dottorato in Ingegneria Biomedica, di Antonino Salerno,
discussa presso l'Università Campus Bio-Medico di Roma in data 20/03/2012.
La disseminazione e la riproduzione di questo documento sono consentite per scopi di didattica e ricerca,
a condizione che ne venga citata la fonte

The four exoskeleton actuators are equipped with optical incremental sensors and redundant potentiometer-based sensors for position measurements. A six-DOF force-torque sensor beneath the horizontal arm rotation module measures forces and torques of the shoulder joint (axis 1–3). The elbow torque is measured by a separate torque sensor (Fig. 12). The third version of ARMin robot will be commercialized by Hocoma as Armeo Power. In order to overcome the misalignment between human shoulder and robot joints Carignan proposed an exoskeleton with five active degrees of freedom for shoulder rehabilitation only [70].

Fig. 16: RUPERT (robotic assisted upper extremity repetitive therapy)

A wearable exoskeletal robot for upper extremity stroke rehabilitation, namely RUPERT [71], is drawn in Fig. 16.

The RUPERT has four actuated degrees-of-freedom driven by compliant and safe pneumatic muscles (PMs) on the shoulder, elbow, and wrist. They are programmed to actuate the device to extend the arm and move the arm in 3-D space and allow movements of shoulder and elbow flexion/extension and humeral internal/external rotation. The gravity of the patient's arm is not compensated. Each one of DoFs of RUPERT is actuated by a Mckibben-type pneumatic muscle actuator. The exoskeleton is instrumented with two type of sensors: joint angle

Tesi di dottorato in Ingegneria Biomedica, di Antonino Salerno,
discussa presso l'Università Campus Bio-Medico di Roma in data 20/03/2012.
La disseminazione e la riproduzione di questo documento sono consentite per scopi di didattica e ricerca,
a condizione che ne venga citata la fonte

sensors to sense the angular position of each DoF and pressure sensors to detect the pressure inside each PM and consequently the force applied by each actuator. The sensors feedback position and force information are also exploited for quantitative evaluation of task performance.

In 2009 Stienen proposed Dampance [72], a passive exoskeleton for tasks 3D of the proximal upper limb.

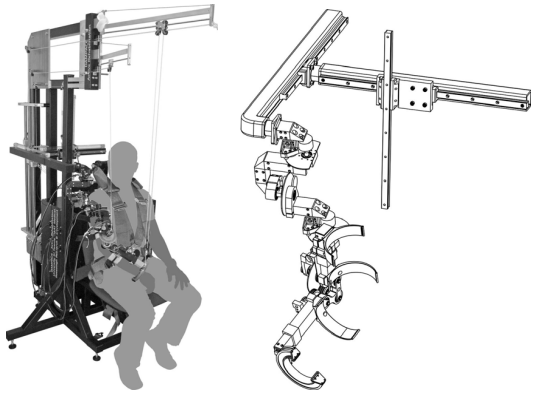

Fig. 17: Dampance Exoskeleton

The Dampace exoskeleton in Fig. 17 combines functional exercises resembling activities of daily living with impairment-targeted force-coordination training.

The rotations of the three joint axes of the shoulder and the one of the elbow can be actively resisted with the hydraulic disk brakes. The joint rotations are decoupled from the joint translations; the robot axes align themselves to the anatomical axes, overcoming some of the traditional difficulties of exoskeletons. The hydraulic disk brakes can resist rotations with up to 50 N m and have a torque bandwidth of 10 Hz for multisine torques of 20 N m. The brakes provide passive control over the movement; the patients' movements can be selectively resisted, but active movement assistance is impossible.

A full-body exoskeleton, named Salford Exoskeleton, was proposed by (Caldwell 2007). The system has seven degrees of freedom for the upper limbs and five degrees of freedom for each of the lower limbs. In this work we consider the

Tesi di dottorato in Ingegneria Biomedica, di Antonino Salerno,
discussa presso l'Università Campus Bio-Medico di Roma in data 20/03/2012.
La disseminazione e la riproduzione di questo documento sono consentite per scopi di didattica e ricerca,
a condizione che ne venga citata la fonte

upper limb exoskeleton only, in Fig. 18. The total weight of the uncompensated upper arm system is less than 2 kg. This low mass is primarily due to the use of a new range of PMAs (Pneumatic Muscle Actuators) as the power source for the system.

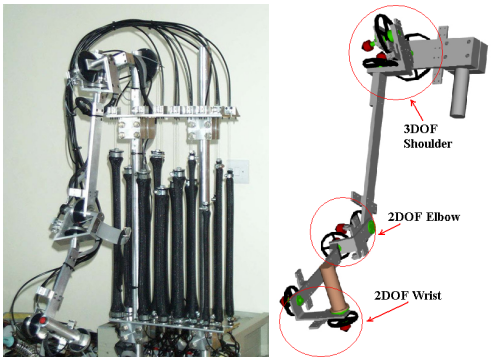

Fig. 18: Salford Exoskeleton (upper limb system)

The structure has three DOFs in the shoulder (flexion/extension, abduction-adduction and lateral-medial rotation), two DOFs at the elbow permitting flexion/extension, pronation/supination of the forearm, and two DOFs. at the wrist (flexion-extension and abduction-adduction). High linearity sensors provide position sensing on each joint, with joint torque sensing achieved by integrating two strain gauges (mounted on internal spokes) inside each joint pulley. This exoskeleton is able to administer robot aided therapy both proximal and distal anatomical districts, whereas in next section the machines for distal upper limb rehabilitation are reviewed.

2.1.3 End-effector and exoskeletal machines for distal upper limb rehabilitation

This section is aimed at providing a review of the robotic system able to train the distal districts of the upper limb. For distal district the wrist and hand are

Tesi di dottorato in Ingegneria Biomedica, di Antonino Salerno,
discussa presso l'Università Campus Bio-Medico di Roma in data 20/03/2012.
La disseminazione e la riproduzione di questo documento sono consentite per scopi di didattica e ricerca,
a condizione che ne venga citata la fonte

intended. The rehabilitative machines are classified in end-effector and exoskeletal for both wrist and hand devices.

Since 2003, there has been a steady increase in the number of devices that assist and train distal upper limb movements such as wrist and/or hand and finger movements (see [73] for a detailed review). Take for example the **Bi-Manu-Track** as *end-effector machine* for the wrist upper limb rehabilitation, and the extension of the MIT-Manus robotic device for wrist training (the **InMotion3** machine) [74] and **RiceWrist** [75] as exoskeletal *machines* for the wrist upper limb rehabilitation.

The Bi-Manu-Track system enables the bimanual passive and active practice of a 1 degree of freedom forearm and wrist movement, namely, forearm pronation/supination and wrist flexion/extension.

The arm trainer was designed to allow the bimanual practice of a 1 DoF pronation and supination movement of the forearm, as well as dorsiflexion and volarflexion of the wrist.

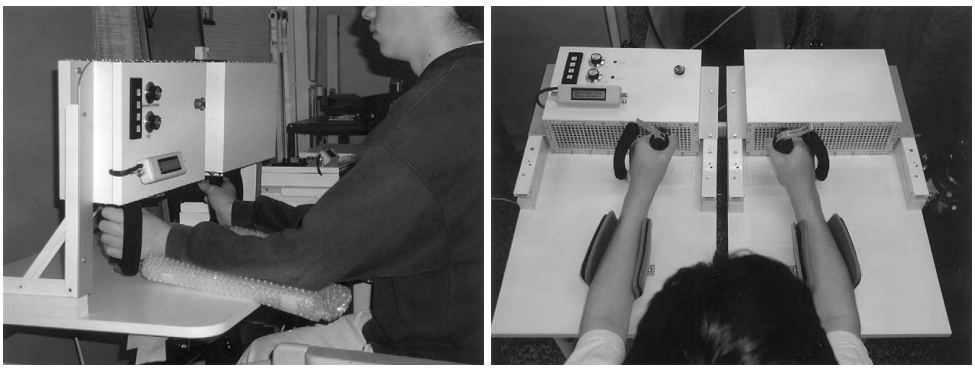

Fig. 19: Bi-Manu-Track system

All exercises can be performed symmetrically or mirror-inverted and in isometric conditions according to the patient's abilities .

Tesi di dottorato in Ingegneria Biomedica, di Antonino Salerno,
discussa presso l'Università Campus Bio-Medico di Roma in data 20/03/2012.
La disseminazione e la riproduzione di questo documento sono consentite per scopi di didattica e ricerca,
a condizione che ne venga citata la fonte

The InMotion3 wrist robot made by Interactive Motion Technologies was proposed by [74]. As shown in Fig. 20, the wrist robot has three active degrees of freedom: abduction–adduction; flexion–extension; pronation–supination.

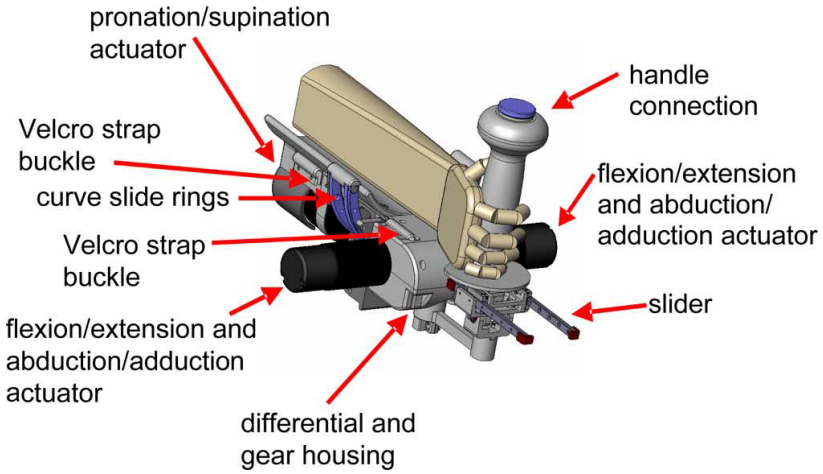

Fig. 20: A solid view of the InMotion3 design

The ranges of motion (ROM) matches the ROM of a normal wrist in everyday tasks, i.e. flexion/extension 60°/60°, abduction/adduction 30°/45°, pronation/supination 70°/70°. Maximum torque for flexion/extension and abduction/adduction is 1.43 Nm and for pronation/supination 1.85 Nm. Achievable impedances range from 0 to 60 Nm/rad and 0 to 1 Nm/rad/s for pronation/supination and 0 to 40 Nm/rad and 0 to 0.45 Nm/rad/s for flexion/extension and abduction/adduction. The two side-mounted actuators are connected to a differential mechanism, which allows for flexion/extension, abduction/adduction movements and their combinations. Joint torque production on the differential is a result of the proper combination of motor torques. Each motor contributes equal components of vertical and horizontal motion of the handle when actuated. When the two motors cooperate, motion is purely abduction/adduction; when the motion generated from these two motors opposes each other, the resulting motion is flexion/extension. The entire differential

Tesi di dottorato in Ingegneria Biomedica, di Antonino Salerno,
discussa presso l'Università Campus Bio-Medico di Roma in data 20/03/2012.
La disseminazione e la riproduzione di questo documento sono consentite per scopi di didattica e ricerca,
a condizione che ne venga citata la fonte

mechanism is mounted onto a curved rack so that it can be actuated from beneath the forearm, enabling pronation and supination movements.

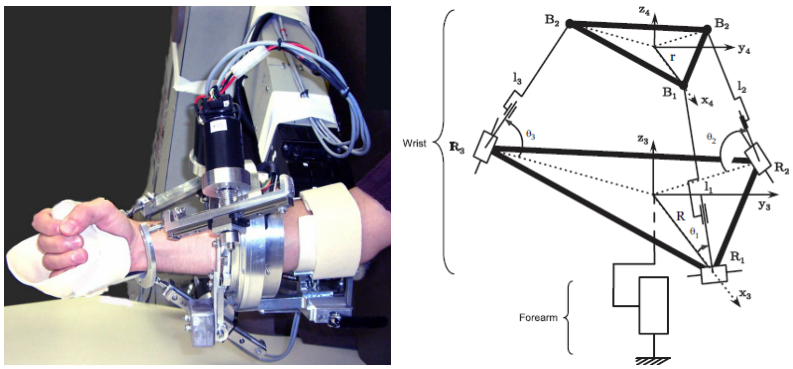

Fig. 21: on the left, subject operating the integrated MIME- RiceWrist System; on the right, kinematic structure of RiceWrist.

The RiceWrist [75] is a four degree-of-freedom upper extremity rehabilitation robot for stroke therapy, to be used in conjunction with the Mirror Image Movement Enabler (MIME) system. The RiceWrist is intended to provide robotic therapy via force-feedback during range-of-motion tasks. The exoskeleton device accommodates forearm supination and pronation, wrist flexion and extension, and radial and ulnar deviation. Joint range of motion and torque output of the electricmotor driven device is matched to human capabilities.

The basic kinematic structure of the RiceWrist is depicted in Fig. 21. The exoskeleton is comprised of a revolute joint at the forearm and a 3-RPS (revolute-prismatic-spherical) serial-in-parallel wrist. The 3-RPS platform consists of a base plate, three extensible links l_1, l_2 and l_3 and a moving plate. The moving plate houses the end-effector that is affixed to the operator during operation. The moving plate is connected to the three extensible links by means of spherical joints spaced at 120° along the circumference of a circle of radius r. The other end of the links connects to the base plate via revolute (pin) joints, which are also spaced at 120° along a circle of radius R. The axes of rotation of the revolute joints are

Tesi di dottorato in Ingegneria Biomedica, di Antonino Salerno,
discussa presso l'Università Campus Bio-Medico di Roma in data 20/03/2012.
La disseminazione e la riproduzione di questo documento sono consentite per scopi di didattica e ricerca,
a condizione che ne venga citata la fonte

oriented along the tangents to this circle. Actuators placed along the link are used to change the link length, thereby moving the top plate. The device has four degrees of freedom corresponding to the rotation of the forearm, height of the wrist platform and 2 DoF in rotation of the top plate of the platform with respect to to the base plate. The choice of a parallel mechanism for the design of the RiceWrist over a serial mechanism was motivated primarily by the compactness of the parallel mechanism. A similar mechanism is the 5 DoFs Haptic Arm Exoskeleton developed by [76] that involves also the elbow joint in the therapy.

A robotic exoskeletal device, named HWARD, for assisting wrist and hand simultaneously was proposed by Takahashi and colleagues in 2005 [77].

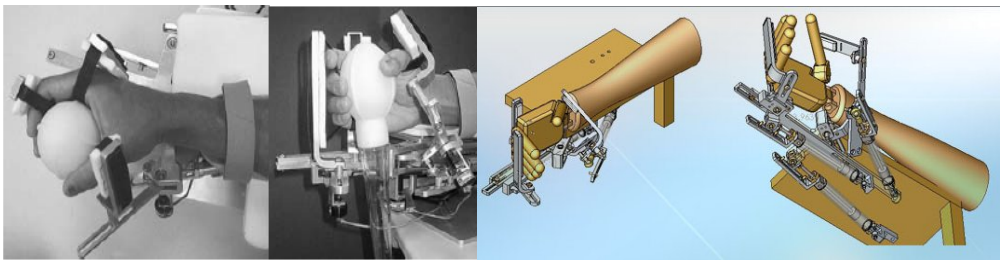

Fig. 22: HWARD device for wrist and hand rehabilitation.

HWARD (Hand-Wrist Assisting Robotic Device) is a 3-DoF mechanism that allows the rotational movement of the fingers, thumb and wrist (see Fig. 22). HWARD allows the movement of the 4 fingers as a single unit about the metacarpophalangeal (MCP) joint with a range of movement (ROM) of approximately 25 to 90 degrees flexion. HWARD allows thumb movement out of the plane of the palm and fingers with an approximate ROM of 90% full extension to 75% of full flexion. Finally, HWARD allows wrist flexion-extension movement with a ROM of approximately 20 degrees extension to 15 degrees flexion.

The device is pneumatically actuated by 3 double-acting air cylinders with bore diameters of 1.59 cm. Each cylinder can produce up to 122.8N (at source pressure of 689kPa) of force, but air pressure is regulated so that the air cylinders produce

Tesi di dottorato in Ingegneria Biomedica, di Antonino Salerno,
discussa presso l'Università Campus Bio-Medico di Roma in data 20/03/2012.
La disseminazione e la riproduzione di questo documento sono consentite per scopi di didattica e ricerca,
a condizione che ne venga citata la fonte

roughly 4-15N, the estimated levels necessary to assist movements. Rotary potentiometers measure the finger, wrist, and thumb joint angles. Microstructure pressure sensors (Honeywell) are mounted on both sides of each air cylinder to measure the pressure levels. The applied forces by the
robot can be computed from data from these sensors. Backdriveability is achieved by minimizing friction in the mechanism (in mechanical design).

As regards the hand rehabilitation, devices to train individual finger movements, simultaneous finger and thumb movements (such as palmar or precision grasp) or a combination of these can be found in the literature. Additionally, in [78], [79], [80], [81][82] robots interacting with the hand for other applications, such as tele-operation, haptic sensation, or force amplification have been presented. A brief summary of hand rehabilitation machines is reported below. They can be grouped in end-effector and exoskeletal hand rehabilitation robots. As concerns end-effector machines for hand rehabilitation, the following examples can be mentioned: HandCARE [83], a cable-actuated rehabilitation system to train hand function; Reha-Digit, a device for repeating controlled passive movements of paralysed fingers developed by [84]; hand-finger rehabilitation machine proposed by [85]; the HapticKnob developed by [86]; Amadeo, a commercially available device that provides endpoint control of each of the hand digits along fixed trajectories [87]; the InMotion hand module designed and developed by [88]; the system for hand opening/closing used in ReachMAN device [89]; the bimanual device for hand rehabilitation developed by [90]; Rutgers Master II developed by [91]. Only the most significant devices are reviewed in detail here.

Tesi di dottorato in Ingegneria Biomedica, di Antonino Salerno,
discussa presso l'Università Campus Bio-Medico di Roma in data 20/03/2012.
La disseminazione e la riproduzione di questo documento sono consentite per scopi di didattica e ricerca,
a condizione che ne venga citata la fonte

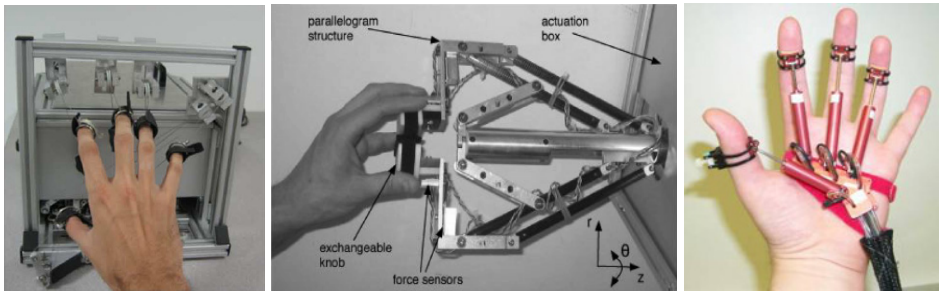

(a) (b) (c)

Fig. 23: Examples of end-effector machines for hand rehabilitation. (a) Hand Care device; (b) Haptic Knob system; (c) The Rutgers Master II.

The *Hand-CARE* [83] is a cable-driven robotic tool, where each finger is attached to a cable loop allowing predominantly linear motion. The interface can assist or resist the subject in opening and closing movements. The device consists of four main parts: (i) Acable-driven system with a frame and pulleys that convey the cable; (ii) A clutch actuation system providing assistive or resistive forces to the fingers; (iii) A sensing system to measure interaction between the subject and the interface; (iv) An arm support, i.e., a versatile system to support the forearm of the subject (Fig. 23(a)). The allowed ROM in flexion of each finger is 0-70° corresponding to a linear motion in the operational space of 8.5 cm. The peak force applied on each finger is 15 N.

The *Haptic Knob* [86] is a two-degrees-of-freedom robotic interface to train opening/closing of the hand and knob manipulation. The device, based on two parallelogram structures holding an exchangeable button shown in Fig. 23(b), offers the possibility to adapt the interface to various hand sizes and finger orientations, as well as to right-handed or left-handed subjects. The interaction with the subject is measured by means of position encoders and four force sensors [Millinewton 2N, LPM-EPFL] located close to the output are used to measure the grasping force and perpendicular (with respect to knob) force applied by the user during movement. The sensors can measure grasping and perpendicular forces of up to 30 N with a resolution of 0.2 N.

Tesi di dottorato in Ingegneria Biomedica, di Antonino Salerno,
discussa presso l'Università Campus Bio-Medico di Roma in data 20/03/2012.
La disseminazione e la riproduzione di questo documento sono consentite per scopi di didattica e ricerca,
a condizione che ne venga citata la fonte

The *Rutgers Master II [91]*, shown in Fig. 23(c), is a haptic interface able to provide force feedback up to 16 N each to fingertip (little finger excluded) designed for dextrous interactions with virtual environments. The structure linking each fingertip to the palm platform has three sensing joints and five degrees of freedom. Each actuator is attached to the base through a spherical joint (2-DoF). Its cylinder shaft can both translate in and out and rotate about the cylinder axis (2-DoF). Finally, the fingertip attachment connects to the cylinder shaft through a cylindrical joint (1-DoF). The actuated flexion motion (relative to the palm) varies from 10° to 120°, the ROM of abduction/adduction (in the plane of the palm) is ± 60°.
It uses custom cylindrical pneumatic actuators arranged in a direct-drive configuration in the palm. All RMII actuators use two Hall-effect sensors to measure the flexion and adduction/abduction angles. An infrared sensor measures the translation of the piston inside an air cylinder. The system doesn't adopt torque/force sensors to detect the interaction force exchanged with the patient.

On the other hand, examples of exoskeletal machines for hand rehabilitation are listed the in following: a device that provides for CPM (continuous passive motion) and CAM (continuous active motion) hand (MCP and PIP Joints) rehabilitation for patients recovering from damage such as flexor tendon repair and strokes proposed by [92]; an exoskeletal pneumatic glove and immersive virtual reality environment for hand rehabilitative training was developed by [93]; the Gifu Haptic Interface, able to produce adduction-abduction and flexion-extension finger movements [94]; the hand rehabilitation system proposed by [95].

Tesi di dottorato in Ingegneria Biomedica, di Antonino Salerno,
discussa presso l'Università Campus Bio-Medico di Roma in data 20/03/2012.
La disseminazione e la riproduzione di questo documento sono consentite per scopi di didattica e ricerca,
a condizione che ne venga citata la fonte

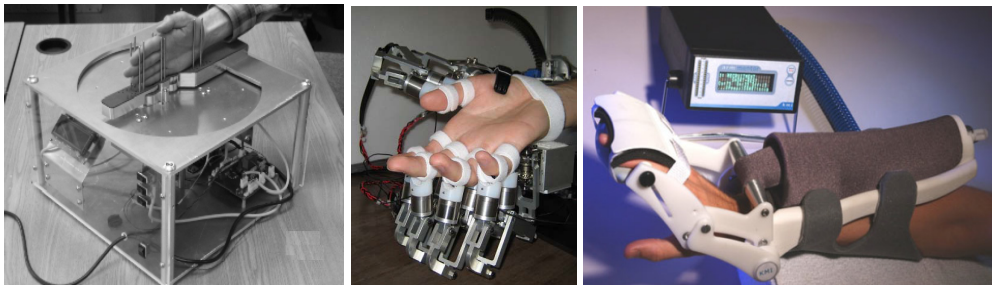

(a) (b) (c)

Fig. 24: (a) Connelly system; (b) GIFU hand rehabilitation system; (c) Koeneman system.

The hand rehabilitation device proposed by [93], shown in Fig. 24(a), is designed as a table-top machine with independent control of the MCP (metacarpophalangeal) and PIP (proximal interphalangeal) joints. During use, the patient places his/her hand within the frame of the device so that their MCP is lined up with the axes of rotation of the first motor. The proximal segment of the fingers between the MCP and the PIP joints rests on the first rotating link (proximal). The extension is slid until the PIP joint is aligned with the axes of rotation of the second motor and the remaining segments (i.e. distal and middle) of the finger rest on the second rotating link (distal). The maximum torque for the device is 4.5 Nm. The FlexiForce sensors (from Tekscan) are used for each joint. The device provides for CPM (continuous passive motion) and CAM (continuous active motion) hand rehabilitation for patients recovering from damage such as flexor tendon repair and strokes. The device is capable of flexing/extending the MCP and PIP joints through a range of motion of 0° to 90° for both the joints independently. During the CPM modes the device utilizes a minimum jerk trajectory model under PD control, moving smoothly and accurately between preselected positions. CAM is the final mode where the device actively resists the movement of the user. The user moves from a start to end position while the device produces a torque to resist the motion. This active resistance motion is a unique ability designed to mimic the benefits of a human therapist.

Tesi di dottorato in Ingegneria Biomedica, di Antonino Salerno,
discussa presso l'Università Campus Bio-Medico di Roma in data 20/03/2012.
La disseminazione e la riproduzione di questo documento sono consentite per scopi di didattica e ricerca,
a condizione che ne venga citata la fonte

The GIFU interface [94] in Fig. 24(b) is a motion assistance mechanism with 18 DoFs: 3 Dofs for 4 fingers (abduction/adduction of MP joint, extension/flextion of MP and PIP joints), 4 DoFs for thumb (abduction/adduction of CM joint, extension/flexion of CM, MP, PI joints), 2 DoFs for wrist motion assistance (abduction/adduction and pronation/supination).

The thumb CM joint has 2 DoFs motions: extension/flexion and abduction/adduction. The latter abduction/adduction produces an arc-like motion of the thumb tip, while the former extension/flexion enables the thumb to touch a fingertips. A C-shaped guide structure guarantees that the conic rotation axis of the motion assistance mechanism matches with that of the human hand.

This structure is constructed by double-tiered parallel links, at the tip of the which the extension/flexion assistance mechanism for thumb is attached. This double parallel-link structure allows the extension/flexion assistance mechanism to always direct to its rotation center. A finger motion assist mechanism is constructed as an exoskeleton of a finger. This mechanism assists the flexion/extension of the CMP and PIP joints and the abduction/adduction of the CMP joint. There are three servo motors with rotary encoders. The first and second servo motors assist the two-DoFs motion of the CMP joint through a differential gear. The third motor assists the flexion/extension of the PIP joint. The finger motion assist mechanism forms two closed loops with the human finger, in which the first and second fixtures are attached to the proximal portion and middle position of human finger, respectively, and the finger joint motion of human is assisted independently. To measure the finger joint torque, a 3-axes force sensor is mounted on each fixture.

In the device proposed by [95] and shown in Fig. 24(c), an air muscle is attached to the proximal forearm. Activation of the air muscle rotates a bar about a pivot point positioned inline with the flexion/extension axis of the wrist. This action extends the wrist and fingers, the opposite action flexes wrist and fingers. Wrist

Tesi di dottorato in Ingegneria Biomedica, di Antonino Salerno,
discussa presso l'Università Campus Bio-Medico di Roma in data 20/03/2012.
La disseminazione e la riproduzione di questo documento sono consentite per scopi di didattica e ricerca,
a condizione che ne venga citata la fonte

extension position is measured by a potentiometer, which is centered inline with the pivot point and thus the wrist flexion/extension axis.

Other exoskeletal devices for hand rehabilitation can be found in [96], [97], [98], [99] and the commercial system CyberGrasp [100];

2.1.4 Machines for arm-hand rehabilitation

Finally, a review of arm-hand rehabilitation machines is proposed. A complete system for arm-hand rehabilitation, named IntelliArm, is presented in [101] and reported in Fig. 25.

(a)

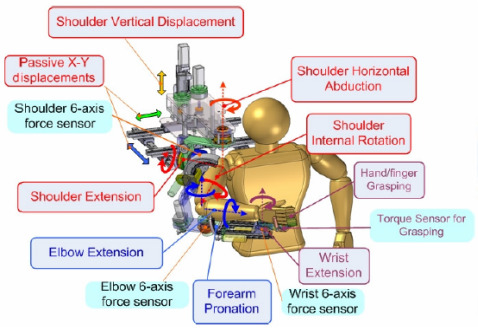

(b)

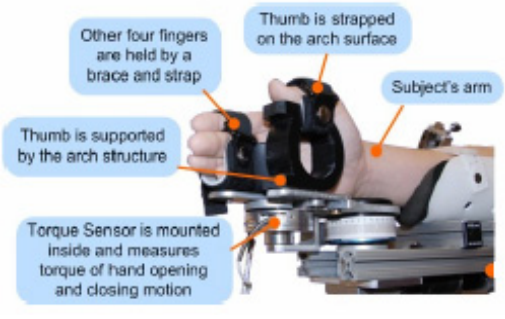

(c)

Fig. 25: IntelliArm system. (a) view of the overall rehabilitative robot; (b) CAD design; (c) Module for hand rehabilitation.

Tesi di dottorato in Ingegneria Biomedica, di Antonino Salerno,
discussa presso l'Università Campus Bio-Medico di Roma in data 20/03/2012.
La disseminazione e la riproduzione di questo documento sono consentite per scopi di didattica e ricerca,
a condizione che ne venga citata la fonte

The IntelliArm is structure with ten degrees of freedom as a whole: four active DoFs and two passive DoFs at the shoulder, two DoFs at the elbow, one DoF at the wrist and one for hand opening/closing mechanism. The shoulder (glenohumeral) movement includes four active DoFs in horizontal abduction/adduction, flexion/extension, internal/external rotation and the vertical displacement of the glenohumeral joint, and two passive DoFs in anterior/posterior and medial/lateral displacement of glenohumeral joint. The elbow movement includes elbow flexion/extension, and forearm supination/pronation while the wrist included flexion/extension. One active DoF drives the hand to open/grasp at MCP and thumb joints – synchronized hand-opening/closing motion, as shown in Fig. 25(c). The adopted sensors are reported in Fig. 25(b) and (c). The torque/force sensors are used for evaluation purposes.
In [102] a compact device named ReachMAN is proposed with only three degrees of freedom to train reaching and manipulation in activities of daily living.

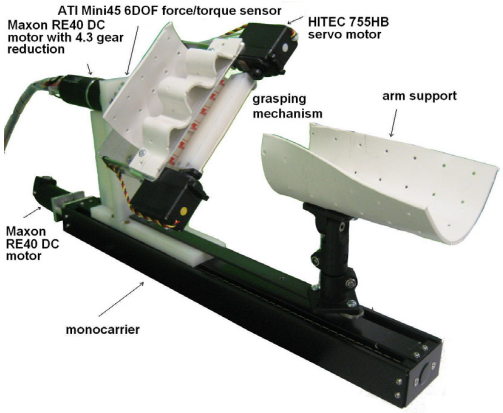

Fig. 26: ReachMAN device.

The 3 DoFs of the ReachMAN robot allows linear reaching movement, supination/pronation and grasping. A monocarrier actuated by a DC motor is used to generate the linear movement. A rotary geared DC motor (with gear reduction of 4.3) is used for supination/pronation, which is attached to the output carriage of

Tesi di dottorato in Ingegneria Biomedica, di Antonino Salerno,
discussa presso l'Università Campus Bio-Medico di Roma in data 20/03/2012.
La disseminazione e la riproduzione di questo documento sono consentite per scopi di didattica e ricerca,
a condizione che ne venga citata la fonte

the monocarrier. This monocarrier is fixed to a stable platform and acts as the robot's base. A grasping mechanism device attached to the rotary DC motor incorporates two servo motors which are used for hand opening/closing exercises. The overall system is shown in Fig. 26.
Two digital encoder are used to measure the linear position and rotary angle. Another digital encoder is used to measure the opening angle of the grasping mechanism. A 6 axis force/torque sensor (ATI Mini45, US) is attached between the grasping mechanism and the rotary actuator to measure interaction forces and torques during arm movements. An arm support attached to the moving monocarrier is added for the patient to rest the forearm. The motion and interaction control is relied on admittance control.

Podobnik and colleagues designed and developed the HARMiS device (hand and arm rehabilitation system) that is intended for use in robot-aided neurorehabilitation and for training of reaching, grasping and transporting virtual objects in haptic environments [103]. The HARMiS consists of an haptic interface HapticMaster and a grasp module mechanism with a wrist support splint mounted on top of the robot arm, as shown in Fig. 27 (a).

Fig. 27: (a) HARMiS system for arm-hand rehabilitation; (b) GENTLE/G arm-hand rehabilitation system.

Tesi di dottorato in Ingegneria Biomedica, di Antonino Salerno,
discussa presso l'Università Campus Bio-Medico di Roma in data 20/03/2012.
La disseminazione e la riproduzione di questo documento sono consentite per scopi di didattica e ricerca,
a condizione che ne venga citata la fonte

The grasp module is a two-axis gimbal with a two degree of freedom. The gimbal is used to carry the weight of the subject's arm and the grasp system and to allow unconstrained movements of the subject's arm. The two DoF are passive each with a load cell for measuring grasp force, one for measuring the force applied by thumb and other for measuring the joint forces applied by index and middle finger. Passive haptic rendering was achieved by adding the elastic cord between the frame and the movable part of the grasp module. The force sensor on the end-point of the robot is used for measuring the interaction forces between the subject and the haptic virtual environment.

Another device based on Haptic Master arm is Gentle/G [104] that integrates the Gentle/S robot [105] with a module for the hand rehabilitation, Fig. 27(b).

Gentle/G allows for relatively large reaching movements in three active degrees of freedom (Haptic Master), coupled to three passive degrees of freedom (Connection Mechanism) to allow arbitrary positioning of the hand and three active degrees of freedom (Grasp Robot Exoskeleton) for hand grasp and release retraining. Grasp robot exoskeleton consists of 3 passive DOF (roll, pitch and yaw of the wrist) and 3 active DOF. The index, middle, ring and small finger are actuated simultaneously (in 2 DOF) and the thumb separately (1 DOF). Optical encoders and precision potentiometers measure joint angles. Force sensing resistors are integrated on the parallel bars of the phalange supports to measure the patient's force input in order to drive the motors using admittance control.

In 2006 Johnson and colleagues developed the ADLER system [106]. The device, able to assist shoulder, elbow and wrist districts, consists of the Haptic Master (Van der Linde et al., 2002) and three typologies of orthoses for supporting patient wrist.

Finally two more machines that involve proximal and distal district are presented: CADEN-7 and UHD. These devices are able to train shoulder, elbow and wrist anatomical joints.

Tesi di dottorato in Ingegneria Biomedica, di Antonino Salerno,
discussa presso l'Università Campus Bio-Medico di Roma in data 20/03/2012.
La disseminazione e la riproduzione di questo documento sono consentite per scopi di didattica e ricerca,
a condizione che ne venga citata la fonte

Cable-Actuated Dextrous Exoskeleton for Neurorehabilitation (CADEN)-7 [107] is an anthropometric 7-DoF powered exoskeleton system shown in Fig. 28(a)

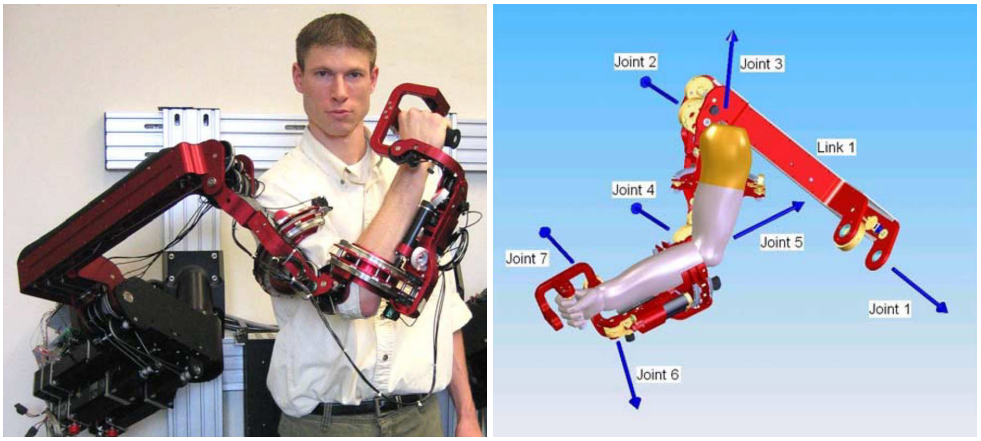

(a) (b)

Fig. 28 : (a) CADEN-7 arm rehabilitative system; (b) CAD model of the exoskeleton.

Articulation of the exoskeleton is achieved about seven single-axis revolute joints: one for each shoulder abduction–adduction (abd-add), shoulder flexion–extension (flx-ext), shoulder internal–external (int-ext) rotation, elbow flx-ext, forearm pronation–supination (pron-sup), wrist flx-ext, and wrist radial–ulnar (rad-uln) deviation. The exoskeletal joints are labeled 1 through 7 from proximal to distal in the order shown in Fig. 28(b).

Proximal placement of motors and distal placement of cable-pulley reductions have led to low inertia, high stiffness links, and backdrivable transmissions with moderate backlash. Redundant position sensors (potentiometer, Midori, Fullerton; shaft encoder, HP), one at either end of the power train, monitor both joint motion and motor position were used. Torque/force sensors have not been employed. A similar approach for simultaneous shoulder, elbow and wrist rehabilitation can also be found in [108].

Tesi di dottorato in Ingegneria Biomedica, di Antonino Salerno,
discussa presso l'Università Campus Bio-Medico di Roma in data 20/03/2012.
La disseminazione e la riproduzione di questo documento sono consentite per scopi di didattica e ricerca,
a condizione che ne venga citata la fonte

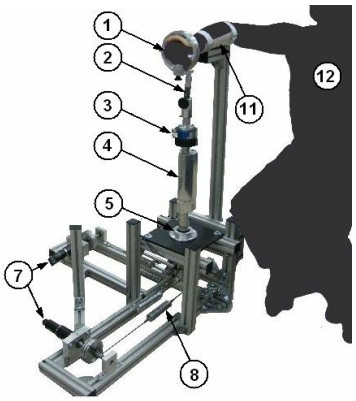

Fig. 29: UHD prototype. 1-handle bar, 2-universal joint, 3-force sensor, 4-sliding mechanism, 5-spherical joint, 7- DC motors with gears and encoders, 8-elastic springs, 11-forearm support ("WRIST" mode) and 12-user.

Universal Haptic Drive (UHD) is a device that enables rehabilitation of either arm ("ARM" mode) or wrist ("WRIST" mode) movement in two degrees of freedom, presented by [109]. The mechanism and adopted sensors are summarized in Fig. 29. The actuation system is based on two sets of DC motors with gears and encoders, which are connected in series with elastic springs to the actuated bar by means of string wires and pulleys. The series elastic actuators generate a desired force calculated from selected impedance parameters and kinematics of the actuated bar. This desired force compared with the force applied on end-effector by the end-user feed in input a conventional proportional force control scheme, which is needed for implementation of impedance control based movement training of each actuated DOF.

2.1.5 Control strategies for rehabilitative robots

The goal of robotic therapy control algorithms is to control robotic devices designed for rehabilitation exercise, so that the selected exercises to be performed by the participant provoke motor plasticity, and therefore improve motor recovery. Currently, however, there is not a solid scientific understanding of how

Tesi di dottorato in Ingegneria Biomedica, di Antonino Salerno,
discussa presso l'Università Campus Bio-Medico di Roma in data 20/03/2012.
La disseminazione e la riproduzione di questo documento sono consentite per scopi di didattica e ricerca,
a condizione che ne venga citata la fonte

this goal can best be achieved. Robotic therapy control algorithms have therefore been designed on an ad hoc basis, usually drawing on some concepts from the rehabilitation, neuroscience, and motor learning literature. One way to group current control algorithms is according to the strategy that they take to provoke plasticity: **assisting**, **challenge-based**, **simulating normal tasks**, and **noncontact coaching**.

The most developed paradigm is the assistive one. Assistive controllers help participants to move their weakened limbs in desired patterns during grasping, reaching, or walking, a strategy similar to "active assist" exercises performed by rehabilitation therapists. The term "challenge-based" controllers refers to controllers that are in some ways the opposite of assistive controllers because they make movement tasks more difficult or challenging. Examples include controllers that provide resistance to the participant's limb movements during exercise, require specific patterns of force generation, or increase the size of movement errors ("error amplification" strategies).

The third paradigm, called haptic simulation, refers to the practice of activities of daily living (ADL) movements in a virtual environment. Haptic simulation has flexibility, convenience, and safety advantages compared to practice in a physical environment.

Finally, there is some work on robotic devices that do not physically contact the participant but instead serve as coaches, helping to direct the therapy program, motivate the participant, and promote motor learning. For such devices, it has been hypothesized that physically embodying the automated coaching mechanism has special merit for motivating participants [110].

Assistance control strategies can be grouped into four conceptual categories: **impedance-based**, **counterbalance-based**, **EMG-based** and **performance-based adaptive assistance**.

The first **Impedance-based** assistive robotic therapy controllers proposed were proportional feedback position controllers [50], [111], [112], [55], [113]. More

Tesi di dottorato in Ingegneria Biomedica, di Antonino Salerno,
discussa presso l'Università Campus Bio-Medico di Roma in data 20/03/2012.
La disseminazione e la riproduzione di questo documento sono consentite per scopi di didattica e ricerca,
a condizione che ne venga citata la fonte

recent controllers have used more sophisticated forms of mechanical impedance than stiffness, including for example viscous force fields [114], [115], creating virtual objects that assist in achieving the desired movement [116], or creating user-definable mechanical limits for complex postural or locomotor movements [117]. Assistive control strategies focus on a common, underlying idea: when the participant moves along a desired trajectory, the robot should not intervene, and if the participant deviates from the desired trajectory, the robot should create a restoring force, which is generated using an appropriately designed mechanical impedance. A variant of impedance-based assistance is triggered assistance, which allows the participant to attempt a movement without any robotic guidance, but initiates some form of (usually) impedance-based assistance after some performance variable reaches a threshold. This form of triggered assistance encourages participant self-initiated movement, which is thought to be essential for motor learning [118], [119]. For example, this triggering technique was used in initial studies with the ARM Guide [57], [120] and MIT-Manus robotic therapy devices [121], [122], which assisted the participant in moving along a minimum jerk trajectory when the participant exceeded a movement error threshold, or moved faster than a velocity threshold, respectively.

Variations of time-triggered assistance have recently been used for the hand grasp robot HWARD [77], and reach and grasp robots Gentle/G [104] and RUPERT [71].

Providing weight counterbalance to a limb is another assistance strategy that has been developed in the framework of **counterbalancing assistance**.

Rehabilitation clinics have a long history of using devices to partially counterbalance the limbs, such as mobile arm supports, overhead slings, arm skateboards or towels that slide on tables, and harnesses for supporting body weight during walking. The use of swimming pools in rehabilitation can also be viewed as variant of this approach: active assistance is provided by virtue of the buoyancy of the body. Recently developed devices implement passive

Tesi di dottorato in Ingegneria Biomedica, di Antonino Salerno,
discussa presso l'Università Campus Bio-Medico di Roma in data 20/03/2012.
La disseminazione e la riproduzione di questo documento sono consentite per scopi di didattica e ricerca,
a condizione che ne venga citata la fonte

counterbalancing schemes in a way that allows a greater range of motion than previous clinical devices [66], [59]. For example, Therapy-WREX, based on the mobile arm support WREX, uses two four-bar linkages and elastic bands to passively counterbalance the weight of the arm, promoting performance of reaching and drawing movements through a wide workspace [66]. A similar approach has been developed for assisting in gait training, counterbalancing the weight of the leg using a gravity-balancing, passive exoskeleton [123]. Non-exoskeleton passive devices that reduce the amount of weight on the participant lower limbs have been developed to assist participants to train standing balance [124], or to keep balance while walking overground [129]. It is also possible to actively generate a counterbalance force through the robot's control system to assist in reaching [125], [53], [130], [131] or walking [132], [133], [134]. This active technique allows the selection of a weight support level via software to meet participants' individual needs, and can take into account other forces that can restrain participant's free movement such as those arising from abnormal tone [57], [111] rather than just gravitational forces.

Some groups have developed robotic devices that employ surface electromyography signals (sEMG) to drive the assistance (**EMG-based assistance**). The EMG signals recorded from selected muscles (i.e pectoralis major, triceps, anterior middle and posterior deltoids, biceps, soleus, gastrocnemius), can be used as an indicator of effort generation to trigger assistance. An example of such an EMG triggered assistance was proposed with the MIT-MANUS robot [121], where EMG signals are collected from different muscles on the shoulder and elbow and, after some signal processing, the assistance is triggered when the processed EMG signals increase above a threshold. Similar approaches are proposed for upper limb rehabilitation in [107], [74], [126].

Adapting control parameters has the potential advantage that the assistance can be automatically tuned to the participant's individual changing needs, both

Tesi di dottorato in Ingegneria Biomedica, di Antonino Salerno,
discussa presso l'Università Campus Bio-Medico di Roma in data 20/03/2012.
La disseminazione e la riproduzione di questo documento sono consentite per scopi di didattica e ricerca,
a condizione che ne venga citata la fonte

throughout the movement and over the course of rehabilitation [121] [127], [128]. Adapting control parameters is a key part of "patient-cooperative training" strategies (**Performance-based adaptation of task parameters**) developed first for the Lokomat, in which the robot adaptively takes into account the patient's intention rather than imposing an inflexible control strategy [127]. It is also a key part of "performance-based, progressive robot-assisted therapy" control strategy developed for MIT-MANUS [121]. In the latter approach the control law is an error-based strategy that adjusts a control parameter from trial to trial based on measured participant performance. A position-feedback type assisting controller was designed that allowed participants freedom to move more quickly than the desired trajectory (i.e. the virtual channel with a moving back wall). The duration of the desired trajectory and the stiffness of the robot controller were modified such that the reaching task was less demanding if the participant was more impaired. For the ARM Guide [128], a similar adaptive update law was proposed and other adaptive approach was proposed in [131], [135], [136], [127], [138], [137] and [140].

The term "**challenge-based controllers**" refers to controllers that in some ways make a task more difficult or challenging, as opposed to the assistive controllers. Challenge-based controllers provides insight that might be missed by focusing solely on assistive-type algorithms. challenge and assistive controllers can be viewed as being different points on the same continuum, a continuum along which task difficulty is modulated to optimally challenge the participant [141].
The challenge-based controllers can be grouped in: **resistive strategies**, **constraint-induced strategies**, **error-amplification strategies**. Resistive exercise refers to the therapeutic strategy of providing resistance to the participant's hemiparetic limb movements during exercise, an approach that has a long history in clinical rehabilitation and clinical rehabilitation devices. There have been a few attempts to incorporate resistive training into robotic therapy.

Tesi di dottorato in Ingegneria Biomedica, di Antonino Salerno,
discussa presso l'Università Campus Bio-Medico di Roma in data 20/03/2012.
La disseminazione e la riproduzione di questo documento sono consentite per scopi di didattica e ricerca,
a condizione che ne venga citata la fonte

Examples of resistive robotic devices that apply constant resistive forces to the affected limb, independent of its position or velocity, have been proposed for reaching and grasping practice [142], [59], [146], [147], [86] and [148]. A more sophisticated resistance proposed in [50] consists of applying a viscous resistance consisting of a resistive force in the movement's direction proportional to the affected limb's velocity. In the rehabilitation literature, the term "constraint-induced" therapy refers to a family of rehabilitation techniques in which the unimpaired limb of persons post stroke is constrained (for example in a sling or with a mitt) to encourage use of the impaired limb [149]. Several robotic therapy control strategies have been developed consistent with the main idea of this strategy, which is to "force use" of the impaired limb. For example, Johnson et al. [150] developed a robotic steering wheel that resists turning when the person poststroke relies too heavily on his unimpaired arm, and showed that this approach encourages use of the impaired limb. Simon et al. [151] developed a robotic control strategy to improve force generation symmetry in the lower limbs, which applies resistance proportional to the difference between the force generated by both legs. For the "Guided Force Training" algorithm [57], [128], subjects reach along a linear rail, and a robot halts the participant's movement if the participant pushes with an abnormally large force perpendicular to the rail. This strategy was inspired by the "active constrained" mode of MIME, which essentially only allowed the participant to move if force generation was toward the target [144]. Assisting-type robotic therapy algorithms have the effect of reducing movement errors – they help the participant do the task better. However, research on motor adaption has emphasized that kinematic errors generated during movement are a fundamental neural signal that drives motor adaptation [136], [137] [152], [154]. Thus, researchers have proposed robotic therapy algorithms that amplify movement errors rather than decrease them developing the error-amplification strategies, e.g. Patton and colleagues [152], [153] and [154]. Several studies have shown that some benefits of error amplification can be achieved by

Tesi di dottorato in Ingegneria Biomedica, di Antonino Salerno,
discussa presso l'Università Campus Bio-Medico di Roma in data 20/03/2012.
La disseminazione e la riproduzione di questo documento sono consentite per scopi di didattica e ricerca,
a condizione che ne venga citata la fonte

distorting visual feedback from the task, rather than by physically altering movements [142], [155] and [143].

In the framework of the **haptic simulation strategies**, Robotic therapy devices can be used as haptic interfaces for interacting with virtual reality simulations of activities of daily living, such as manipulating objects [69], [125], [156], [86], [88], [157], [158], [159], [70], [139]. Potential advantages of this approach over training in physical reality include: a haptic simulator can create many different interactive environments simulating a wide range of real-life situations, quickly switch between these environments without a "set-up" time, automatically grade the difficulty of the training environment by adding or removing virtual features, make the environments more interesting than a typical rehabilitation clinic (e.g. walking through Paris versus down a hospital hallway), automatically "reset" itself if objects are dropped or misplaced, and provide novel forms of visual and haptic feedback regarding performance. A variable of virtual environments was suggested by [145], where real objects for manipulation were presented robotically.

2.2 State of the art on robotic and prosthetic hands

The hand is the most dexterous organ ("device") humans are endowed with [21] which also entails the major complexity in the mechanical structure. In robotics, the development of robotic hands capable of dexterous manipulation tasks is still a real challenge. Under a technical viewpoint, for applications requiring few movements with high accuracy, robotics often offers solutions that are also stronger or faster than human hands [22]; these mechanical solutions are generally very specific tools (ranging from pliers up to simplified hands) that always have reduced degree of freedoms with respect to the human hand and high dexterity in

Tesi di dottorato in Ingegneria Biomedica, di Antonino Salerno,
discussa presso l'Università Campus Bio-Medico di Roma in data 20/03/2012.
La disseminazione e la riproduzione di questo documento sono consentite per scopi di didattica e ricerca,
a condizione che ne venga citata la fonte

specific contexts. However, when they are required to perform new tasks or are moved to environments with changing dynamic characteristics, their performances inevitably go down and performances of human hands still remain incomparable. Analysis of the literature shows that robotic hands often result from a trade-off among between the application and the level of anthropomorphism, thus influencing the choice of the number, the kinematics and the viscoelastic characteristics of the fingers, the choice of actuated/unactuated degrees of freedom, the complexity of sensory system, the design of the control, etc.

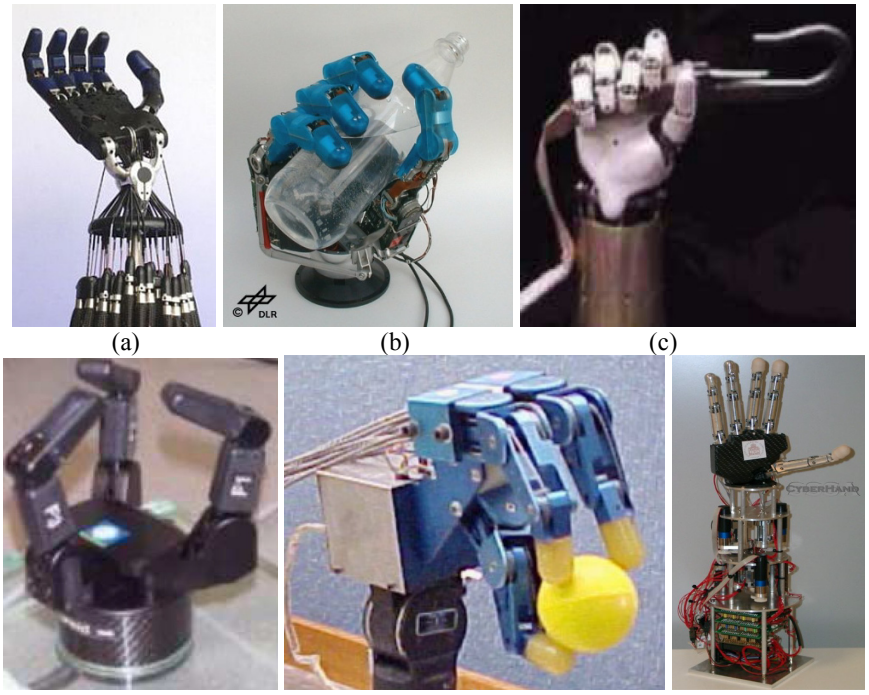

Fig. 30: A series of pictures of robotic hands: (a) Shadow Hand; (b) DLR Hand II; (c) Robonaut Hand; (d) Barrett Hand; (e) Okada hand; (f) CyberHand.

In the following an overview of the most meaningful examples of robotic hands is reported. Although first papers on this topic can be dated already in the sixties [23], the first very robotic prototype of hand is the Okada Hand, a three finger,

Tesi di dottorato in Ingegneria Biomedica, di Antonino Salerno,
discussa presso l'Università Campus Bio-Medico di Roma in data 20/03/2012.
La disseminazione e la riproduzione di questo documento sono consentite per scopi di didattica e ricerca,
a condizione che ne venga citata la fonte

tendon actuated hand with 11 DOF [24] developed in 1979. In the same period also the Stanford JPL hand [25] appeared. It had size comparable with the human hand and integrated an array of tactile sensors on the fingertips. The Utah/MIT hand [26] is instead a pneumatic hand aimed at ensuring a safe contact in grasping with the fingertips, the phalanges and the palm. In 1988 the concept of underactuation was fully exploited in the Belgrade USC hand [27], endowed of 18 degrees of freedom, of which just 4 actuated. A commercially available robotic hand is the Barrett Hand [28], whose aspect is much closer to a plier than a human hand. It has three fingers, each embedding one motor. With the technological advancements above all in electronic components and micromechanics, the level of anthropomorphism of the robotic hands got higher and higher. For example, in 1992 the three-fingered UB hand II and successive versions [29][30], [31] were developed at the Bologna University. It included 11 degrees of freedom in the hand and 2 degrees-of-freedom in the wrist. In 1993 the Anthrobot-II dexterous hand [32] was introduced as an example of anthropomorphic hand, which has 5 tendon-actuated fingers, each of them with 4 degrees of freedom. Then GRASPAR was presented, that is a three fingers hand purposely developed for grasping with one motor per finger [33].

At the beginning of 1997, a first version of the DLR hand was presented. The second one appeared in the 2000 [34], [35], [36]. The DLR hand I has four fingers with 18 degrees of freedom, but only 13 actuated. The actuators (electrical revolute motor) are placed inside the fingers so to have a compact device (although its size is higher than human hand). Concerning the sensory system, this hand include an x-y force sensors on the fingertips as contact sensors, potentiometer for the position of joints. The DLR hand I has been designed with typical features that are useful when executing particular tasks or to enhance general performances during grasping and manipulation [36]: first of all fingers can be bent backwards so to increase the grasping abilities; then another important factor is the role of the palm: indeed, if appropriately used, it adds a lot to the

Tesi di dottorato in Ingegneria Biomedica, di Antonino Salerno,
discussa presso l'Università Campus Bio-Medico di Roma in data 20/03/2012.
La disseminazione e la riproduzione di questo documento sono consentite per scopi di didattica e ricerca,
a condizione che ne venga citata la fonte

stability of a power grasp. So, mimicking an anthropomorphic behaviour, the DLR hand I is able to reconfigure its palm according to the type of the task to perform (power grasp, fine manipulation, etc.) allowing two configurations: a "flat" palm configuration and an opposing fingers configuration. Another key aspect to take into account when performing particular tasks, such as catching or playing piano is the speed. To this purpose DLR hand I has a high speed of the joints (about 382 deg/s). From the redesign of the DLR hand I, the DLR/HIT-Hand II [248] was developed. It consists of 5 fingers with a total of fifteen dofs. To achieve a high degree of modularity, all five fingers are identical. Each finger has three dofs and four joints, last two joints are mechanically coupled. All actuators, gears, the electronics and communication controllers for one finger are fully integrated in the finger's base or the finger's body directly. The motor measures only 20mm in diameter and 10mm in height, weights only 15g. The rated speed and torque of the motor are 6000 rpm and 3.2 mNm respectively. In the finger distal joint, a 2.1:1 mechanical transmission is realized by a timing belt instead of bevel gears, so that the transmission noise is much quiet. The coupling mechanism in the last two joints of the finger is realized by steel wires with fasten mechanism. This makes the transmission ration exactly 1:1 in the whole movement range. Also at the base joint actuation unit, two tiny harmonic drivers with timing belts have replaced planetary gears and bevel gears.

In 1998 LMS [37] hand was presented: in this case the device included also the forearm with the pneumatic actuation system within it. Among the five fingered hands, it is worth to mention the DIST hand [38] and the Robonaut hand [39], developed by the NASA for space applications. In 2000 Karlsruhe and Tokyo University developed an underactuated robotic five fingered hand for grasping with 24 joints but only one actuated degree of freedom [40]. In the same year the Ultralight hand was developed by Karlsruhe Research Center with pneumatic actuators located inside the fingers [41]. Again in 2000 Light presented a myoelectric controlled lightweight hand prosthesis [42]. Other five fingered hands

Tesi di dottorato in Ingegneria Biomedica, di Antonino Salerno,
discussa presso l'Università Campus Bio-Medico di Roma in data 20/03/2012.
La disseminazione e la riproduzione di questo documento sono consentite per scopi di didattica e ricerca,
a condizione che ne venga citata la fonte

are the GIFU hand [43], with 16 actuated degrees of freedom by DC motors, and the commercial model, the Shadow hands, developed by Shadow Robot Company Ltd including inside the forearm the pneumatic actuation system. In 2005 RL1 hand [44] with three fingers actuated by only one motor was developed.

As regards the prosthetic hands, upper-limb prostheses are not yet dexterous enough to provide function comparable to healthy limbs. Commonly used upper-limb prosthetics range from a hook to a single-degree-of-freedom (opening and closing) mechanism using myoelectric control.
Upper-limb prosthetics with multiple degrees of freedom typically use sequential control methods, with locking mechanisms or switches used to separately activate each joint. Commercial prosthetic hands are basically simple grippers with few degrees of freedom (DOFs), a limited biomorphic appearance, and one actuator able to exert high grasping forces. Take for example the Sensorhand speed made by Ottobock (http://www.ottobock.com/). This prosthetic hand consists of three finger with one degree of freedom only. Consequently, the control is very simple but robust: a couple of commands sent by the user myoelectric signals control gripper opening and closure. The maximum exercisable force is 100 N, with the grasp force proportional to myoelectric signal. A novel multiarticulated prosthetic hand, i.e. the i-LIMB hand (http://www.touchbionics.com) was introduced in the market by Touch Bionics. This hand is the first-to market prosthetic device with five individually powered digits. It is manufactured using high-strength plastics and looks like a real human hand. It has two main improvements compared to other commercial prostheses: first, speed and grip-strength sensors allow the control system to independently stop each digit; second, the possibility of moving the opposition plane of the thumb by means of a passive joint. The result is that the hand is capable of different grasping patterns such as precision (tridigit), power, and lateral grips. Nevertheless, concerning the control strategy, the device

Tesi di dottorato in Ingegneria Biomedica, di Antonino Salerno,
discussa presso l'Università Campus Bio-Medico di Roma in data 20/03/2012.
La disseminazione e la riproduzione di questo documento sono consentite per scopi di didattica e ricerca,
a condizione che ne venga citata la fonte

still uses a traditional two-input EMG system to open and close the hand's fingers that does not differ from those available in other commercial prosthetic hands.

For the last decade, the research focus in upper-limb prosthetics has been in the anthropomorphic arm and hands capable of neural interface. The Cyberhand [46], with a single degree of freedom per finger, aims to interface with both afferent and efferent pathways, providing true feedback for the user. The ACT hand [47] is designed around the central tenant that an anatomically correct hand can be operated by the same neural signals used to operate the muscles in the original hand.
In 2007 a gas actuated hand prosthesis was presented with 9 actuated degrees of freedom [45].
The prosthetic hands aim at substituting the functionality of a missing human hand. Therefore in addition to a natural and cosmetic apparence, requirements of lighthness and sensory feedback are requested. As previously shown, the prosthetic hand present only few actuated degree of freedom and very simple control law proportional to myoelectric commands. On the other hand, robotic hands shows higher manipulation capabilities by exploiting a large number of actuated joints (meanly three/four per finger) in the mechanical design.

2.3 Main issues to address and proposed solutions

The control strategy mentioned in section 2.1.5 highlights that a plethora of control strategies has been proposed in scientific literature. Only few comparative studies can be found in literature and estabilishing which control strategy entails the best results in terms of motor recovery of the patient is still debated and goes beyond the thesis purposes. In this thesis the impedance-based assistance strategy of end-effector rehabilitative machines is taken into account.

Tesi di dottorato in Ingegneria Biomedica, di Antonino Salerno,
discussa presso l'Università Campus Bio-Medico di Roma in data 20/03/2012.
La disseminazione e la riproduzione di questo documento sono consentite per scopi di didattica e ricerca,
a condizione che ne venga citata la fonte

In the framework of assistance control strategies (impedance-based) is typically assumed that the robot intervention is dependent on the deviation of the upper limb trajectory from a reference trajectory planned by manipulator.

In order to assist the impaired limb of the patient, it is generally assumed that desired motion is a minimum-jerk virtual trajectory [19], [55], being the jerk the third derivative of the position. This reference trajectory (typically corresponding to linear path) is generated exploiting a predetermined polynomial arch length function, but this concept is difficult to customize to different typologies of stroke patients. The first part of this thesis investigates if it is possible to assist the impaired limb of the patient as a human therapist does in the traditional therapy. In [121] a performance-based control approach is proposed, but adapting offline the control gains and duration of the whole end effector trajectory. *One of the main objectives of this thesis is to demonstrate that it's possible to tune online trajectory features of an end effector rehabilitative machine according to patient need*. In other words, this work tries to address the question: "Is feasible to generate a reference trajectory (robot side) as similar as possible to the trajectory generated by motor control of a human therapist? ". The assumption is that adopting the submovements theory, mentioned in section 1.1, is possible to plan on line a desired trajectory of a robot by reproducing the human motor control output for the upper limb. The trajectory can be changed in real time according to motor task requirement and patient impairments. The motion features can be modified on the basis of proprioceptive and exteroceptive sensors of the rehabilitative robot in order to provide an assistance as similar as possible to human therapist. Chapter 3 is aimed at providing these evidence.
Another key point highlighted by state of the art analysis is that in case of active assistance of the robot on patient's limb, control design typically resorts to traditional approaches, e.g. stiff PID voltage control (i.e. a proportional-integral-derivative action), compliance control and impedance control [160], [161]. The

Tesi di dottorato in Ingegneria Biomedica, di Antonino Salerno,
discussa presso l'Università Campus Bio-Medico di Roma in data 20/03/2012.
La disseminazione e la riproduzione di questo documento sono consentite per scopi di didattica e ricerca,
a condizione che ne venga citata la fonte

term *compliance control* is referred to interaction control based on a proportional-derivative action plus gravity compensation; on the other hand, impedance control refers to inverse dynamics interaction control.

The mentioned types of control can ensure robustness and ease of implementation, especially in the case of PID and compliance control (which do not require estimating robot dynamics), but highly nonlinear phenomena able to strongly degrade robot performance, such as friction, are typically not accounted for in the design of the control system and mechanical structure of the machines for robot aided rehabilitation. In order to overcome this issue a compensation for friction and tuning robot compliance by means of an interaction control law based on inverse dynamics compensation is proposed. Additionally, among the above mentioned control algorithm only the impedance control (term referred to inverse dynamics control) exploits the interaction force feedback in the control loop. In fact in case of compliance or PID control friction and force applied on external environment by robot are rejected as disturbs.

When the robot interacts with a patient these physical quantities cannot be neglected. Generally the force feedback is provided by torque/force sensors, but in this thesis aims at exploiting a sensorless approach where the interaction forces exchanged between robot and patient are monitored of the motor currents in order to achieve the limitation of the masses and wires at the robot end-effector and costs containment. The *friction compensation* and the *implementation of an impedance control with force feedback provided by motor currents monitoring* are the main objectives of chapter 4 where the CBM-Motus rehabilitative machine [63] is taken as case-study.

Finally *in the field of assistive robotics the main objective of this work is determining the optimal hand configuration that fits object characteristics and ensures a stable grasp*. In fact, for manipulation aids, robotic and prosthetic hands the ability to realize smooth movements and to obtain a stable grasp has a primary importance. For this reason, one issue that the present work tries to address is to

Tesi di dottorato in Ingegneria Biomedica, di Antonino Salerno,
discussa presso l'Università Campus Bio-Medico di Roma in data 20/03/2012.
La disseminazione e la riproduzione di questo documento sono consentite per scopi di didattica e ricerca,
a condizione che ne venga citata la fonte

develop a bio-inspired control approach for determining posture, contact points with the object and trajectory of the fingers of a robotic hand during the grasping action. Such as action can be decomposed in reaching (the hand approaches the object to be grasped), pre-shaping (fingers assume the configuration most suitable to ensure a stable grasp) and grasping (the object is actually grasped).

In order to reduce the complexity of the control that ensures the stability of grasping, it appears convenient to find the optimal grasping configuration. During the pre-shaping phase, in fact, on the basis of the physical characteristics of the object to be grasped, such as shape and weight, the hand, while approaching the object, assumes the configuration most suitable for seizing. During this phase, the contact points between fingers and object allowing a stable grasp are also located, and the trajectory to be followed by fingers in order to grasp the object in the determined points is planned. Thus, pre-shaping plays a fundamental role in order to guarantee a stable grasp, and, for this reason, the control algorithm proposed in chapter 5 is focussed on pre-shaping and reaching phases by finding the optimal contact points by means a technique coming out studies on human. The control algorithm has been applied to a robotic hand with 20 DoF [248] as explained in chapter 5. The choice of the implementation of the control strategy on such as robotic hand was determined by the possibility to exploit the dexterous capabilities impossible to achieve with current prosthetic hands. Applications to prosthetic field is also envisaged.

Tesi di dottorato in Ingegneria Biomedica, di Antonino Salerno,
discussa presso l'Università Campus Bio-Medico di Roma in data 20/03/2012.
La disseminazione e la riproduzione di questo documento sono consentite per scopi di didattica e ricerca,
a condizione che ne venga citata la fonte

Chapter 3

Submovement-based control

This chapter presents a novel control approach for robot motion and interaction control that is inspired by neuroscientific studies on the intermittency nature of motor control in humans. Robot motion is generated by dynamic sequences of elementary motion units (called submovements) that, on-line modulated, can achieve accurate motion or else force regulation. A feasibility study on the predetermined static sequence of submovements and the dynamic sequence generator implementation are presented. The dynamic submovement sequence generation is grounded on the adaptive behaviour of four oscillators. Control performance in free space and in interaction with a purely elastic environment can be managed by dynamically changing features of motion units in the current

Tesi di dottorato in Ingegneria Biomedica, di Antonino Salerno,
discussa presso l'Università Campus Bio-Medico di Roma in data 20/03/2012.
La disseminazione e la riproduzione di questo documento sono consentite per scopi di didattica e ricerca,
a condizione che ne venga citata la fonte

sequence. The theoretical formulation of the control strategy and the application to robot point-to-point motion in free and in constrained space are provided in simulated environment and by means trials on available robot. A comparative analysis with a traditional PD control is also carried out. The chapter is structured in six main sections. Section 3.1 focuses on the investigation of the human motor control presented in scientific literature and how it can be exploited for robot motion and interaction control; Section 3.2 presents the general control architecture; Section 3.3 provides a feasibility study on the proposed approach with submovements of predetermined features. Section 3.4 describes the implementation methods of the control approach able to generate dynamically submovements with features according to task requirements in free space and in interaction with the external environment. Finally Sect. 3.5 and 3.6 are focussed on validation of the method in simulated environment and by means trials on MIT-Manus robotic system respectively.

3.1 Introduction to submovements theory

The observation of biological systems can be regarded as an important source of inspiration for the development of new control schemes robust and adaptable enough to safely and efficiently interact with unstructured environments. In particular, there is a wide number of studies on human motor control [162]-[171] supporting the theory that reaching and pointing movements are the result of sequences of discrete motion units, called submovements, attributed to the intermittency of neural control in movement generation and sensory-motor coordination. They include observations of slow movements, eye saccades, cyclical movements, ballistic movements, movements of developing infants, movements requiring high accuracy, children and also post-stroke patients [169].

Tesi di dottorato in Ingegneria Biomedica, di Antonino Salerno,
discussa presso l'Università Campus Bio-Medico di Roma in data 20/03/2012.
La disseminazione e la riproduzione di questo documento sono consentite per scopi di didattica e ricerca,
a condizione che ne venga citata la fonte

Studies on motion kinematics in adults ([189]; [190]), children [197] and also stroke patients [196] show that continuous movements such as reaching of the upper limb can be regarded as composed of discrete units.
Furthermore, the analysis of hand pointing movements in [168] provides evidence for two kinematic invariants in the Cartesian space, which are typically used to control robots operating in conditions of human-robot interaction, i.e. the hand trajectories are approximately straight segments, and the tangential hand velocity for different movements always appears to have a bell-shaped profile. This kinematic behaviour is attributed to an optimization criterium, consisting of minimizing end-point smoothness [170].

Not-bell-shaped hand movement profiles could be actually seen as a composition of several bell-shaped velocity profiles occurring in sequence. The common assumption was that a primary, ballistic movement is produced to cover the major portion of the distance to the target. If the primary movement misses the target, secondary submovements are performed or after the end of the main movement (corrective submovements, [191]), or by overlapping the main movement (overlapping submovements – OSMs [192], [189], [193], [194], [171], [195], [185]).
Velocity profiles of the main movement and those of both corrective and overlapping submovements were considered to share a common shape, differing only in amplitude (peak velocity) and duration as shown in Fig. 31.

Tesi di dottorato in Ingegneria Biomedica, di Antonino Salerno,
discussa presso l'Università Campus Bio-Medico di Roma in data 20/03/2012.
La disseminazione e la riproduzione di questo documento sono consentite per scopi di didattica e ricerca,
a condizione che ne venga citata la fonte

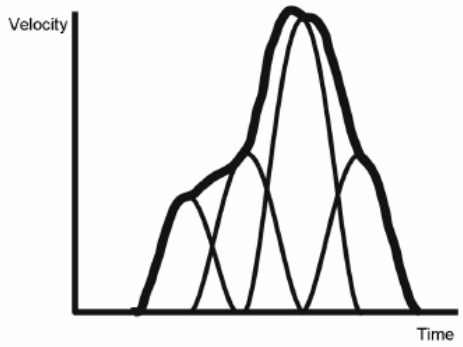

Fig. 31: Example of complex movement represented as its velocity profile on a single axis. The overall movement (thick black line) can be expressed as the sum of underlying overlapping submovements (light lines) **[165]**.

The motion units shape is debated but in different studies it was analytically selected in order to satisfy the minimum-jerk constraint [189], [194], [171] or determined empirically [193], [196].

From the above-mentioned studies, a common factor can be observed in the composition of submovements: they seem to be characterized by constant behaviors in terms of duration, frequency, and mutual overlapping [165], [171] and a properly optimized scaling of amplitude and number. Based on the experimental results in the literature, the hypothesis was formulated that the neural controller embedded in the brain works intermittently, sending short "bellshaped" velocity commands to each limb segment that are modulated in accordance with limb intrinsic inertia and muscle recruitment method. In particular, from human data reported in [171], it was observed that big and heavy limb segments with wide muscle recruitment method, such as the upper arm (from shoulder to wrist), seem to receive "long" (0.5 s) bell-shaped velocity commands, overlapped each other by 0.25 s. "Shorter" velocity commands were observed in the wrist [185] and, further, in the hand fingers motion [186].
As extensively discussed in [172], experimental data on humans (healthy and stroke patients) seem to be consistent with the hypothesis that the neural controller

Tesi di dottorato in Ingegneria Biomedica, di Antonino Salerno,
discussa presso l'Università Campus Bio-Medico di Roma in data 20/03/2012.
La disseminazione e la riproduzione di questo documento sono consentite per scopi di didattica e ricerca,
a condizione che ne venga citata la fonte

embedded in the brain works intermittently, sending short "bell-shaped" velocity commands to each limb segment, which are modulated in accordance with limb intrinsic inertia and muscle recruitment method: the number of adjustments is reflected in the number of submovements that make up the action. Submovements seem to be characterized by constant behaviors in terms of duration, frequency, and mutual overlapping and by a properly optimized scaling of amplitude and number.

Taking inspiration from the above mentioned study on humans, this work wants to investigate the feasibility of an interaction control for robots, able to modulate point-to-point motion accuracy as well as the applied force, by composing motion units and dynamically changing submovement features (in particular their number and amplitude). Several solutions can be found in the literature on the control of robot manipulators interacting with the working environment (see [173], [174], [175] for a survey). Furthermore, previous attempts of controlling robots by means of sequences of simple motion templates or else learning motor primitives can also be mentioned [176], [177][178]. In [177] the authors using the terms of motion template and motion primitive to indicate a set of simple action in which can be decomposed a complex action or activity. This approach was employed in the field of reinforcement learning. A similar approach can be found in [178] for controlling a humanoid robot. Similar ideas are exploited in [187] to convert dynamic movement primitives in motor planning and execution by means learning from demonstration.

Further studies in [188] are focussed on motion primitive employment for handwrite modelling. In particular, the authors speculate that coupling of the low level primitive model, and the higher level timing model during inference can produce good reconstructions of handwriting, with shared primitives for all characters modelled, where a segment of movement in superposition is meant for primitive.

Tesi di dottorato in Ingegneria Biomedica, di Antonino Salerno,
discussa presso l'Università Campus Bio-Medico di Roma in data 20/03/2012.
La disseminazione e la riproduzione di questo documento sono consentite per scopi di didattica e ricerca,
a condizione che ne venga citata la fonte

However, differently from them, this work relies on the definition of motion unit (i.e. submovement) introduced in neuroscience for humans and is grounded on the direct observation of human mechanisms involved in upper-limb motion generation [172] for composing them.

The control approach presented here proposes that the trajectory planner is no longer a pure generator of trajectory; it is also in charge of tuning motion accuracy or else interaction force in lieu of a specific control law. In [180] we preliminarily presented this approach by resorting to pre-determined sequences of submovements, statically generated. In view of an application to unstructured environments and, mainly, to human-robot interaction, this work proposes a technique based on non linear systems (i.e. oscillators) for dynamically generating submovement sequences in accordance with task requirements, with the main expected advantage of increasing system adaptability. The use of non-linear dynamic systems, such as oscillators, is not new in the literature. For instance, oscillators or coupled oscillators are employed to model physical phenomena, such as spatial pattern formation with reaction diffusion systems, reaction diffusion (Turing) mechanisms, cardiac electro-physiology and fireflies synchronization. For a detailed review, see [181]. In robotics, oscillators and coupled oscillators are typically used for producing the oscillatory motion of swimming and walking [179], [182]. To our knowledge, no previous examples of use of oscillators for dynamic submovement generation can be found.

3.2 Proposed approach

An important and original point of this work is to try to answer to the question "Can submovement composition achieve robot motion and interaction control through occurrence and amplitude modulation?". Assumed that this is plausible in

Tesi di dottorato in Ingegneria Biomedica, di Antonino Salerno,
discussa presso l'Università Campus Bio-Medico di Roma in data 20/03/2012.
La disseminazione e la riproduzione di questo documento sono consentite per scopi di didattica e ricerca,
a condizione che ne venga citata la fonte

humans [195], a new paradigm of robot control was developed which exploits and emphasizes the role of composition of tunable sequences of submovements in generating very accurate or else very adaptable motion behavior. This entails a completely new paradigm of motion generation and control, that is introduced in the block scheme depicted in Fig. 32.

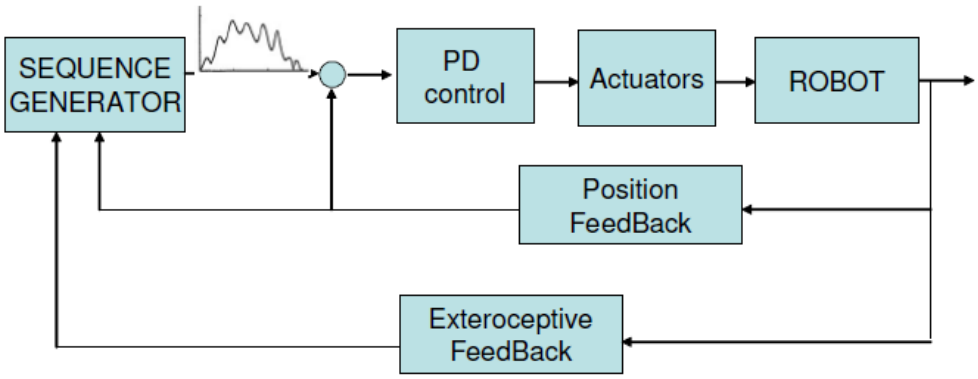

Fig. 32: Block scheme of the bio-inspired control based on submovements composition.

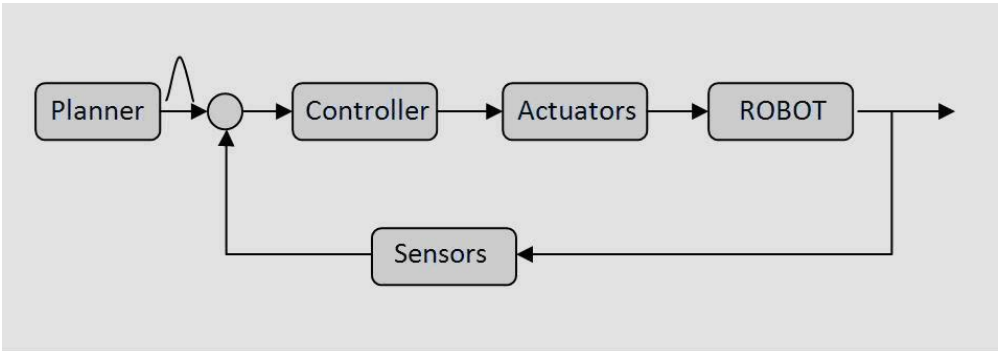

Fig. 33: Block scheme of a traditional control.

When comparing this novel approach to the traditional control scheme presented in Fig. 33 the key points that need to be underlined are the following:

- The standard trajectory planner in Fig. 33 typically aims at generating the whole trajectory of the end effector with a level of precision increasing with the level of structured environment and specificity of the task. In Fig. 1 this module is replaced by a new trajectory planner (called *sequence*

Tesi di dottorato in Ingegneria Biomedica, di Antonino Salerno,
discussa presso l'Università Campus Bio-Medico di Roma in data 20/03/2012.
La disseminazione e la riproduzione di questo documento sono consentite per scopi di didattica e ricerca,
a condizione che ne venga citata la fonte

generator) closed in the feedback loop, which online generates new sequences of submovements, opportunely scaled in amplitude and occurrence. The sensory feedback will contribute to submovements tuning in order to achieve accuracy or else compliance as required by the task context.

- The low level control can always be realized by means of standard PD (i.e. proportional-derivative) control, without focusing on the development of complex control laws for achieving compliant or else very stiff robot behavior. This solution has two important implications as it always exploits robustness and stability of traditional PD torque control in the feedback loop and, on the other hand, it requires a unique tuning of the PD control gains. Fine motion tuning will be managed by the sequence generator module.

To summarize, exploiting only proprioceptive and exteroceptive feedback the management of the motion accuracy in free space and interaction control with external environment is relied on trajectory planner by modulating on-line the generated sequence of submovements. The PD control has an stabilizing action only.

Before to continue with the dynamic submovements generator implementation an important point to clarify is to understand if it is feasible the motion generation by using submovement theory. Section 3.3 tries to address this issue by means predetermined sequence of submovements highlighting the benefits of the novel approach with respect to the traditional approach. Section 3.4 describes in detail the dynamic submovements generator able to tune on-line the sequence of motion units in order to achieve accuracy or else compliant behaviour.

Tesi di dottorato in Ingegneria Biomedica, di Antonino Salerno,
discussa presso l'Università Campus Bio-Medico di Roma in data 20/03/2012.
La disseminazione e la riproduzione di questo documento sono consentite per scopi di didattica e ricerca,
a condizione che ne venga citata la fonte

3.3 Feasibility study on predetermined sequence of submovements

3.3.1 Static submovement composition

By analogy with the human studies on unconstrained point-to-point movements [168], robot trajectory is planned with the objective of generating the smoothest motion to bring the end effector from the initial position to the final position in a given time. The resulting trajectory is named minimum-jerk trajectory; it is linear and described by the following parametric representation

$$x\big(s(t)\big) = x_i + \frac{s(t)}{\|x_f - x_i\|}\left(x_f - x_i\right) \tag{3.1}$$

where x (0) = x_i, $x\left(\|x_f - x_i\|\right) = x_f$ and s(t) is the arc length. The origin of the end-effector frame moves from x_i to x_f in a time t_f . The arc length then goes from the value s = 0 at t =0 to the value s = s_f (path length) at t = t_f.

The timing law along the path is described by the function s(t) and answers the optimization criterion of maximizing motion smoothness by minimizing jerk, i.e. the first time derivative of Cartesian acceleration. It is a fifth order polynomial function in time expressed as

$$s(t) = a_5t^5 + a_4t^4 + a_3t^3 + a_2t^2 + a_1t + a_0 \tag{3.2}$$

where t is the time instant and a_i (i = 0 . . . 5) are the polynomial coefficients to be determined by using initial and final motion conditions. The resulting Cartesian

Tesi di dottorato in Ingegneria Biomedica, di Antonino Salerno,
discussa presso l'Università Campus Bio-Medico di Roma in data 20/03/2012.
La disseminazione e la riproduzione di questo documento sono consentite per scopi di didattica e ricerca,
a condizione che ne venga citata la fonte

trajectory is a straight line between initial and final positions with a bell-shaped velocity profile given by

$$\dot{s}(t) = 5a_5 t^4 + 4a_4 t^3 + 3a_3 t^2 + 2a_2 t + a_1 \tag{3.3}$$

In the traditional control approach, end-effector trajectory is planned through a unique parametric function expressed by eqs. (3.1), (3.2) describing motion from initial point x_i up to final point x_f in a time interval t_f.

Taking inspiration from recent studies of neuroscience, the main assumption of the approach proposed in this work (Fig. 32) is that robot motion is not generated by a unique function; on the contrary, it comes out from the composition of several motion units (in the following named 'submovements'), each described by eqs. (3.1), (3.2).

Minimum-jerk submovements can be uniquely described by three parameters [165]: the amplitude of the peak A_i, the time at which the peak occurs u_i, and the duration of the movement ω_i. They allow writing the bell-shaped profile of each submovement as

$$\dot{s}_i(t, u_i, \omega_i, A_i) = \frac{A_i}{1.875}\left(30\left(\frac{t - \left(u_i - \omega_i/2 \right)}{\omega_i} \right)^2 - 60\left(\frac{t - \left(u_i - \omega_i/2 \right)}{\omega_i} \right)^3 + 30\left(\frac{t - \left(u_i - \omega_i/2 \right)}{\omega_i} \right)^4 \right) \tag{3.4}$$

for $u_i - \frac{\omega_i}{2} \le t \le u_i + \frac{\omega_i}{2}$ and 0 otherwise. The area under a minimum-jerk curve (3.4) is equal to $\omega_i A_i / 1.875$. Relation (3.4) comes out from eq. (3.2) for a given final arc length and null velocity and acceleration at the initial and final time instants. The complete point-to-point movement is generated by overlapping several submovements described by eq. (3.4) (3.4)), having different features in

Tesi di dottorato in Ingegneria Biomedica, di Antonino Salerno,
discussa presso l'Università Campus Bio-Medico di Roma in data 20/03/2012.
La disseminazione e la riproduzione di questo documento sono consentite per scopi di didattica e ricerca,
a condizione che ne venga citata la fonte

terms of amplitude A_i, peak time u_i and duration ω_i. The resulting velocity profile is given by

$$\dot{s} = \sum_{i=1}^{n} \dot{s}_i(t, u_i, \omega_i, A_i) \tag{3.5}$$

where n is the total number of submovements, empirically defined. The main role of the sequence generator module in Fig. 32 is to generate sequences of submovements by defining total number of motion units and amplitude, peak time and duration of each of them in accordance with task requirements.
It is assumed that submovements have duration ω_i and mutual overlapping ov_i constant (i.e. $\omega_i = \omega$ and $ov_i = ov$ for each i). Note also that, due to symmetry of each $\dot{s}_i$ with respect to the peak, mutual overlapping can be calculated as $ov = u_i - u_{i+1} + \omega$ for i = 1 . . . n.

Relying on the neuroscientific literature on the intermittent nature of motor outputs, as explained in Sect. 3.1, it is assumed that bell-shaped motion units are 0.5 s long (i.e. ω = 0.5 s) and overlapped each other by 0.25 s (i.e. ov = 0.25 s). The global submovement frequency f is defined as the inverse of the distance between two consecutive peaks and is equal to 4 Hz in case of ω = 0.5 and ov = 0.25 (Fig. 34). The total number of submovements N is given by $N = f \cdot t_f - 1$, being t_f the total motion duration.

Tesi di dottorato in Ingegneria Biomedica, di Antonino Salerno,
discussa presso l'Università Campus Bio-Medico di Roma in data 20/03/2012.
La disseminazione e la riproduzione di questo documento sono consentite per scopi di didattica e ricerca,
a condizione che ne venga citata la fonte

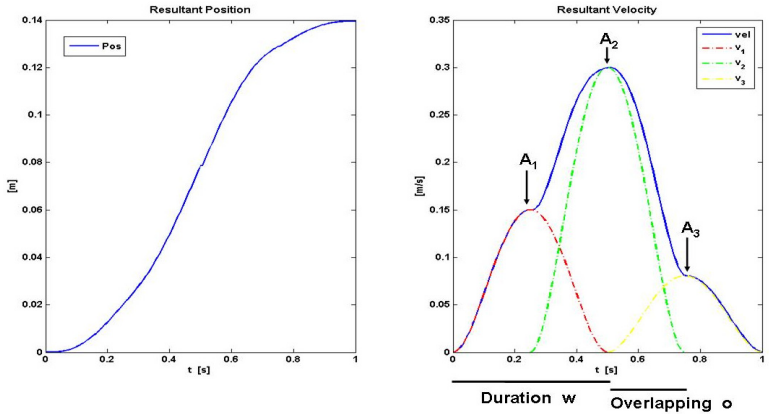

Fig. 34: Representative trajectory generated by three submovements (left); Submovement parameters (right)

The immediate consequence of these data is that the sequence generator has to modulate just two of the four parameters characterizing motion, i.e. the number of motion units n and the amplitude of each unit A_i. A general rule to vary n and A_i with the total path length s_f and duration t_f can be extracted by eq. (3.3) applied to each temporal window lasting $\omega = 0.5$ s and centered at $u_i = 0.25$ s. This yields

$$s_i\left(u_i + \frac{\omega_i}{2}, A_i\right) = \frac{8}{15} A_i \omega_i \tag{3.6}$$

and

$$s_f = \sum_{i=1}^{n} s_i\left(u_i + \frac{\omega_i}{2}, A_i\right) \tag{3.7}$$

being $s_i\left(u_i + \frac{\omega_i}{2}, A_i\right)$ the path length of each submovement. Analogously,

$$t_f = \sum_{i=1}^{n} \omega_i - \sum_{i=1}^{n} ov_i = n \cdot \omega - n \cdot ov \tag{3.8}$$

being ov_i the mutual overlapping between two contiguous submovements.

Tesi di dottorato in Ingegneria Biomedica, di Antonino Salerno,
discussa presso l'Università Campus Bio-Medico di Roma in data 20/03/2012.
La disseminazione e la riproduzione di questo documento sono consentite per scopi di didattica e ricerca,
a condizione che ne venga citata la fonte

3.3.2 PD control

The control block in Fig. 32 represents a standard torque controller in Cartesian space based on proportional and derivative actions. Consider the general form of robot dynamics, expressed as

$$B(q)\ \ddot{q} + C(q,\dot{q})\ \dot{q} + F_v \dot{q} + F_S(q,\dot{q}) + g(q) = \tau - J(q)^T h \qquad (3.9)$$

where B(q) is robot inertia matrix, q, $\dot{q}$, $\ddot{q}$ are vectors of joint position, velocity and acceleration, respectively, $C(q,\dot{q})\dot{q}$ is the vector of centrifugal and Coriolis torques, $F_V\,\dot{q}$ is the viscous friction, $F_S(q,\dot{q})$ is the static friction, g(q) is the gravitational torque vector and τ is the torque vector acting on the robot joints. In case of interactions, $J^T(q)h$ is the torque contribution due to interaction force h exerted by the environment on the robot.
The PD control in the Cartesian space is described by the following law

$$\tau = J^T(q)K_P\tilde{x} + J^T(q)K_D\dot{\tilde{x}} + g(q) \qquad (3.10)$$

where $\tilde{x} = x_d - x$ is the position error in the Cartesian space, $\dot{\tilde{x}} = \dot{x}_d - \dot{x}$ is the velocity error, x_d is the reference trajectory coming out from the trajectory planner, x is the actual end effector trajectory and g(q) is the estimate of the gravitational torques acting on the joints. Matrices K_P and K_D are the (m x m) stiffness and damping matrices, respectively, being m the dimension of the Cartesian space.
In a traditional control approach, PD control in eq. (3.10) can achieve position or else compliance regulation by opportunely tuning robot stiffness and damping matrices with respect to the environment visco-elastic properties. In fact, it can be

Tesi di dottorato in Ingegneria Biomedica, di Antonino Salerno,
discussa presso l'Università Campus Bio-Medico di Roma in data 20/03/2012.
La disseminazione e la riproduzione di questo documento sono consentite per scopi di didattica e ricerca,
a condizione che ne venga citata la fonte

demonstrated that, in the free space (h = 0) and provided a full rank Jacobian matrix, position error asymptotically converges to zero with a rate depending on K_P . On the contrary, in the interaction with the environment (h ≠ 0) control law (3.10) serves as compliance control, being at the equilibrium

$$\tilde{x} = K_P^{-1} h \tag{3.11}$$

for full rank Jacobian. The interaction with the external force h is regulated by means of the compliance matrix K_P^{-1}.

The PD control in the Cartesian space was chosen for the control system in Fig. 32 because (i) it is very simple and robust; (ii) it is applicable in the free space as well as in the interaction. Therefore, it allows demonstrating that a new control paradigm can be conceived where accurate control of motion as well as of interaction is obtained by means of opportunely varied sequences of motion units in lieu of either sophisticated position and interaction control laws, or re-tuning and smart regulation of control gains. Just one tuning of the PD control gains is required for the robot, that are kept constant during the submovement sequences. In other words, it is possible to reduce the position error, or else vary interaction force, by acting on the sequence of submovements instead of acting on PD gains such as in the traditional approach. This also guarantees that robot operating conditions are always far from motor saturation and instability, possibly caused by excessively high gains.

3.3.3 Experimental tests and results

Experimental tests were aimed at proving the feasibility to achieve motion control and interaction control by properly modulating sequences of submovements, once

Tesi di dottorato in Ingegneria Biomedica, di Antonino Salerno,
discussa presso l'Università Campus Bio-Medico di Roma in data 20/03/2012.
La disseminazione e la riproduzione di questo documento sono consentite per scopi di didattica e ricerca,
a condizione che ne venga citata la fonte

PD control gains are defined. To this purpose, block scheme in Fig. 32 was implemented on the MIT-Manus robot manipulator available in our lab [209] and presented in section 2.1.1. It is a 2 degree-of-freedom manipulator, reproducing the planar motion of shoulder and elbow rotational joints of the upper limb in a workspace of 0.40 x 0.40 m.

Two experimental sessions were carried out. The first one consisted of experimental trials of free motion in the plane and investigated the relationship between submovements properties and motion accuracy. Details are presented in Sect. 3.3.3.1. The latter consisted of experimental trials of impact against an obstacle and interaction with a purely elastic environment. It was aimed at analyzing the effect of sequences of submovements on force regulation. Details on the experimental setup and results are reported in Sect. 3.3.3.2.

3.3.3.1 Motion control results

For experimental trials of motion in the *free space*, the robot was commanded to move in eight different Cartesian directions from the initial position $P_i = [0.0\ 0.0]^T$ m, with a radius of 0.14 m. Motion duration could be set to $t_f = 1$ s, $t_f = 2$ s or else $t_f = 3$ s, with an adjustment time of 0.5 s. Further, the linear reference trajectory was planned both with the traditional approach based on the time law in eq. (3.2) and with the new approach based on the overlap of motion units expressed by eqs. (3.4) - (3.5). Control parameters for the PD control were set to $K_P = \text{diag}\{750;\ 750\}$ N/m and $K_D = \text{diag}\{50;\ 50\}$ Ns/m. Fig. 35 reports end-effector trajectory, position error in norm and velocity profile for point-to-point movements lasting 1 s and generated by the traditional trajectory planner (3.2) with a single bell for 0.14 m linear path.

Tesi di dottorato in Ingegneria Biomedica, di Antonino Salerno,
discussa presso l'Università Campus Bio-Medico di Roma in data 20/03/2012.
La disseminazione e la riproduzione di questo documento sono consentite per scopi di didattica e ricerca,
a condizione che ne venga citata la fonte

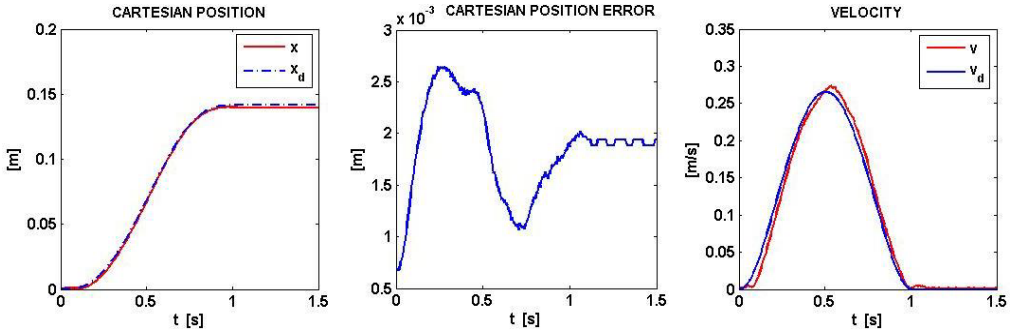

Fig. 35: End-effector trajectory, position error and velocity profile for a PD control in a traditional scheme; motion duration is 1 s and control gains are K_P = diag{750; 750} N/m and K_D = diag{50; 50} Ns/m.

In order to assess the effect of submovements properties on motion accuracy in the free space, sequences of motion units were generated for the same linear path. They differed each other for the amplitude of each submovement and the total number; submovement duration and overlap were fixed to 0.5 s and 0.25 s, as explained in the previous section. Submovement amplitude was chosen in order to guarantee that the total xy path was 0.14 m. Table I reports the mean value of Cartesian position error for different compositions of a fixed number of submovements in a sequence.

Trajectory planner	Mean err [m]	Peak err [m]
trad 1 s	0.0018	0.0026
trad 2 s	0.0017	0.0022
trad 3 s	0.0016	0.0023
$A_1 = 0.3;\ A_2 = 0.15;\ A_3 = 0.0803$	0.0018	0.0031
$A_1 = 0.0803;\ A_2 = 0.3;\ A_3 = 0.15$	0.0016	0.0028
$A_2 = 0.3;\ A_1 = A_3 = 0.1152$	0.0017	0.0027
$A_1 = A_2 = A_3 = 0.177$	0.0016	0.0023
$A_1 = A_2 = ... = A_7 = 0.0758$	0.0015	0.0018
$A_1 = A_2 = ... = A_{11} = 0.0542$	0.0014	0.0016

TABLE I: mean position and peak error for traditional control (1-2-3 s of motion duration), and different submovements configuration in free space

Tesi di dottorato in Ingegneria Biomedica, di Antonino Salerno,
discussa presso l'Università Campus Bio-Medico di Roma in data 20/03/2012.
La disseminazione e la riproduzione di questo documento sono consentite per scopi di didattica e ricerca,
a condizione che ne venga citata la fonte

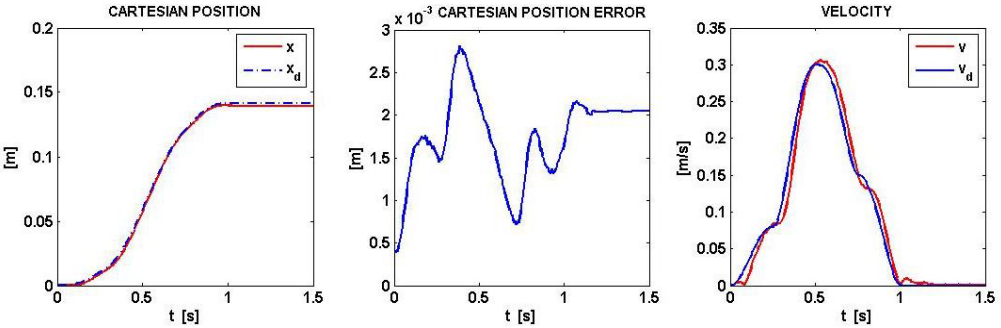

Fig. 36: End-effector trajectory, position error and velocity profile for a point-to-point motion generated by three submovements with $A_1 = 0.0803$; $A_2 = 0.3$; $A_3 = 0.15$ m/s.

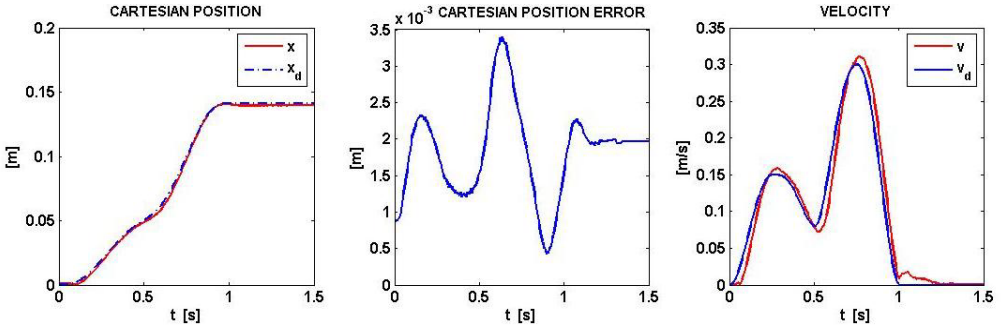

Fig. 37: End-effector trajectory, position error and velocity profile for a point-to-point motion generated by three submovements with $A_1 = 0.15$; $A_2 = 0.0803$; $A_3 = 0.3$ m/s.

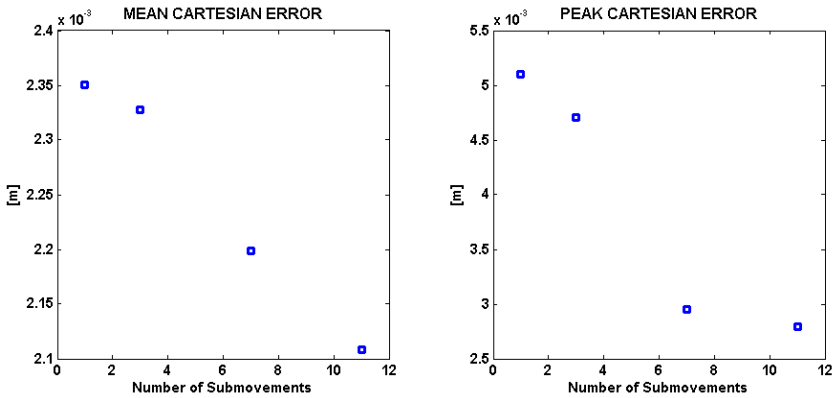

Fig. 38: End-effector mean and peak position error generated by increasing the number of submovements with KP = diag{500; 500} N/m.

Moreover, Fig. 36 and Fig. 37 depict two representative situations of error time course in the case of two different compositions of three submovements with different order in the sequence, i.e. ($A_1 = 0.0803$; $A_2 = 0.3$; $A_3 = 0.15$) m/s in Fig.

Tesi di dottorato in Ingegneria Biomedica, di Antonino Salerno,
discussa presso l'Università Campus Bio-Medico di Roma in data 20/03/2012.
La disseminazione e la riproduzione di questo documento sono consentite per scopi di didattica e ricerca,
a condizione che ne venga citata la fonte

36 and (A_1 = 0.15; A_2 = 0.0803; A_3 = 0.3) m/s in Fig. 37. The total duration of movement is t_f = 1 s. The experimental results showed that submovements order in the sequence, symmetry with respect to the central submovement and total number of submovements affect motion accuracy. It can be observed that time position of peak error and mean value of the error change with the submovements order. Time position of peak error follows time position of the highest bell. Mean value of the error is smaller when the highest bell-shaped velocity is in the middle. It corresponds to describe a global velocity profile that is smoother and slower at the beginning and at the end of the motion (Fig. 36), thus avoiding jerky movements as in Fig. 37. Fig. 38 proves that sequences of submovements can be regarded as sequences of corrective actions able to continuously adjust and refine robot movement choosing the right sequence of submovements. It shows how the mean and peak position error in the operational space change with respect to the number of motor primitives for K_P = diag{500; 500} N/m and K_D = diag{50; 50} Ns/m. It is worth noticing that the error decreases with the increase of the number of submovements; the reason is that motion becomes slower and more accurate as an indirect effect of subsequent corrective actions. The error decreases notably with the increase of submovement number up to 3 mm for 11 submovements.

3.3.3.2 Interaction control results

For experimental trials of impact against an obstacle, an experimental setup involving the impact of the robot end effector against a wall was constructed. A vertical obstacle was located in the middle of the trajectory from P_i to P_f and robot kinematic and dynamic parameters were registered through position sensors at the joints and a load cell at the end effector. Fig. 39 and Fig. 40 report time evolution of end-effector trajectory, error, velocity and impact force for two representative cases of peak force modulation.

Tesi di dottorato in Ingegneria Biomedica, di Antonino Salerno,
discussa presso l'Università Campus Bio-Medico di Roma in data 20/03/2012.
La disseminazione e la riproduzione di questo documento sono consentite per scopi di didattica e ricerca,
a condizione che ne venga citata la fonte

Control parameters for the PD control were kept constant to K_P = diag{750; 750} N/m and K_D = diag{50; 50} Ns/m, as for the motion in the free space. In Fig. 39 a peak force of ≈ 50 N is generated in the impact by a sequence of three submovements with amplitudes (A_1 = 0.3; A_2 = 0.15; A_3 = 0.0803) m/s. On the other hand, changing the order (A_1 = 0.3; A_2 = 0.0803; A_3 = 0.15) m/s, the peak force reduces to ≈ 40 N (Fig. 40); the same value of peak force is obtained whenever a high bell is followed by the shortest bell (i.e. A_2 = 0.0803), or else when the three bells have an increasing order. This entails that force peak is lower when impact occurs with minor velocity, that is during the time interval of the shortest bell. Furthermore, bells order in the sequence also affects impact time instant, as it implies a change of initial motion velocity. When the highest bell is at the beginning of the sequence (A_1 = 0.3 m/s), impact time occurs before 0.5 s; on the other hand, when the shortest bell moves at the beginning (A_1 = 0.0803 m/s) impact instant time shifts around 0.7 s. Table II summarizes impact time instants and peak force values for different cases of trajectory planning. Peak force values for the traditional control are lower because of lower acceleration profiles.

Tesi di dottorato in Ingegneria Biomedica, di Antonino Salerno,
discussa presso l'Università Campus Bio-Medico di Roma in data 20/03/2012.
La disseminazione e la riproduzione di questo documento sono consentite per scopi di didattica e ricerca,
a condizione che ne venga citata la fonte

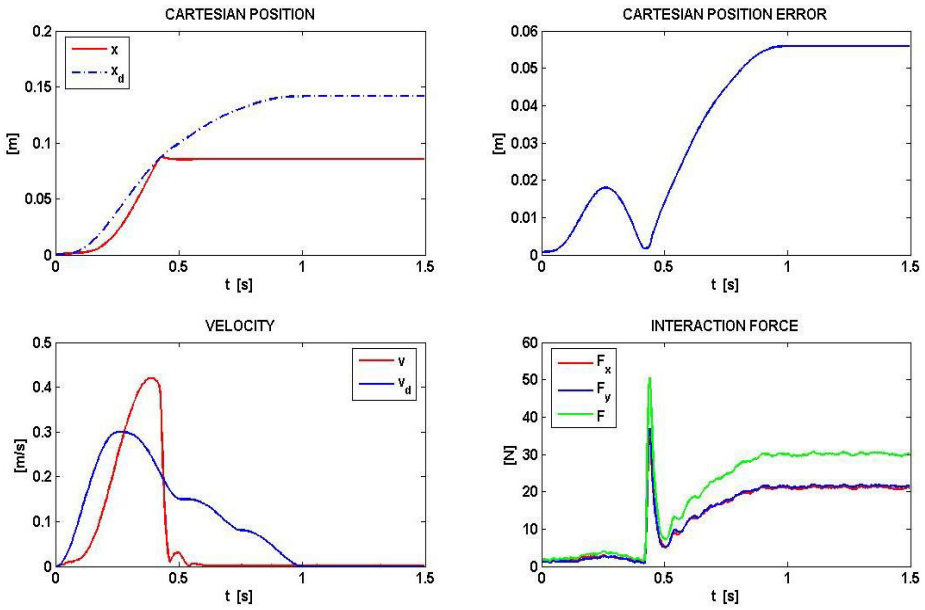

Fig. 39: End-effector trajectory, position error velocity profile and impact force for impact experiments with three submovements having $A_1 = 0.3$; $A_2 = 0.15$; $A_3 = 0.08$ m/s.

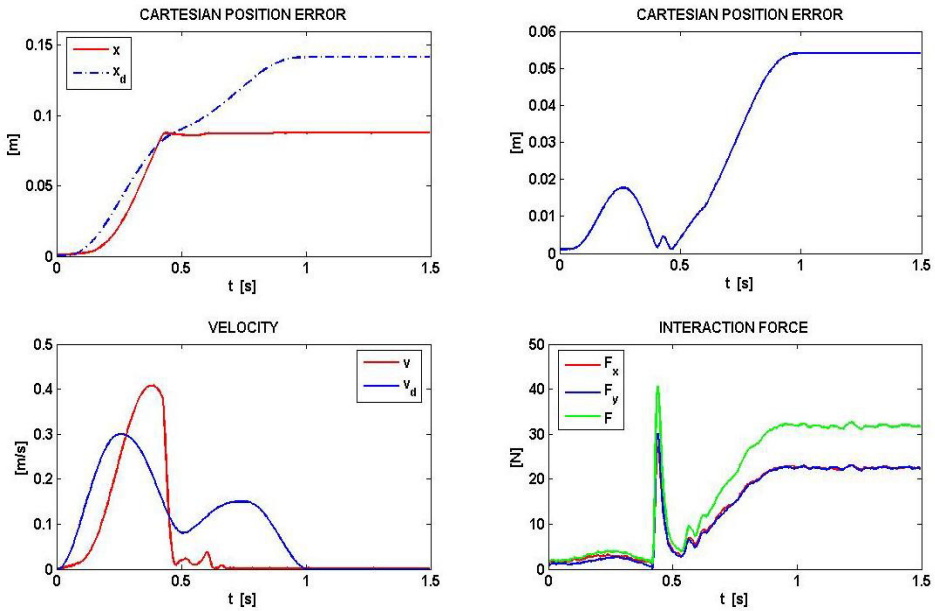

Fig. 40: End-effector trajectory, position error velocity profile and impact force for impact experiments with three submovements having $A_1 = 0.3$; $A_2 = 0.0803$; $A_3 = 0.15$ m/s.

Tesi di dottorato in Ingegneria Biomedica, di Antonino Salerno,
discussa presso l'Università Campus Bio-Medico di Roma in data 20/03/2012.
La disseminazione e la riproduzione di questo documento sono consentite per scopi di didattica e ricerca,
a condizione che ne venga citata la fonte

Trajectory Planner	Peak Force [N]	Time [s]
trad	29.9	0.58
$A_1 = 0.3;\ A_2 = 0.15;\ A_3 = 0.0803$	50.5	0.42
$A_1 = 0.3;\ A_2 = 0.0803;\ A_3 = 0.15$	40.6	0.42
$A_1 = 0.15;\ A_2 = 0.3;\ A_3 = 0.0803$	47.6	0.545
$A_1 = 0.15;\ A_2 = 0.0803;\ A_3 = 0.3$	39.6	0.76
$A_1 = 0.0803;\ A_2 = 0.15;\ A_3 = 0.3$	43.5	0.735
$A_1 = 0.0803;\ A_2 = 0.3;\ A_3 = 0.15$	53.9	0.6

Table II: Peak force values and peak force instant in impact experiments for traditional control and different submovements configuration

Finally, the effect of the number of submovements on the level of force applied in the interaction with an external environment was investigated. To this purpose, the robot was commanded to move from $P_i = [0.0 \quad 0.0]^T$ m to $P_f = [0.1 \quad 0.1]^T$ m while an elastic force (with stiffness coefficient of 10 N/m) was applied at the end effector.

The experimental trials were carried out with (i) the traditional trajectory planner in eq. (3.2) and different values of K_P matrices; (ii) with sequences of submovements as expressed in eqs. (3.4)–(3.5), by varying number n of motion units (see Tab. III). Fig. 41 and Fig. 42 draw time evolution of end-effector trajectory, error, velocity and interaction force in the case of fixed K_P gains (i.e. K_P = diag{750; 750} N/m) and two different values of number of motion units, n = 3 and n = 11. From Tab. III it can be observed that in the traditional approach force increases with proportional control gains as well as in the proposed novel approach force increases with the number n of submovements. Furthermore, for n = 11 approximately the same levels of interaction force produced by K_P = diag{950; 950} N/m can be achieved.

Tesi di dottorato in Ingegneria Biomedica, di Antonino Salerno,
discussa presso l'Università Campus Bio-Medico di Roma in data 20/03/2012.
La disseminazione e la riproduzione di questo documento sono consentite per scopi di didattica e ricerca,
a condizione che ne venga citata la fonte

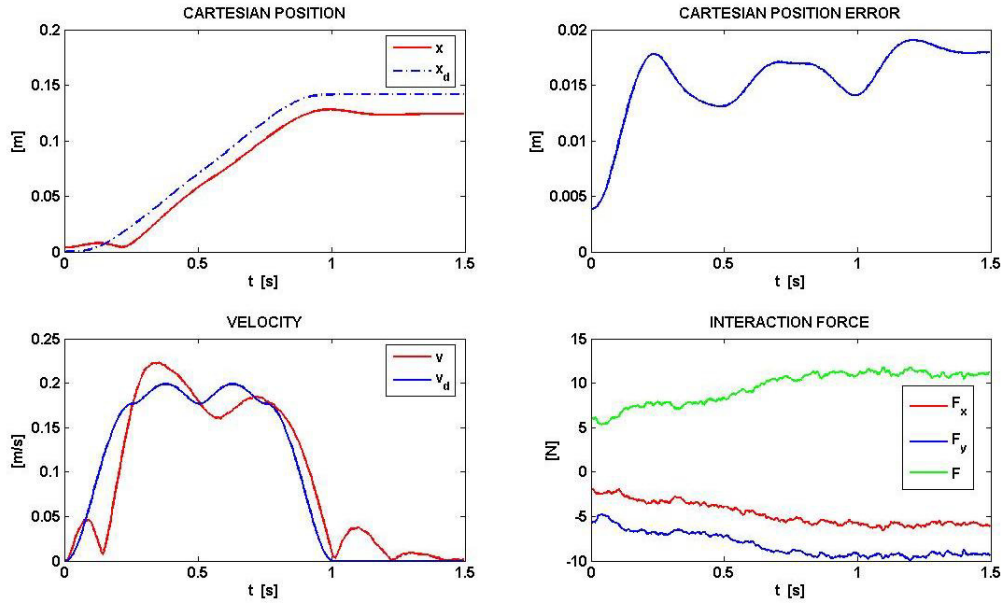

Fig. 41: End-effector trajectory, position error velocity profile and force in interaction experiments with three submovements having same amplitude $A_i = 0.177$.

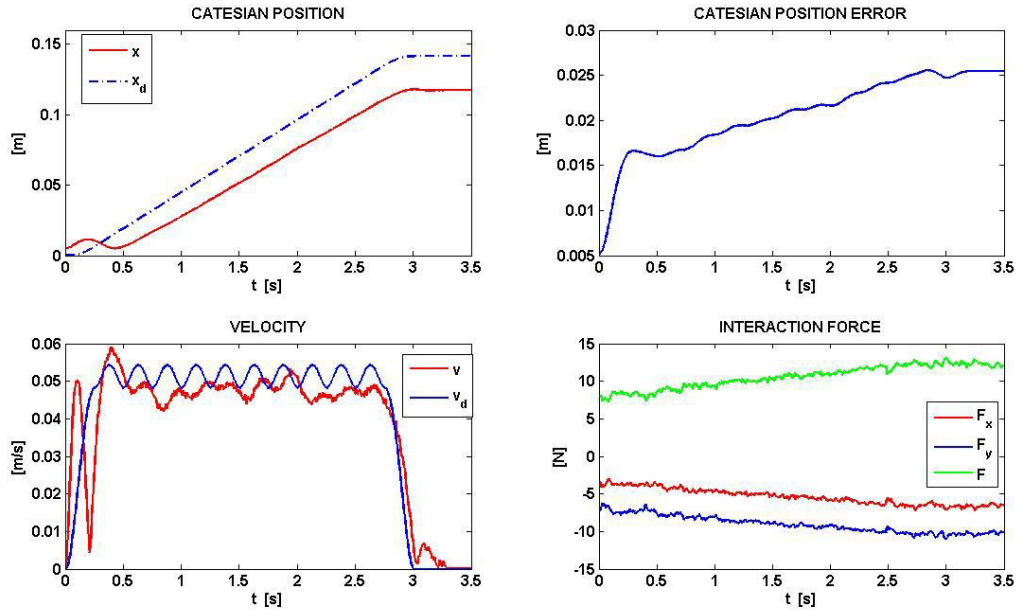

Fig. 42: End-effector trajectory, position error velocity profile and force in interaction experiments with eleven submovements having same amplitude $A_i = 0.05$.

Tesi di dottorato in Ingegneria Biomedica, di Antonino Salerno,
discussa presso l'Università Campus Bio-Medico di Roma in data 20/03/2012.
La disseminazione e la riproduzione di questo documento sono consentite per scopi di didattica e ricerca,
a condizione che ne venga citata la fonte

Trajectory planner	Mean Force [N]	Peak Force [N]
trad Kp 750 Kd 50	9.980085	12.074551
trad Kp 950 Kd 50	10.802723	13.084462
$A_1 = A_2 = A_3 = 0.177$	7.863171	9.847114
$A_1 = A_2 = ... = A_{11} = 0.054$	10.563841	13.144350

Table III: mean force and peak force values in interaction experiments for traditional control and different submovements configurations.

The experimental results of the feasibility study showed that: (i) In motion control, positioning accuracy was related to submovements amplitude and number. In particular, amplitude increase caused a degradation of position error, whereas an increase of the number of motion units determined error improvement and, correspondingly, velocity reduction. Further, a dependence on motion units order and symmetry in a single sequence was also observed, thus demonstrating that a global smoother bell-shaped velocity profile improved performance; in positioning tasks. (ii) In interaction control, experimental results showed that peak force and occurrence of peak force could be regulated by properly ordering submovements in a sequence during the impact. Furthermore, the number of motion units notably affected the average level of exerted force. An increase of the interaction force with the number of submovements was observed, comparable to the increase generated by PD control with higher stiffness gains in the traditional approach. However, safety is guaranteed by the low motion velocity. Next section is aimed at addressing to the development of an automatic sequence generator module that dynamically modifies features of submovements sequences, based on sensory feedback, and is able to perform online trajectory generation and, also, interaction control.

Tesi di dottorato in Ingegneria Biomedica, di Antonino Salerno,
discussa presso l'Università Campus Bio-Medico di Roma in data 20/03/2012.
La disseminazione e la riproduzione di questo documento sono consentite per scopi di didattica e ricerca,
a condizione che ne venga citata la fonte

3.4 Dynamic sequence generator based on oscillators

3.4.1 Theoretical formulation

The most delicate issue that a static composition cannot solve is how to determine the proper number of submovements and the value of A_i for each submovement in order to achieve a desired level of accuracy or force. To this purpose, the adoption of oscillators is proposed to dynamically generate sequences of elementary motion units. This work resorts to the same type of oscillators presented in [178]. However, differently from learning by imitation algorithms in [178], here oscillator dynamic behaviour is directly exploited to modulate submovement amplitude according to robot sensory feedback, without involving neural networks. The sequence generator based on oscillators has to be able to dynamically produce a linear point-to-point motion, with an overall bell-shaped velocity. Accordingly, the velocity profile and the arc length s are provided as output from the oscillators.

The dynamic system used to implement the oscillator (retrieved by [178]) can be expressed by the following equations

$$\begin{aligned} \tau \dot{y} &= z + f \\ \tau \dot{z} &= \alpha_z \left(\beta_z \left(y_m - y \right) - z \right) \\ \tau \dot{\phi} &= 1 \\ \tau \dot{r} &= -\mu \left(r - r_0 \right) \end{aligned} \tag{3.12}$$

where y_m is a known goal state, α_z, β_z are time constants, τ is a temporal scaling factor, y, z, ϕ, r are the state variables and f is a non-linear contribution to be defined. For f = 0 and a suitable parameter settings, these equations lead to a globally stable linear dynamical system having y_m as a unique attractor point.

Tesi di dottorato in Ingegneria Biomedica, di Antonino Salerno,
discussa presso l'Università Campus Bio-Medico di Roma in data 20/03/2012.
La disseminazione e la riproduzione di questo documento sono consentite per scopi di didattica e ricerca,
a condizione che ne venga citata la fonte

Choosing f as follows

$$f = \frac{\sum_{i=1}^{k} \psi_i \omega_i^T \bar{v}}{\sum_{i=1}^{k} \psi_i} \tag{3.13}$$

and

$$\bar{v} = [r\cos(\phi) \quad r\sin(\phi)]^T \tag{3.14}$$

yields to a coupled system because of the coupling between $\bar{v}$ and eqs. (3.12). Imposing in (3.13) $\psi = \exp\left(-h_i\left(\mathrm{mod}(\phi, 2\pi) - c_i\right)^2\right)$ with $c_i \in [0, 2\pi]$, the non-linear system described by eqs. (3.12) is able to generate a stable limit cycle. Fig. 43 (left side) shows a typical trend of the state variables, obtained integrating the non-linear system with the fourth order Runge-Kutta method when $y_m = 1$, $\alpha = 8s^{-1}$, $\beta = 2s^{-1}$, $\tau = 0.05$, $r_0 = 1.5$, $k = 3$, $h_1 = h_2 = h_3 = 0.5$, $c_1 = 0.25$, $c_2 = 0.5$, $c_3 = 0.75$, $\omega_1 = \omega_2 = \omega_3 = [0.3 \quad 0.3]^T$, $\mu = 2$, with initial conditions $\phi(t = 0) = 3.4050$, $r_0(t = 0) = 0.0995$, $z(t = 0) = 0.0211$ and $y(t = 0) = 0.9874$. On the other hand, Fig. 43 (right side) shows that, after a transient, a stable limit cycle is established.

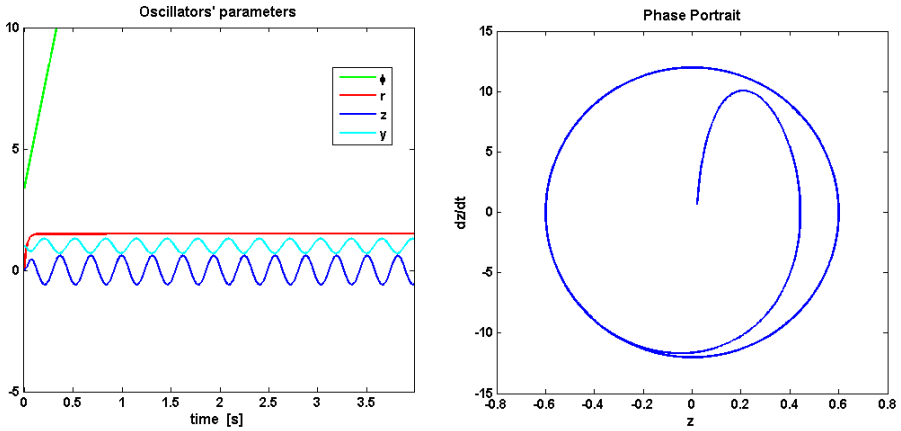

Fig. 43: Evolution of the state variables ϕ, r, z and y, on the left; Limit cycle in the projection (z, $\dot{z}$) of the phase portrait, on the right.

Tesi di dottorato in Ingegneria Biomedica, di Antonino Salerno,
discussa presso l'Università Campus Bio-Medico di Roma in data 20/03/2012.
La disseminazione e la riproduzione di questo documento sono consentite per scopi di didattica e ricerca,
a condizione che ne venga citata la fonte

It is worth noticing that ϕ has a linear time course and r(t) converges to r_0; instead, an oscillation is established for variables y and z. The system response time mainly depends on τ and r_0. Further, a change of τ implies a linear variation of the pseudo-period of y oscillation and, simultaneously, a non-linear variation of y oscillation amplitude. On the contrary, a change of τ and r_0 entails a direct modification of period and amplitude of z oscillation, respectively. Hence, in order to handle the lowest number of parameters and regulate independently amplitude and period of the oscillation, z oscillation is preferred to y oscillation. Finally, in order to address the requirement on the bell shaped velocity profile, the absolute value of state variable z of four oscillators with equal parameters and appropriately dephased is taken into account. Consequently, relationship (3.5) becomes

$$\dot{s} = \sum_{i=1}^{4} z_i \tag{3.15}$$

Integrating eq. (3.15) with a trapezoidal method, the arc length to insert in relation (3.1) describing a point-to-point parametric motion function can be obtained. In Fig. 44 an example of velocity profile and arc length planned with this novel approach based on four oscillators is drawn. The absolute value of each z hemi-oscillation is regarded as a single submovement where: overlapping with the subsequent submovement depends on the initial conditions imposed to the oscillators; oscillation frequency (i.e. the number of submovements) and submovement amplitude depend on the values of τ and r_0, respectively. In the representative Fig. 44 $\tau = 0.16$ has been chosen for each oscillator and $r_{0,1} = 0.15$, $r_{0,2} = r_{0,4} = 0.2$, $r_{0,3} = 0.25$ where $r_{0,i}$ refers to r_0 parameter of the oscillator i. The eqs. (3.12) form the core of the sequence generator shown in Fig. 32.

Tesi di dottorato in Ingegneria Biomedica, di Antonino Salerno,
discussa presso l'Università Campus Bio-Medico di Roma in data 20/03/2012.
La disseminazione e la riproduzione di questo documento sono consentite per scopi di didattica e ricerca,
a condizione che ne venga citata la fonte

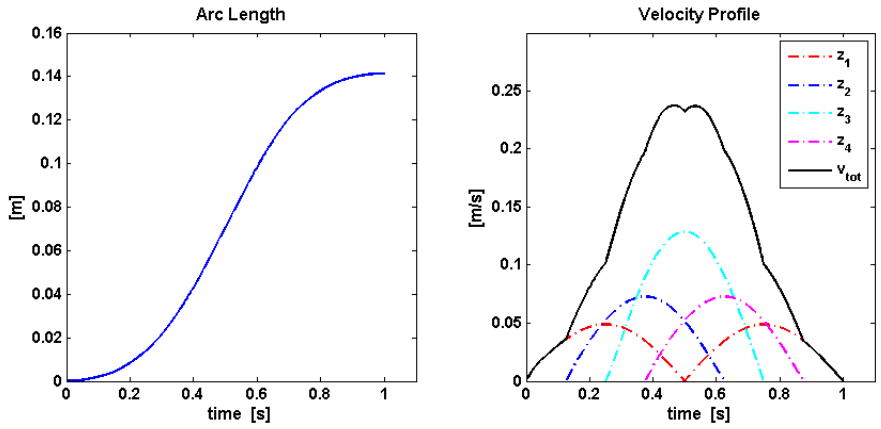

Fig. 44: Submovements generation using four oscillators. The black line represents the overall velocity profile composed of 5 submovements equals in amplitude. Each submovement has a duration of 0.5 s and overlapping of 0.375 s.

As shown in Fig. 45, in order to satisfy the task requirements (i.e. x_i, x_f, motion accuracy and desired force F_d) and sensory feedback, the pattern modulator module (explained in Sect. 3.4.3) provides the $r_{0,i}$ value to each oscillator to regulate the oscillation amplitude. Composing z-oscillation of each oscillator by means of eq. (3.15) with time dephase of 0.125 s, the velocity profile $\dot{s}$ is generated. In order to produce the desired position x_d, a numerical integration of the velocity profile is carried out at each sample time.

The dynamic generation of sequences of submovements (pattern modulator module) resorts to a relationship, experimentally retrieved, between the oscillator parameters and robot performance in free space and constrained space. It is presented in details in Sect. 3.4.3.

Tesi di dottorato in Ingegneria Biomedica, di Antonino Salerno,
discussa presso l'Università Campus Bio-Medico di Roma in data 20/03/2012.
La disseminazione e la riproduzione di questo documento sono consentite per scopi di didattica e ricerca,
a condizione che ne venga citata la fonte

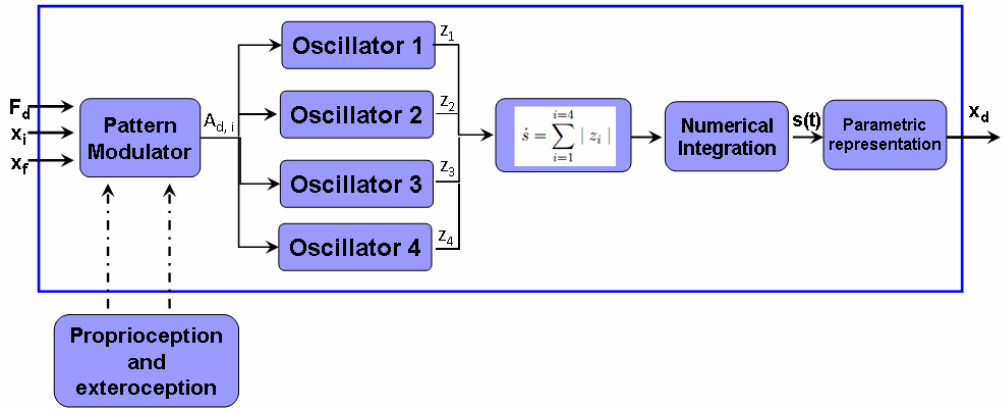

Fig. 45: Block scheme of the submovement-based trajectory planner.

3.4.2 Oscillator characterization

In this section the characterization of the oscillator dynamic features to achieve position and force regulation of a robot manipulator is proposed.

The main strength of the approach based on oscillators is its capability to keep motion continuity within the stability limits also in presence of perturbation. The perturbation of an oscillator basically generates a variation of the oscillation parameters, without compromising output continuity. For a detailed stability analysis of the proposed limit cycle see [183] and [184].

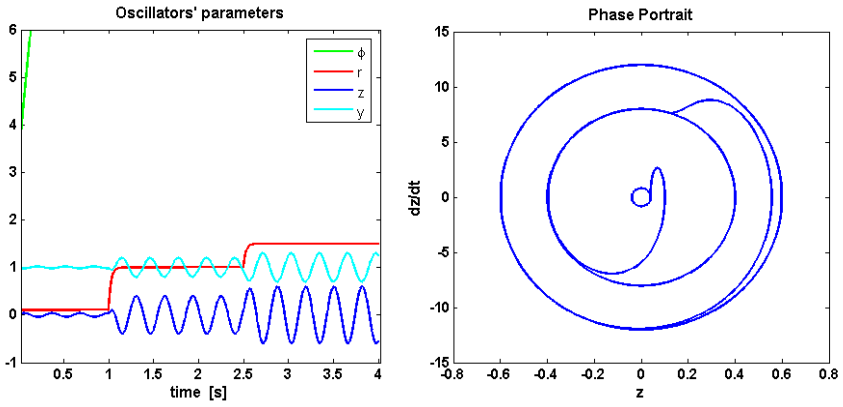

Fig. 46: Response of the oscillator to external perturbations on the left; Phase portrait of the response of the oscillator to external perturbations, on the right.

Tesi di dottorato in Ingegneria Biomedica, di Antonino Salerno,
discussa presso l'Università Campus Bio-Medico di Roma in data 20/03/2012.
La disseminazione e la riproduzione di questo documento sono consentite per scopi di didattica e ricerca,
a condizione che ne venga citata la fonte

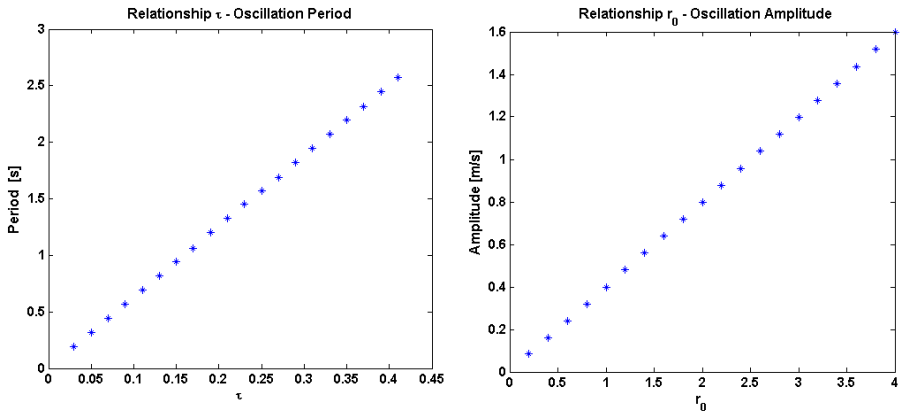

Fig. 47: On the left relationship between τ and oscillation period; on the right, relationship between r_0 and oscillation amplitude.

In Fig. 46 (left side) an example of response of variable z in eq. (3.12) is reported. When r changes, the oscillation dynamically adapts its behaviour by changing the amplitude.

Note that, as shown in phase portrait of Fig. 46 (right side) the system hops from a limit cycle to another without discontinuity. Variable z and its oscillation are studied in order to extract the oscillator parameters, given a desired submovement amplitude A and its duration of 0.5 s. Fig. 47 (left side) shows that the period of oscillation linearly increases with τ, when the other parameters are kept constant; it can be observed that an oscillation with period 1 s, corresponding to a submovement duration of 0.5 s, can be obtained for τ = 0.16. Fig. 47 (right side) reports the linear relationship between r_0 and the oscillation amplitude when oscillator parameters are kept constant and τ = 0.16.

The corresponding analytical relation is reported below

$$r_0 = 2.521\,A - 0.01934 \tag{3.16}$$

Similarly, the retrieved relationship between the oscillation period P and τ parameter is

$$P = 6.389\,\tau - 0.01845 \tag{3.17}$$

Tesi di dottorato in Ingegneria Biomedica, di Antonino Salerno,
discussa presso l'Università Campus Bio-Medico di Roma in data 20/03/2012.
La disseminazione e la riproduzione di questo documento sono consentite per scopi di didattica e ricerca,
a condizione che ne venga citata la fonte

Inverting the eq. (3.17) can be found that $\tau = 0.16$ is needed to obtain an oscillation period of 1 s and consequently submovements lasting 0.5 s.
From relationship (3.16) is clear how an oscillation of desired amplitude can be set. In the Section 3.4.3 is clarified how the amplitude A of the submovement is chosen according too task requirements (i.e. motion accuracy and force level to achieve).

3.4.3 Pattern modulator implementation

As above mentioned the pattern modulator is aimed at provide to oscillators the desired amplitude according to task requirements. The pattern modulator module is grounded on experimentally retrieved relationships between oscillation amplitude and motion accuracy (or interaction force to achieve).
This section is aimed at retrieving a dynamic relationship between submovement features and robot performance in motion and interaction control. To achieve this goal, an experimental relationship of submovement features with robot position error and applied force was investigated by means of several trials in free and constrained space.

3.4.3.1 Experimental relation between submovements and motion accuracy

Experimental tests on the MIT-Manus robotic system [209] available in our lab were carried out, in order to investigate the relationship between submovement properties and motion accuracy, with special focus on the variation of robot position error with submovement number and amplitude.

Tesi di dottorato in Ingegneria Biomedica, di Antonino Salerno,
discussa presso l'Università Campus Bio-Medico di Roma in data 20/03/2012.
La disseminazione e la riproduzione di questo documento sono consentite per scopi di didattica e ricerca,
a condizione che ne venga citata la fonte

Note that (i) position error is calculated as the difference in norm between desired and current position in the Cartesian space; (ii) the procedure reported in following was applied

to the eight main directions of the MIT-Manus planar workspace in Fig. 48; however, for brevity, it is explained only for one direction. The robot was commanded to move from the initial position $P_i = [0.0 \;\; 0.0]^T$m to the final position $P_f = [-0.1 \;\; 0.1]^T$m. Control parameters for the PD control were set to K_P = diag{500; 500} N/m and K_D = diag{20; 20} Ns/m.

Sequences of motion units with pre-defined features were generated for the same linear path. They differed each other for the amplitude of each submovement and the total number; submovement duration and overlap were fixed to 0.5 s and 0.375 s, as explained in the Sect. 3.3.1. System accuracy was evaluated for an increasing number of submovements, i.e. from one (as in a traditional planner) up to eleven. For each number of submovements five experimental trials were carried out. Mean and peak error in the Cartesian space were calculated for each group of trials. Fig. 49 reports the obtained experimental results of robot accuracy as a function of the number of submovements. Each point in the graph represents a trial in free space. It can be observed that robot accuracy improves with the number of submovements. The plateau obtained for a number of submovements greater than 5 is due to the maximum level accuracy achievable by the robot.

Tesi di dottorato in Ingegneria Biomedica, di Antonino Salerno,
discussa presso l'Università Campus Bio-Medico di Roma in data 20/03/2012.
La disseminazione e la riproduzione di questo documento sono consentite per scopi di didattica e ricerca,
a condizione che ne venga citata la fonte

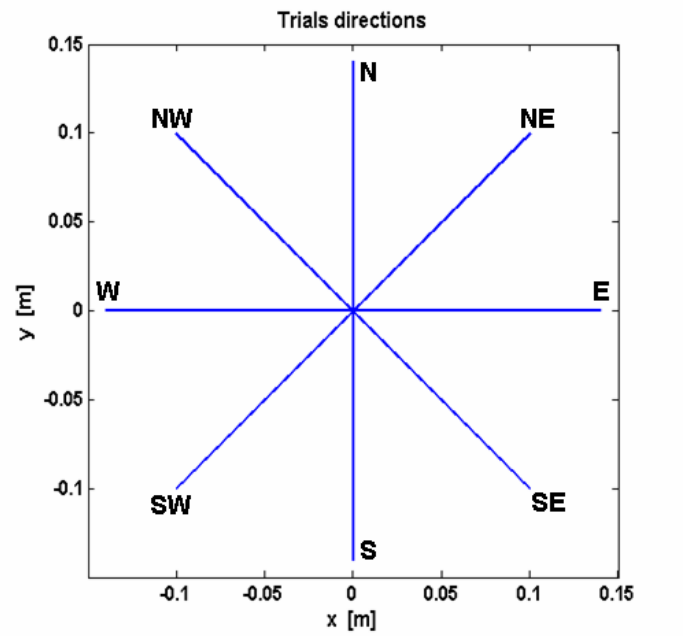

Fig. 48: Directions of the MIT-Manus workspace used for experimental trials in free space

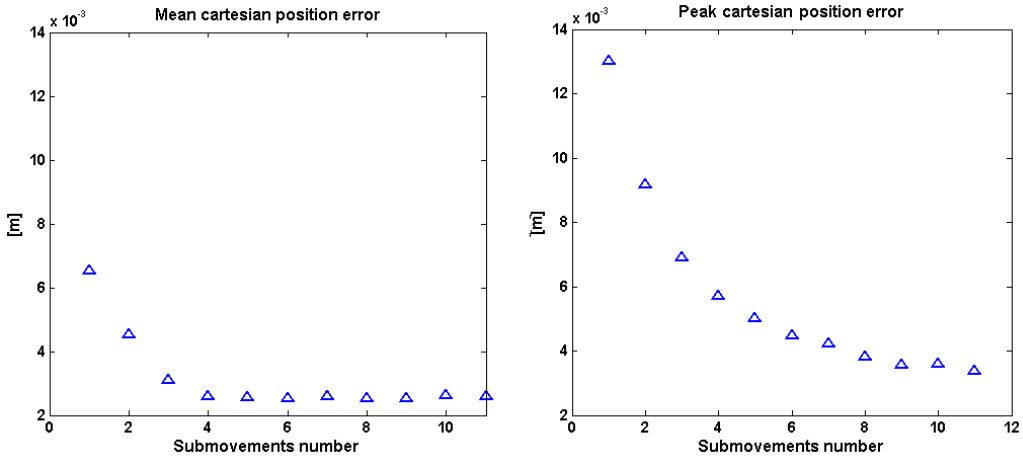

Fig. 49: Experimental data on robot accuracy vs. number of submovements.

Through MATLAB curve fitting toolbox the following relation between Cartesian position error E and number of submovements N was obtained, with 95 percent confidence bounds and Pearson coefficient $\rho^2 = 0.9905$.

$$N = 5.487 \cdot 10^{-5} E^{-2.13} + 0.6284 \qquad (3.18)$$

Tesi di dottorato in Ingegneria Biomedica, di Antonino Salerno,
discussa presso l'Università Campus Bio-Medico di Roma in data 20/03/2012.
La disseminazione e la riproduzione di questo documento sono consentite per scopi di didattica e ricerca,
a condizione che ne venga citata la fonte

where N is rounded to the greatest integer value, thus yielding an improvement of system performance. N represents the number of submovements with equal amplitude used by the static trajectory planner in order to perform the experimental sessions. Moreover, from the experimental session, the relation between number N and amplitude of submovements A resulted to be

$$A = \frac{0.5303}{N} \tag{3.19}$$

Therefore, from relations (3.18) and (3.19), it is possible to reconstruct the desired amplitude of oscillation A, once the current cartesian position error E is obtained by the feedback loop shown in Fig. 32.

3.4.3.2 Experimental relation between submovements and applied force

As for the accuracy, the relationship between submovement features and force applied on the external environment was experimentally retrieved. To this purpose, experimental trials of impact against an obstacle were carried out with the MIT-Manus robotic system. A vertical obstacle was located in the middle of the trajectory from $P_i = [0.0 \;\; 0.0]^T$ to $P_f = [-0.1 \;\; 0.1]^T$m and robot positions and forces were registered through position sensors mounted at joints and a force/torque sensor mounted at the end effector.
Control parameters for the PD control were kept constant to K_P = diag{500; 500} N/m and K_D = diag{20; 20} Ns/m, as for the motion in the free space. The technique employed to plan the trajectory was exactly the same used in section 3.4.3.1, i.e. a static sequence of submovements, each lasting 0.5 s and overlapped of 0.375 s.

Tesi di dottorato in Ingegneria Biomedica, di Antonino Salerno,
discussa presso l'Università Campus Bio-Medico di Roma in data 20/03/2012.
La disseminazione e la riproduzione di questo documento sono consentite per scopi di didattica e ricerca,
a condizione che ne venga citata la fonte

Fig. 50 shows the experimental relation between the peak force F applied in the impact and the number of submovements N. As expected, the peak force values decrease with the number of submovements, because the end-effector velocity at the impact instant decreases when the number of submovements increases.

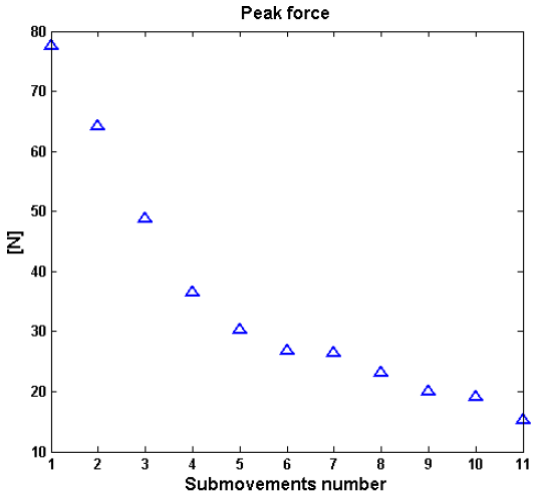

Fig. 50: Experimental data on peak force value vs. number of submovements.

Fitting the experimental data yields

$$N = 5.053\exp\left(-\left(\frac{F-13.91}{11.6}\right)^2\right) + 9.762\exp\left(-\left(\frac{F+42.72}{82.97}\right)^2\right) \qquad (3.20)$$

with 95 percent confidence bounds and Pearson coefficient $\rho^2 = 0.9933$.

Thus, substituting eq. (3.20) in eq. (3.19) leads to a relationship between desired force and amplitude of the oscillation. Once defined a force level to achieve, eqs. (3.20) and (3.19) provide the inputs to (3.16) in order to set the amplitude of oscillation in the oscillator, as explained in subsection 3.4.2.

Tesi di dottorato in Ingegneria Biomedica, di Antonino Salerno,
discussa presso l'Università Campus Bio-Medico di Roma in data 20/03/2012.
La disseminazione e la riproduzione di questo documento sono consentite per scopi di didattica e ricerca,
a condizione che ne venga citata la fonte

3.5 Validation in simulated environment

In order to prove the validity of the proposed approach, a preliminary validation in a simulated environment was carried out. It was aimed at demonstrating the feasibility of achieving robot motion control or else force regulation by means of sequences of submovements dynamically generated by four oscillators, once oscillator parameters are defined.

To this purpose, the block scheme in Fig. 32 was implemented in Matlab/Simulink and the fourth order Runge-Kutta method was chosen as solver. As mentioned above, the modelled robotic system was the MIT-Manus controlled by a PD control with gains K_P = diag{500; 500} N/m and K_D = diag{20; 20} Ns/m. The MIT-Manus was modelled adopting the Lagrangian formulation. The dynamic sequence generator was implemented through four oscillators. It produced submovements with duration 0.500 s and overlapping 0.375 s, corresponding to $\tau = 0.16$ for a total number of 5 submovements. The number of planned submovements is a constrained parameter. In fact it depends on τ, the overlapping and the duration imposed for the overall movement (i.e. 1 s for the simulated trials).

As regards control performance in the free space, simulation tests of point-to-point movements were carried out along a radius of 0.14 m from initial position $P_i = [0.0 \;\; 0.0]^T$ m in 1.0s, in eight different Cartesian directions rotated of 45 each other, shown in Fig. 48.

A comparative analysis with a traditional minimum-jerk planner, based on a polynomial velocity function, was carried out on the same movements, with the same control gains (i.e. Fig. 51 and Fig. 52).

Tesi di dottorato in Ingegneria Biomedica, di Antonino Salerno,
discussa presso l'Università Campus Bio-Medico di Roma in data 20/03/2012.
La disseminazione e la riproduzione di questo documento sono consentite per scopi di didattica e ricerca,
a condizione che ne venga citata la fonte

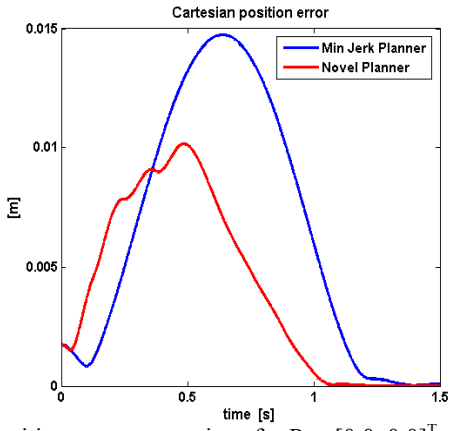

Fig. 51: Cartesian position error comparison for $P_i = [0.0 \;\; 0.0]^T$ and $P_f = [-0.1 \;\; 0.0]^T$m

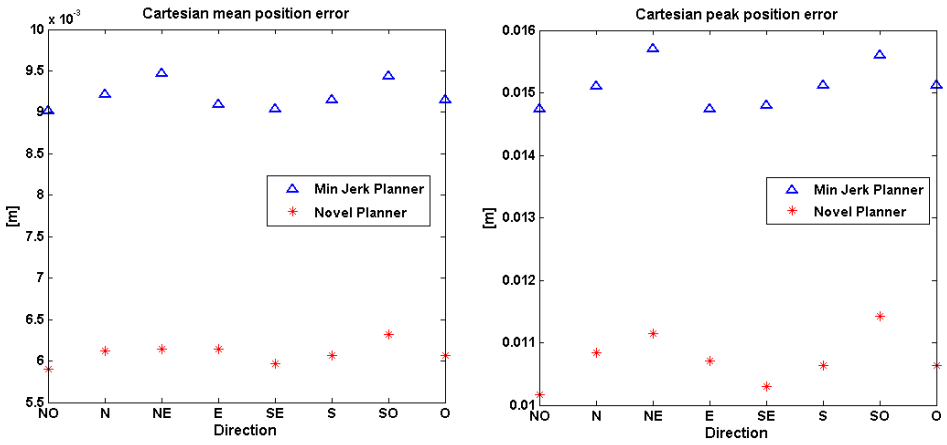

Fig. 52: Mean and peak position error comparison in eight directions.

Note that at the end of the trial the error provided by submovements based control converges to zero faster than traditional control approach with the set control gain K_P and K_D (see Fig. 51). Fig. 51 shows the Cartesian position error obtained with the two planners in one direction, whereas Fig. 52 reports mean and peak position error in all the eight directions. The proposed approach based on the oscillators determined a position error meanly lower of 3 - 4 mm with respect to the traditional control approach. Fig. 53 shows the on-line modulation of submovement features for a representative reaching task from initial position $P_i = [0.0 \;\; 0.0]^T$ m and final position $P_f = [-0.1 \;\; 0.1]^T$ m in 1.0 s. It is worth noticing that the missing smoothness of the velocity profile in Fig. 53 is due to corrective

Tesi di dottorato in Ingegneria Biomedica, di Antonino Salerno,
discussa presso l'Università Campus Bio-Medico di Roma in data 20/03/2012.
La disseminazione e la riproduzione di questo documento sono consentite per scopi di didattica e ricerca,
a condizione che ne venga citata la fonte

actions taken by sequence generator in order to achieve the task requirements in free space in terms of acuracy. A similar behaviour is shown in the studies on humans [165], [195] and [257].

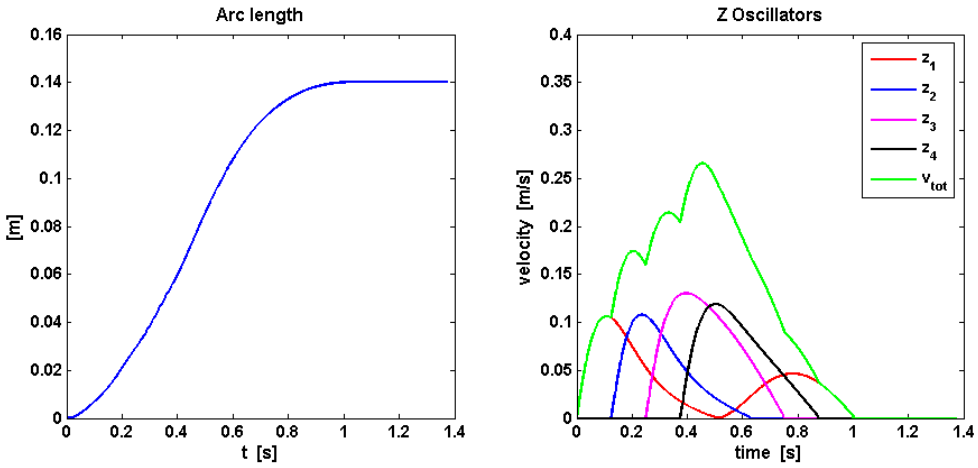

Fig. 53: Planned arch length and velocity profile provided by amplitude modulation of the submovements in free space.

Gain K_P [N/m]	Mean err [m]	Peak err [m]
500	0.009018	0.014740
550	0.008489	0.013843
600	0.008018	0.013047
650	0.007596	0.012335
700	0.007216	0.011696
750	0.006872	0.011119

Table IV: Mean position error and peak error in case of traditional control for 1 s of motion duration and increasing KP values.

It is also worth noticing that the accuracy improvement shown by the submovement-based approach is comparable to the improvement obtained in a traditional PD control, by increasing K_P gains from 500 N/m to 750 N/m (see table IV).

On the other hand, as regards control validation in the constrained space, robot interaction with an elastic environment with stiffness K = 1000 N/m was

Tesi di dottorato in Ingegneria Biomedica, di Antonino Salerno,
discussa presso l'Università Campus Bio-Medico di Roma in data 20/03/2012.
La disseminazione e la riproduzione di questo documento sono consentite per scopi di didattica e ricerca,
a condizione che ne venga citata la fonte

simulated. The produced elastic force F_e is $F_e = K(x - x_e)$, being $x_e = [0.05\ 0.05]^T$m.

The simulated interaction trials were aimed at validating the relationship force-r_0 found in Sect. 3.4.3.2. A point-to-point motion was planned from $P_i = [0.0\ \ 0.0]^T$ to $P_f = [0.1\ \ 0.1]^T$m in 1 s. In the first part of the movement (i.e. up to x_e) the same r_0 value was set for the 4 oscillators; at the beginning of the interaction with the elastic environment r_0 value was modified by using the eqs. (3.16), (3.19), (3.20) according to force feedback, in order to achieve a desired force $F_d = 20$ N. When the measured force level F_e is $F_d - 5 \leq F_e \leq F_d + 5$, with the threshold chosen as 25 per cent of the desired force value, the r_0 value was set to zero, thus producing a smooth decay of velocity.

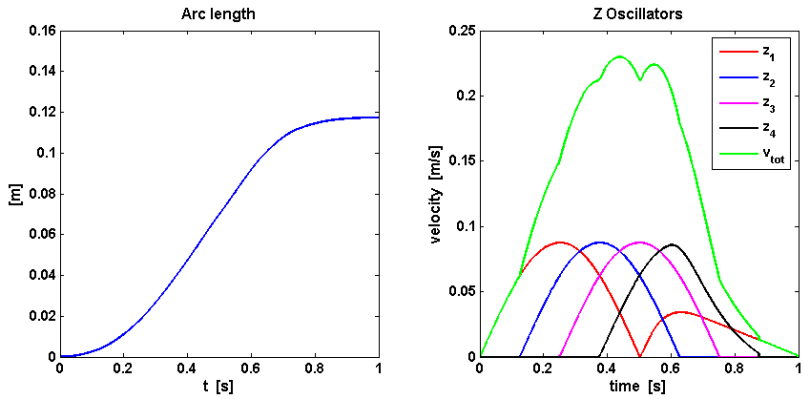

Fig. 54: Planned arc length and velocity profile dynamically generated to achieve desired force F_d.

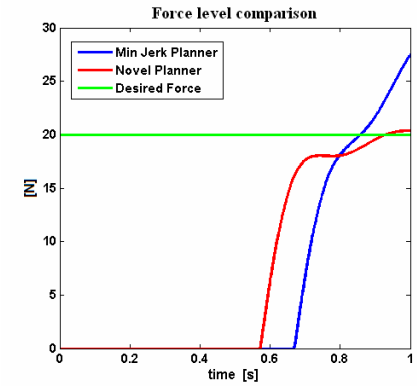

Fig. 55: Force level comparison between traditional minimum-jerk and submovement-based approach with control gains K_P = diag{500; 500} N/m and K_D = diag{20; 20} Ns/m.

Tesi di dottorato in Ingegneria Biomedica, di Antonino Salerno,
discussa presso l'Università Campus Bio-Medico di Roma in data 20/03/2012.
La disseminazione e la riproduzione di questo documento sono consentite per scopi di didattica e ricerca,
a condizione che ne venga citata la fonte

Fig. 54 and Fig. 55 report, respectively, the arc length, velocity profile dynamically generated with the submovement-based planner and the force levels obtained with a traditional minimum-jerk planner and the dynamic submovement generator.

As regards the planned arc length in Fig. 54 can be noticed that the force regulation is converted in a position regulation. In other words the non linear systems, that implement the four oscillators, plan an arc length approximatively of 0.12 m, instead of 0.14 m in order to achieve the desired force level. Observe in Fig. 55 that the dynamic submovement generator converges to desired force F_d whereas the minimum-jerk control approach reach the force level coming out from the equilibrium between environment and robot stiffness. Furthermore, table V points out that, by keeping K_P gain equal to 500 N/m , submovement modulation allows achieving the same level of force obtained in a traditional PD control with K_P = 350 N/m.

Gain K_P [N/m]	Force [N]
500	27.480859
450	26.194747
400	24.820003
350	20.222521
300	18.613506
250	17.254733

Table V: Force values for a traditional PD control for decreasing K_P gains

In order to evaluate the adaptability to achieve different force requirements, several interaction trials were carried out with different desired forces F_d to accomplish. In the same operating conditions above described in terms of trial direction, control gains and external environment to interact, the case of F_d equal to 25 N is highlighted in Fig. 56 by comparing the performance of traditional and submovement-based approaches.

Tesi di dottorato in Ingegneria Biomedica, di Antonino Salerno,
discussa presso l'Università Campus Bio-Medico di Roma in data 20/03/2012.
La disseminazione e la riproduzione di questo documento sono consentite per scopi di didattica e ricerca,
a condizione che ne venga citata la fonte

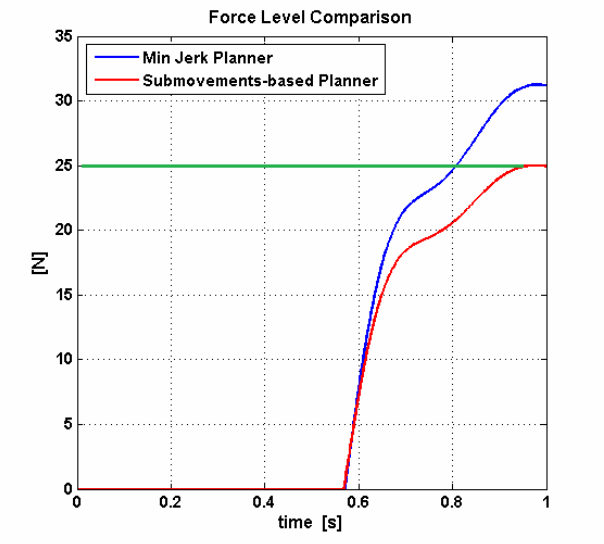

Fig. 56: Force level comparison between traditional minimum-jerk and submovement-based approach with control gains K_P = diag{500; 500} N/m and K_D = diag{20; 20} Ns/m. The desired force is set to 25 N.

It's worth noticing that the force convergence to the desired value is guaranteed by employing the submovement-based trajectory planner. On the other hand, the traditional approach is not able to on-line regulate the force applied on external environment. Additionally, taking into account Fig. 55 and Fig. 56, an adaptation to different desired force at robot end-effector can be noticed in the submovement-based planner performance. Therefore in view of applications to unstructured environment, the submovement-based planner shows a more adaptive behaviour than traditional approach.

3.6 Experimental validation

The proposed control approach was also validated by means of experimental trials in the free space with the MIT-Manus robot arm. A PD control with gains K_P = diag{500; 500} N/m and K_D = diag{20; 20} Ns/m was used as control law for the

Tesi di dottorato in Ingegneria Biomedica, di Antonino Salerno,
discussa presso l'Università Campus Bio-Medico di Roma in data 20/03/2012.
La disseminazione e la riproduzione di questo documento sono consentite per scopi di didattica e ricerca,
a condizione che ne venga citata la fonte

robot. In the real systems, the dynamic sequence generator was implemented through four oscillators.

The fourth order Runge-Kutta method was chosen as solver for the numerical integration of the non linear systems on the real robot at each sample time. The dynamic sequence generator was implemented in C programming language. The sequence generator produced submovements with 0.500 s of duration and 0.375 s of overlapping, $\tau = 0.16$ and a total number of submovements equal to 5 for a trial lasting 1 s.

The experimental tests consisted of point-to-point movements carried out in 1.0 s along a radius of 0.14 m, starting from the initial position $P_i = [0.0 \;\; 0:0]^T$ m. The point-to-point movements were repeated five times in eight different Cartesian directions rotated of 45 each other as proposed in the previous section. Fig. 59 shows the on-line modulation of submovement features for a representative reaching task from initial position $P_i = [0.0 \;\; 0.0]^T$ m to final position $P_f = [0.1 \;\; 0.1]^T$ m in 1.0 s. A comparative analysis with a traditional minimum-jerk planner, based on a polynomial velocity function, was carried out on the same movements, with the same control gains.

Fig. 57 shows the Cartesian position error obtained with the two planners in one direction (i.e. $P_i = [0.0 \;\; 0.0]^T$ m and $P_f = [0.1 \;\; 0.1]^T$ m), whereas Fig. 58 reports mean and peak position error in all the eight directions. Note that the error provided by submovement-based control converges to zero faster than traditional control with the set control gain K_P and K_D (Fig. 57). Moreover, the control based on the oscillators determined a position error meanly lower of 4 mm with respect to the traditional approach and more isotropic robot behavior in the entire workspace. It is also worth noticing that the accuracy improvement shown by the submovement-based approach is comparable to the improvement obtained in a traditional PD control, by increasing K_P gains from 500 N/m to 700 N/m (see table VI) in the same direction, labelled as NE direction in Fig. 58. It is worth noticing that the missing smoothness of the velocity profile in Fig. 59 is due to

Tesi di dottorato in Ingegneria Biomedica, di Antonino Salerno,
discussa presso l'Università Campus Bio-Medico di Roma in data 20/03/2012.
La disseminazione e la riproduzione di questo documento sono consentite per scopi di didattica e ricerca,
a condizione che ne venga citata la fonte

corrective actions taken by sequence generator in order to achieve the task requirements in free space in terms of acuracy. A similar behaviour is shown in the studies on humans [165], [195] and [257].

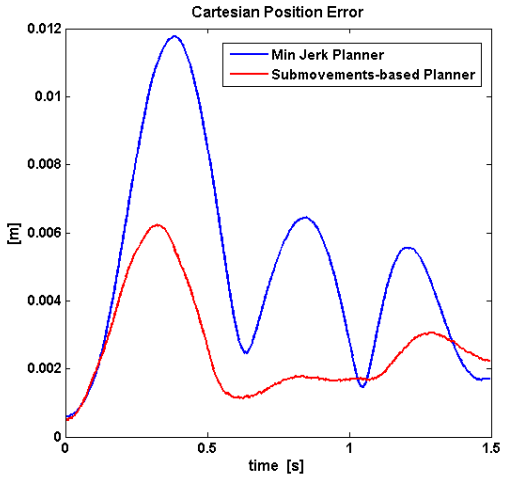

Fig. 57: Cartesian position error for a point-to-point motion from $P_i = [0.0 \;\; 0.0]^T$ to $P_f = [0.1 \;\; 0.1]^T$m in 1 s. A comparison with a traditional minimum-jerk planner is shown.

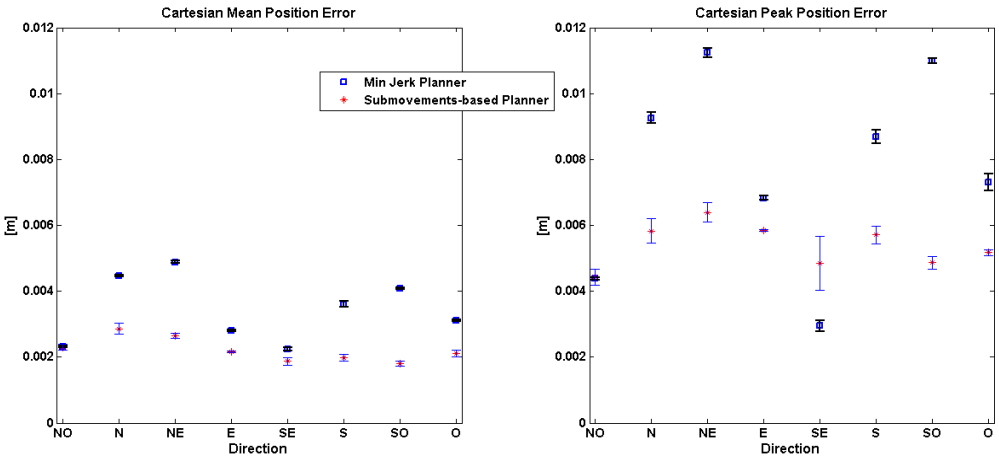

Fig. 58: Mean and peak cartesian position error comparison between traditional and submovement-based planner in eight directions.

Tesi di dottorato in Ingegneria Biomedica, di Antonino Salerno,
discussa presso l'Università Campus Bio-Medico di Roma in data 20/03/2012.
La disseminazione e la riproduzione di questo documento sono consentite per scopi di didattica e ricerca,
a condizione che ne venga citata la fonte

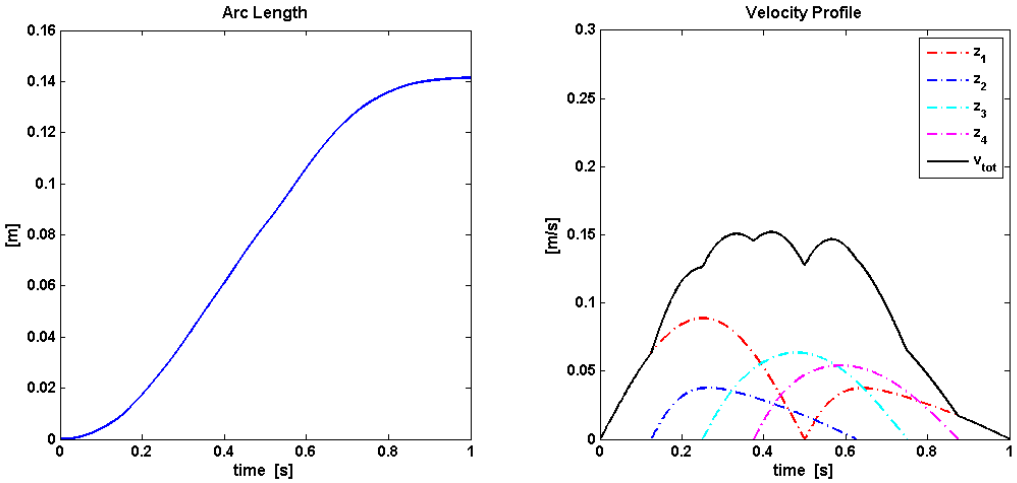

Fig. 59: Planned arch length and velocity profile provided by amplitude modulation of the submovements generated for trial in free space from $P_i = [0.0 \;\; 0.0]^T$ to $P_f = [0.1 \;\; 0.1]^T$m.

Gain K_P [N/m]	Mean err [m]	Peak err [m]
500	0.005187	0.011840
600	0.004018	0.009047
700	0.003216	0.007196
900	0.002872	0.004019

Table VI: Mean position error and peak error in case of traditional control for 1 s of motion duration and increasing KP values with $P_i = [0.0 \;\; 0.0]^T$ and $P_f = [0.1 \;\; 0.1]^T$m

3.7 Analysis of the submovement-based control performance

This section is aimed at discussing pros and cons of the submovement-based control with respect to the traditional approach with reference to the simulated and experimental results presented in sections 3.3, 3.5 and 3.6.

The novel control approach was firstly presented as sequence of submovements generated with predetermined features. The experimental results demonstrated that motion accuracy and force level could be regulated by keeping the control gains constant. The regulation action achieved by means of different sequences of submovements is comparable to that obtained by changing the control gains in the traditional PD approach. Indeed, in motion control, positioning accuracy depends

Tesi di dottorato in Ingegneria Biomedica, di Antonino Salerno,
discussa presso l'Università Campus Bio-Medico di Roma in data 20/03/2012.
La disseminazione e la riproduzione di questo documento sono consentite per scopi di didattica e ricerca,
a condizione che ne venga citata la fonte

on submovements amplitude and number. In particular, motion accuracy can be improved with an increase of the number of motion units. In the interaction, experimental results showed that the force level could be regulated by properly ordering submovements in a sequence. In fact, the variation of the interaction force is related to the number of submovements, comparable to the increase generated by PD control with higher stiffness gains in the traditional approach.

The previously mentioned considerations show the method potentiality, but the regulation action in terms of motion accuracy and applied force are obtained by means of offline submovement modulation. The real strength of the submovement-based control approach is obtained with the dynamic sequence generator implementation, in charge of on-line generating sequences of elementary motion units. Indeed, relying on four oscillators opportunely dephased and modulated in amplitude, the trajectory planner may on-line generate motion units changing features in accordance with task requirements.

Therefore the main advantage of the submovement-based control approach with respect to the traditional control is the possibility to on-line modulate the robot behaviour (i.e. motion accuracy and applied force) during the motor task execution. This result cannot be achieved by adopting the traditional PD control approach.

In order to meet the task requirements, the modulation of the desired motion was based on analytical functions experimentally identified on a 2-dof robot arm.

The results of the sequence generator validation presented in sect. 3.5 and 3.6 showed that in the free space the use of the dynamic sequence generator achieves position regulation with different accuracy as traditionally done with offline gains change in a tradition PD control. In addition, as well as accuracy improvement with respect to a traditional PD control with the same gains, the robot presents a more isotropic behaviour in all workspace directions even if the MIT-Manus mechanical structure is anisotropic. In the interaction control, the submovement-based approach was able to achieve a force regulation action in real-time

Tesi di dottorato in Ingegneria Biomedica, di Antonino Salerno,
discussa presso l'Università Campus Bio-Medico di Roma in data 20/03/2012.
La disseminazione e la riproduzione di questo documento sono consentite per scopi di didattica e ricerca,
a condizione che ne venga citata la fonte

comparable to the effect of offline control gain change in a traditional PD control. Additionally, the adaptability of the submovement-based control approach to different force level to on-line achieve has been shown in Sect. 3.5. These results cannot be achieved by employing a standard PD controller during the reaching task execution, but an offline tuning of the control gains is needed.

On the other hand, the main drawback of the motion generation by exploiting the composition of motion units is the initial workspace characterization in free and interaction motion conditions carried out in order to retrieve the analytical relationships of the pattern modulator. However this laborious work has to be carried out once and is strongly dependent on the mechanical structure of the employed robot.

Additionally, the robot behaviour during task different from the point-to-point motion has not been evaluated. For instance, a possible choice of task in motion control is the planning of a circular trajectory. As previously shown in section 3.6, a more isotropic robot behaviour is expected in case of submovements-based control with respect to traditional approach during the tracking of the circular trajectory. Indeed, considered the trials carried out on MIT-Manus system in free space, the dynamic sequence generator has shown comparable performance in all workspace directions, on the other hand the traditional PD control approach is dependent on the motion direction. Therefore, involving the circular path all workspace directions, it is legitimate to expect a uniform performance during the task execution with submovement-based control approach. As regards tasks execution different from point-to-point motion in interaction conditions, a dependence on task is expected. Take for example tasks as impact against an obstacle and continuous interaction with an elastic environment. In the first case the force level is dependent on the end effector velocity at impact time instant and this parameter can be easily handled by the sequence generator. The latter case is managed as explained in section 3.5. Basically the robot performance in

Tesi di dottorato in Ingegneria Biomedica, di Antonino Salerno,
discussa presso l'Università Campus Bio-Medico di Roma in data 20/03/2012.
La disseminazione e la riproduzione di questo documento sono consentite per scopi di didattica e ricerca,
a condizione che ne venga citata la fonte

interaction conditions by employing the submovement-based control approach is task-dependent. This entails that a further characterization could be needed.

Tesi di dottorato in Ingegneria Biomedica, di Antonino Salerno,
discussa presso l'Università Campus Bio-Medico di Roma in data 20/03/2012.
La disseminazione e la riproduzione di questo documento sono consentite per scopi di didattica e ricerca,
a condizione che ne venga citata la fonte

Chapter 4

Current-based impedance control

This chapter presents an interaction control approach for a rehabilitation machine with unnegligible friction and low performance in impedance regulation. A current-based impedance control is developed in order to compensate for friction by means of inverse dynamics, and to enhance control performance in the interaction with the patient by means of force feedback, without growing system inertia as proposed in section 2.3. To this purpose, servo-amplifier motor currents are monitored to provide force feedback in the interaction, thus avoiding the need of force sensors mounted at the robot end effector. The control law has been applied to the CBM-Motus upper-limb rehabilitation machine by modelling robot kinematics and dynamics, whereas static and dynamic friction properties are

Tesi di dottorato in Ingegneria Biomedica, di Antonino Salerno,
discussa presso l'Università Campus Bio-Medico di Roma in data 20/03/2012.
La disseminazione e la riproduzione di questo documento sono consentite per scopi di didattica e ricerca,
a condizione che ne venga citata la fonte

experimentally estimated. The current-based impedance control performance in free space and in interaction with external environment have been compared with impedance control without force feedback.

4.1 Introduction and objective

The design of a robotic machine for robot-aided neuro-rehabilitation develops in a highly collaborative research scenario where roboticists, neuroscientists and medical doctors contribute to define system specifications. The main reason is that the human subject (i.e. the patient exposed to the rehabilitation therapy) plays a key-role in the design in view of the tight and continuous physical human-robot coupling [198], [19], [199]. The robot helps the subject to carry out part of the task that she/he is not able anymore to perform autonomously, with a level of assistance that can be adapted to her/his residual abilities [121], [200]. Requirements such as accuracy, repeatability, pre-programmed movements and task specificity (typical of industrial or service robots [201], [202]) yield to priorities imposed by the close physical contact with the user, such as safety, reliability, robustness, adaptability, and back-driveability (i.e. low mechanical impedance). All these features depend on the robot mechanical and control design [203], [204], [205] and can be addressed by means of a mechatronic approach, where the optimal combination of mechanics and control is searched in order to answer requirements coming from the specific application context.

As seen in section 2.1, several examples of robotic machines for rehabilitation can be found in the literature. The machines presented in section 2.1 can be also classified in two main groups, according to design approaches followed.

The first one consists of adapting or re-configuring industrial robots for use in rehabilitation [48], [62], [49]. This approach has the consequent critical drawback that low impedance comparable to the human arm cannot practically be obtained,

Tesi di dottorato in Ingegneria Biomedica, di Antonino Salerno,
discussa presso l'Università Campus Bio-Medico di Roma in data 20/03/2012.
La disseminazione e la riproduzione di questo documento sono consentite per scopi di didattica e ricerca,
a condizione che ne venga citata la fonte

being machines intrinsically position-controlled. Despite the use of active force feedback to enhance robot responsiveness, back-driveability required to move smoothly and rapidly in compliance with patients' actions [206] is not achieved. High inertia, anisotropy of dynamic properties and low acceleration capabilities are often the main responsible for that [207], [208].

The second approach consists of designing robots specifically conceived for tight human-machine interaction and includes two main classes of systems [62]:

- Class I machines. They resort to mechanical solutions able to intrinsically enhance system backdriveability, with the main purpose of making user perceive a very low mass, as for haptic interfaces [210], [76]. They have low mechanical inertia and friction, fine tuning of viscoelastic properties, and high cost [212], [213], [209], [74].
- Class II machines. They have a simple mechanical structure, no back-driveability, unnegligible inertia, possible presence of friction and a low cost. Although presenting some limitations, Class II machines are very interesting for their applicability to remote rehabilitation (i.e. telerehabilitation)[211], justified by the low-cost and the simplicity of functioning mode.

For both Class I and Class II systems, control design typically resorts to traditional approaches, e.g. stiff PID voltage control (i.e. a proportional-integral-derivative action), compliance control and impedance control [160], [161]. By analogy with [201], [214], in this thesis the term compliance control is referred to interaction control based on a proportional-derivative action plus gravity compensation; on the other hand, impedance control refers to inverse dynamics interaction control. The three above mentioned types of control can ensure robustness and ease of implementation, especially in the case of PID and compliance control (which do not require estimating robot dynamics).

Although rehabilitation robotic machines are a paradigmatic example of mechatronic system, quite surprisingly, highly nonlinear phenomena able to

Tesi di dottorato in Ingegneria Biomedica, di Antonino Salerno,
discussa presso l'Università Campus Bio-Medico di Roma in data 20/03/2012.
La disseminazione e la riproduzione di questo documento sono consentite per scopi di didattica e ricerca,
a condizione che ne venga citata la fonte

strongly degrade robot performance, such as friction, are typically not accounted for in their design.

Friction models proposed in the literature [222], [223] point out the complexity of the physical phenomenon and the variability of its features with temperature and different lubrication conditions. From here the difficulty in managing it and the tendency to neglect it. Main studies on friction compensation are in the fields of industrial and service robotics. Friction is experimentally identified and compensated by the control [224], [225], [226], and its variability in the robot workspace is faced with adaptive control laws [227], [228], [229]. The issue, however, still remain neglected in rehabilitation robotics.

In this work, the case of rehabilitation robots with high friction and reduced capability of visco-elastic regulation is considered, and an interaction control able to cope with these two issues is proposed. **Key points** of the control system (named `current-based impedance control') are:

- Compensating for *friction* and tuning robot compliance by means of an interaction control law based on inverse dynamics compensation;
- Closing the control loop on measured electric currents, in lieu of traditionally used force sensors, in addition to position feedback. Current monitoring plays a fundamental role in fine tuning of robot impedance during interaction by providing an indirect force feedback in the control loop.

Previous examples of robot control based on current monitoring or force sensorless approaches can be found in the literature. They resort to artificial neural networks [215] and neuro-fuzzy approaches [216], [217] for current characterization in structured environment, or else to observers for force/torque estimation [218], [219], and are typically applied to the industrial context, such as for indirect cutting force measurement [215], [216]. Only recently, an extension to force control of a mechanical finger for prosthetics has been published [220]. The use of servo-amplifier motor currents in the control loop in lieu of a force sensor

Tesi di dottorato in Ingegneria Biomedica, di Antonino Salerno,
discussa presso l'Università Campus Bio-Medico di Roma in data 20/03/2012.
La disseminazione e la riproduzione di questo documento sono consentite per scopi di didattica e ricerca,
a condizione che ne venga citata la fonte

is unusual in rehabilitation robotics. Here, it is proposed because of the twofold benefit of avoiding an increase of mechanical inertia and wiring problems caused by a force sensor mounted at the robot end effector, and improving control performance with respect to traditional control based on sole position feedback. A servo-amplifier motor current characterization based on a linear regression analysis is proposed in this chapter and an application to impedance control is carried out.

The CBM-Motus robotic machine has been used for validating the proposed approach [63]. It has been conceived for applications of tele-rehabilitation [221], thus aiming to be highly dependable, low cost and portable. The resulting machine is light, compact and robust to be moved to and mounted at the patient's site with no or small need for specialized skills. However, friction is unnegligible and makes difficult visco-elastic regulation in the interaction with the patient. This work originates from the study of this specific machine; however, the approach is conceived in order to be generalized to non-redundant rehabilitation robotic machines with electric actuation and to redundant robot with some precaution.

CBM-Motus mechanical design, kinematics and dynamics are described in Sect. 4.2. Section 4.3 concentrates on the experimental identification of robot static and dynamic friction; a parameter identification procedure based on a least-squares technique is used to estimate dynamic friction. Section 4.4 provides the theoretical formulation of current-based impedance control, while Sect. 4.5 reports data coming from the experimental validation. Finally, a comparison between control with and without friction compensation as well as with a traditional impedance control based on sole position feedback is also carried out in Sect. 4.5.

4.2 CBM-Motus robotic machine

Tesi di dottorato in Ingegneria Biomedica, di Antonino Salerno,
discussa presso l'Università Campus Bio-Medico di Roma in data 20/03/2012.
La disseminazione e la riproduzione di questo documento sono consentite per scopi di didattica e ricerca,
a condizione che ne venga citata la fonte

4.2.1 Mechanical Design

The CBM-Motus is a planar robot for the neuro-rehabilitation of the upper limb with a workspace of 0.5 x 0.5 m. It has a Cartesian kinematic structure consisting of two modules, each corresponding to an actuated axis. As shown in Fig. 60(a) each module includes six pulleys with the same radius (R = 0.025 m) and two timing belts (9.4 mm wide, reinforced with a glass fiber cord). Two couples of pulleys (on the left in Fig. 60(a)) are mounted on the same shaft, while one pulley per module is directly driven by the motor with no reduction gearing interposed. Two belts for each module are mounted in such a way that the points along the segments AB and CD move vertically with the same speed.

A grinded stainless steel bar is fixed to a couple of such points, e.g. P and P' in Fig. 60(a). The second module is connected to the robot frame with a rotation of 90° with respect to the first module. The end-effector of the robot, i.e. the handle grasped by the patient, is connected to both bars, at their minimum distance points, through a couple of orthogonal prismatic joints, rigidly linked together to make a single compound joint, in the following referred to as double prismatic joint. Friction at each prismatic joint (still remaining unnegligible because of the sliding motion) is reduced by means of linear ball bushings.

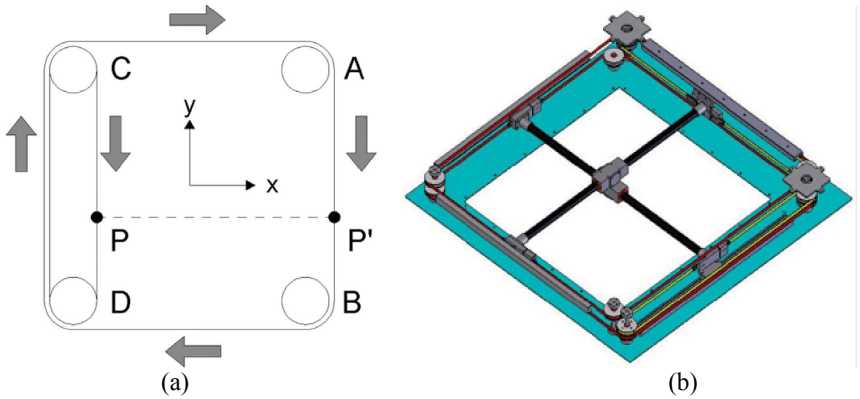

(a) (b)

Fig. 60: (a) Schematic of a single kinematic module comprising 6 pulleys and 2 belts. P and P0 move vertically with the same speed; (b) Overview of the two assembled kinematic modules. The rigid bars slide in a double prismatic joint and are connected to the driving belts.

Tesi di dottorato in Ingegneria Biomedica, di Antonino Salerno,
discussa presso l'Università Campus Bio-Medico di Roma in data 20/03/2012.
La disseminazione e la riproduzione di questo documento sono consentite per scopi di didattica e ricerca,
a condizione che ne venga citata la fonte

Both ends of each bar are connected to driving belts, as shown in Fig. 60(b). The outer prismatic joints (P_1, . . ., P_4) correspond to the segments of the belts to which the two bars (1 and 2) are connected (see Fig. 61(a)). The two bars slide through the compound prismatic joint (A+B), to which the end-effector (E) is connected. This patented kinematic architecture [64] has the main feature of ensuring a good rigidity of the robot with relatively small moving masses, because the double prismatic joint assures that only tensile forces are transmitted to the belts. In order to balance vertical loads and axial forces caused by friction at prismatic joints, both ends of the bars are supported by a ball-bearing supported wheel running in a rail.

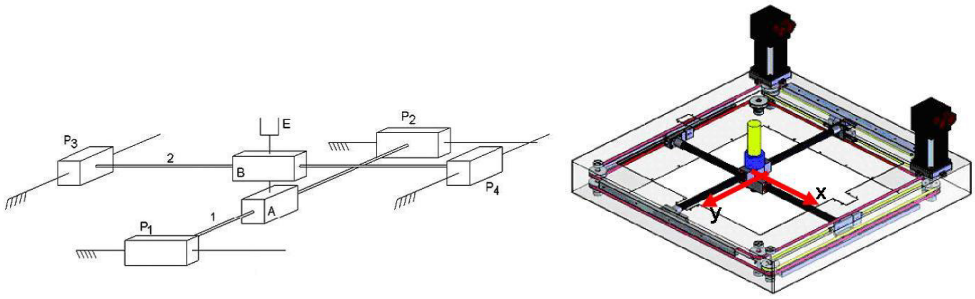

(a) (b)

Fig. 61: (a) CBM-Motus kinematic scheme; (b) rendering of the complete system with the reference frame.

The two modules are directly driven by DC servomotors (Aerotech BM 250) with rated torque of 2 Nm and peak torque of 5 Nm. Being R = 0.025 m the radius of the pulleys, the rated force which the robot is able to exert is 80 N for each axis, with a peak force of 200 N. For safety purpose, the maximum exercisable force was limited via software to 50 N. The overall dimensions of the robot frame are 0.83 x 0.82 x 0.11 m^3. The total mass (frame and motors included) is less than 30 kg. The overview of the system is shown in Fig. 62.

Tesi di dottorato in Ingegneria Biomedica, di Antonino Salerno,
discussa presso l'Università Campus Bio-Medico di Roma in data 20/03/2012.
La disseminazione e la riproduzione di questo documento sono consentite per scopi di didattica e ricerca,
a condizione che ne venga citata la fonte

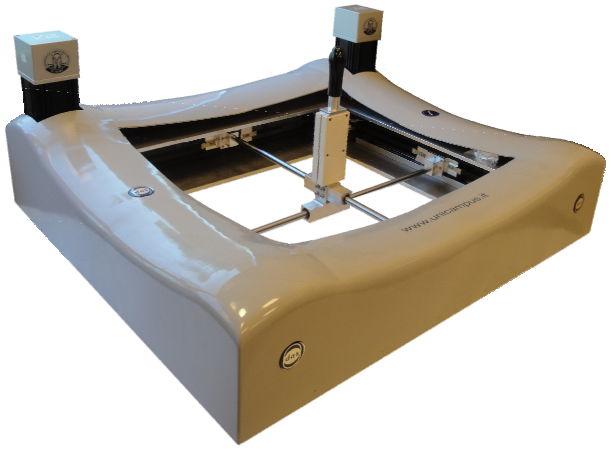

Fig. 62: Overview of the real robot.

4.2.2 Robot kinematics and dynamics

The CBM-Motus robot can be regarded as a Cartesian manipulator with two linear joints d_1 and d_2. Robot kinematics (Fig. 61 (a) and (b)) is very simple. The end-effector Cartesian position and the Jacobian matrix can be expressed as:

$$\begin{bmatrix} x \\ y \end{bmatrix} = \begin{bmatrix} d_1 \\ d_2 \end{bmatrix} \qquad J = \begin{bmatrix} 1 & 0 \\ 0 & 1 \end{bmatrix} \tag{4.1}$$

The Lagrangian formulation can be used to derive the robot dynamic model. Thus, consider the following Lagrangian equations

$$\frac{d}{dt}\frac{\partial L}{\partial \dot{q}_i} - \frac{\partial L}{\partial q_i} = \xi_i \qquad i = 1,2. \tag{4.2}$$

where L = T - U is the difference between system kinetic energy T and potential energy U, $q_i = d_i$, and ξ_i is the generalized force vector associated to q_i. Note that,

Tesi di dottorato in Ingegneria Biomedica, di Antonino Salerno,
discussa presso l'Università Campus Bio-Medico di Roma in data 20/03/2012.
La disseminazione e la riproduzione di questo documento sono consentite per scopi di didattica e ricerca,
a condizione che ne venga citata la fonte

due to the planar structure of the robot, gravitational energy is structurally compensated. Hence, L includes only kinetic energy T that is expressed as

$$T = \frac{1}{2} m_{l1} \dot{d}_1^2 + \frac{1}{2} m_{l2} \dot{d}_2^2 + \frac{1}{2} I_{m1} \frac{\dot{d}_1^2}{R^2} + \frac{1}{2} I_{m2} \frac{\dot{d}_2^2}{R^2} \tag{4.3}$$

In eq. (4.3) m_{l1} and m_{l2} (with $m_{l1} = m_{l2} = 2.026$ kg) indicate the translating masses, including bars, belts and handle; $\omega_{m1} = d_1/R$ and $\omega_{m2} = d_2/R$ are the motor angular velocities; $I_{m1} = I_m + 6\ I_p$ and $I_{m2} = I_{m1}$ are the moments of inertia due to the two motors ($I_m = 7.8 \times 10^5$ kg m^2) and the six pulleys ($I_p = 4.12 \times 10^5$ kg m^2). CAD values and motor data sheet values were used for calculating the inertial terms in (4.3).

By resolving eqs. (4.2) the following robot dynamic model is obtained

$$B(q)\ddot{q} + C(q,\dot{q})\dot{q} = \xi, \tag{4.4}$$

being $\xi = \tau - F_V \dot{q} - F_S(q,\dot{q})$. In particular, τ is the joint torque vector, $F_V\ \dot{q}$ is the viscous friction, $F_S(q,\dot{q})$ is the static friction,

$$B = \begin{bmatrix} m_{l1} + \frac{I_{m1}}{R^2} & 0 \\ 0 & m_{l2} + \frac{I_{m2}}{R^2} \end{bmatrix} \tag{4.5}$$

is the inertia matrix (independent from robot configuration), $C(q,\dot{q})\dot{q} = [0 \quad 0]^T$ is the vector of centrifugal and Coriolis torques. The obtained robot dynamic model thus demonstrates the homogeneity of robot dynamics, being the inertia matrix constant with the configuration.

Tesi di dottorato in Ingegneria Biomedica, di Antonino Salerno,
discussa presso l'Università Campus Bio-Medico di Roma in data 20/03/2012.
La disseminazione e la riproduzione di questo documento sono consentite per scopi di didattica e ricerca,
a condizione che ne venga citata la fonte

4.3 Friction identification

In [63] the model of the robot was developed and evaluated in simulation, thus neglecting friction. Here, the values of static friction forces were experimentally obtained. A set of experimental trials in the robot workspace were carried out in order to define the minimum value of electric currents needed to move the end effector. For each trial, the value of static friction force for each axis was extracted by means of the following relation

$$F_{Si} = \frac{K_t I_i}{R} \qquad i = 1,2 \tag{4.6}$$

where K_t = 0.19 Nm A^{-1} is the motor torque-current constant, taken from the data sheet, R is the pulley radius and I is the current of the actuated motor. Using Student's t-distribution, the confidence interval of friction measurement can be expressed as

$$\overline{F}_{Si} \pm \frac{t_{\alpha,N-1}\sigma_i}{\sqrt{N}} \tag{4.7}$$

where $\overline{F}_{Si}$ is the true mean of the static friction force, σ is the standard deviation and $t_{\alpha,N-1}$ is t-value for N = 10 trials and statistical significance α = 0.05. For the two linear joints, the following values were obtained

$$F_{S1} = (2.02 \pm 0.24)N \qquad F_{S2} = (2.43 \pm 0.32)N \tag{4.8}$$

On the other hand, as regards viscous friction, a parameter identification procedure based on a least-squares technique was applied [214]. Note that all the other robot dynamic parameters were known, being extracted from the CAD model, and were used in the identification procedure to identify viscous friction

Tesi di dottorato in Ingegneria Biomedica, di Antonino Salerno,
discussa presso l'Università Campus Bio-Medico di Roma in data 20/03/2012.
La disseminazione e la riproduzione di questo documento sono consentite per scopi di didattica e ricerca,
a condizione che ne venga citata la fonte

coefficients F_{vi} of diagonal matrix F_v in eq. (4.4). To this purpose, the linearity property of robot

dynamic model with respects to dynamic parameters was used, as described in the following

$$\bar{\tau} = Y(q,\dot{q},\ddot{q})\pi \tag{4.9}$$

where $\boldsymbol{\pi}$ is the unknown parameters (p x 1) vector, $\bar{\tau}$ is the n x 1 vector of measured joint torques and $Y(q,\dot{q},\ddot{q})$ is the (n x p) regression matrix, considering that n indicates robot degrees of freedom (i.e. dof) and p the number of unknown dynamic parameters.

For the CBM-Motus, vector $\bar{\tau}$, matrix Y and vector $\boldsymbol{\pi}$ can be written as follows

$$\begin{aligned} &\bar{\tau} = \tau - \mathrm{B}(\mathrm{q})\ddot{q} - F_S(q,\dot{q}) \\ &Y = \begin{bmatrix} q_1 & 0 \\ 0 & q_2 \end{bmatrix}; \qquad \pi = \begin{bmatrix} F_{V1} \\ F_{V2} \end{bmatrix} \end{aligned} \tag{4.10}$$

Remembering that n is the number of robot dof and p the number of unknown dynamic parameters, and assuming that M represents the number of trials and N the number of time instants for each trial, eq. (4.9) becomes

$$\tilde{\tau} = \begin{bmatrix} \tau_{11} \\ \vdots \\ \tau_{N1} \\ \vdots \\ \tau_{1M} \\ \vdots \\ \tau_{NM} \end{bmatrix} = \begin{bmatrix} Y_{11} \\ \vdots \\ Y_{N1} \\ \vdots \\ Y_{1M} \\ \vdots \\ Y_{NM} \end{bmatrix} \pi = \bar{Y}\pi, \tag{4.11}$$

being $\bar{Y}$ a (nNM x p) matrix, and the convergence of the method is guaranteed for nN >> p [214]. In order to identify viscous friction coefficients, twenty trials were carried out in the workspace, each lasting 1 s with sample time of 10 ms.

Tesi di dottorato in Ingegneria Biomedica, di Antonino Salerno,
discussa presso l'Università Campus Bio-Medico di Roma in data 20/03/2012.
La disseminazione e la riproduzione di questo documento sono consentite per scopi di didattica e ricerca,
a condizione che ne venga citata la fonte

The unknown vector π of viscous friction coefficients was obtained by inverting eq. (4.11) by means of left pseudo-inverse matrix of $\overline{Y}$, as follows

$$\pi = \left(\overline{Y}^T \overline{Y}\right)^{-1} \overline{Y}^T \overline{\tau}\,, \tag{4.12}$$

thus yielding the following values (expressed in Ns/m)

$$\pi = \begin{bmatrix} F_{V1} \\ F_{V2} \end{bmatrix} = \begin{bmatrix} 3.42 \\ 4.59 \end{bmatrix} \tag{4.13}$$

As expected, dry friction was unnegligible being the value of static friction around 4 - 5% of the maximum force value that the robot can generate (50 N); it requires 0.25 A along x and 0.30 A along y to be won, that is about 60% of average current values in normal operating conditions during a point to point motion in free space lasted 2 s (current mean value is 0.42 A along x and 0.47 A along y). On the other hand, viscous friction reaches 2.1% and 2.7% of the maximum force value along x and y axis, respectively, in normal operating conditions of 0.3 m/s in unconstrained motion.

The procedure was automatized in order to account for the dependence of the friction parameters on environmental conditions. Thus, friction parameters are evaluated every time the machine is turned on.

However friction parameters might depend on the force applied to the end effector and, more in general, on the robot configuration. In order to address this issue by avoiding calculating friction values for each configuration, the identification procedure was carried out in the worst region of the robot workspace, i.e. where friction is the highest, and the obtained values were used in the control scheme for friction compensation. However the terms retrieved by friction identification procedure are mean values in the considered robot workspace, an experimental relationship between force applied to the end effector and friction parameters has

Tesi di dottorato in Ingegneria Biomedica, di Antonino Salerno,
discussa presso l'Università Campus Bio-Medico di Roma in data 20/03/2012.
La disseminazione e la riproduzione di questo documento sono consentite per scopi di didattica e ricerca,
a condizione che ne venga citata la fonte

not been identified. The effect of such a choice on robot control are shown in the experimental section.

4.4 Theoretical formulation of current-based impedance control

In the literature, common approaches to rehabilitation robot control are compliance control (i.e. a PD control action plus gravity compensation) [55], [74], that is purely based on position feedback, or impedance control (i.e. inverse dynamics control) [230], [49] that is based on position feedback with (optionally) force feedback. The use of force feedback simplifies control action and improves its performance in the interaction. For the CBM-Motus the approach based on impedance control was chosen. However, in order to keep inertia low and solve wiring issues, the use of a force sensor mounted at the end effector was avoided.
Thus, two formulations of impedance control were developed and compared. They are:

- Impedance control purely based on position feedback: incremental encoders mounted on the motor shafts are used to read joint positions and indirectly regulate interaction force.
- Impedance control based on servo-amplifier current feedback (namely `current-based impedance control'): measure of servo-amplifier electric current is used as an indirect measure of interaction force and fed back in addition to position readings from the encoders. The approach is particularly interesting as (i) it ensures high performance similarly to impedance control with force feedback; (ii) it does not require force sensors and solves problems related to the increase of the apparent inertia perceived by a human user (due to force sensor mass), wiring issues and costs of the sensors. It is general and can be applied to rehabilitation

Tesi di dottorato in Ingegneria Biomedica, di Antonino Salerno,
discussa presso l'Università Campus Bio-Medico di Roma in data 20/03/2012.
La disseminazione e la riproduzione di questo documento sono consentite per scopi di didattica e ricerca,
a condizione che ne venga citata la fonte

robotic machine with electric actuation, where inertia and acceleration are typically low.

The choice of impedance control in lieu of compliance control is motivated by the need of compensating for dry and viscous friction, that resulted unnegligible from the identification procedure of robot dynamic parameters (eqs. (4.8), (4.13)) and from experimental tests on the robot (see the experimental section 4.5). Compliance control cannot solve motion problems due to friction, being independent on robot dynamics (except for gravity).

The two formulations of impedance control are reported in the following. Both of them refer to the general form of robot dynamics in the interaction with the patient, expressed as

$$B(q)\ \ddot{q} + C(q,\dot{q})\ \dot{q} + F_v\dot{q} + F_S(q,\dot{q}) + g(q) = \tau - J(q)^T h \qquad (4.14)$$

where $J^T(q)h$ is the torque contribution due to interaction force h exerted by the patient on the robot and g(q) is the vector of gravitational torques. For impedance control with purely position feedback, the control law can be written as

$$\tau = B(q)\ \ddot{q} + C(q,\dot{q})\ \dot{q} + F_v\dot{q} + F_S(q,\dot{q}) + g(q) \qquad (4.15)$$

Substituting (4.15) in (4.14) leads to

$$\ddot{q} = y - B^{-1}(q)\, J^T(q)\, h \qquad (4.16)$$

that reveals the existence of a non-linear coupling term $B^{-1}(q)J^T(q)h$ due to contact forces, which makes the relation between $\ddot{q}$ and y dependent on robot joint configuration q.

Choosing for acceleration y the following expression

Tesi di dottorato in Ingegneria Biomedica, di Antonino Salerno,
discussa presso l'Università Campus Bio-Medico di Roma in data 20/03/2012.
La disseminazione e la riproduzione di questo documento sono consentite per scopi di didattica e ricerca,
a condizione che ne venga citata la fonte

$$y = J^{-1}(q)M_d^{-1}(M_d\ddot{x}_d + K_D\dot{\tilde{x}} + K_P\tilde{x} - M_d\dot{J}(q,\dot{q})\dot{q}) \tag{4.17}$$

where J is the Jacobian matrix, $\tilde{x} = x_d - x$ and $\dot{\tilde{x}} = \dot{x}_d - \dot{x}$ are position and velocity errors, respectively, between the planned trajectory xd and the actual trajectory x, yields

$$M_d\ddot{x}_d + K_D\dot{\tilde{x}} + K_P\tilde{x} = M_d J(q)B^{-1}(q)J^T(q)h \tag{4.18}$$

The robot behaves as a generalized mechanical impedance regulated through mass matrix M_d, stiffness matrix K_P and damping matrix K_D. The impedance control with purely position feedback does neither decouple nor linearize robot dynamics, because of the absence of a force sensor at the end effector; however the desired mechanical behaviour is still ensured. At equilibrium the elastic term continues balancing the exerted force even if indirectly.

Note that in the special case of CBM-Motus, inertia and Jacobian matrices are independent on robot configuration and diagonal. This entails that, in this specific case, impedance control with purely position feedback can decouple and linearize robot dynamics; however, the balance with the external force is still indirect.

On the other hand, in the case of current-based impedance control, eqs. (4.15) - (4.18) modify as follows.

Control law is defined as

$$\tau = B(q)y + F_V\dot{q} + F_S + g(q) + J^T(q)h(I) \tag{4.19}$$

where h(I) is the interaction force extracted from sensed current I. The addition of $J^T(q)h(I)$ allows decoupling and linearize robot dynamics, thus yielding

Tesi di dottorato in Ingegneria Biomedica, di Antonino Salerno,
discussa presso l'Università Campus Bio-Medico di Roma in data 20/03/2012.
La disseminazione e la riproduzione di questo documento sono consentite per scopi di didattica e ricerca,
a condizione che ne venga citata la fonte

$$\ddot{q} = y \tag{4.20}$$

Finally, adaptation with respect to interaction force is obtained by means of y, that is defined as

$$y = J_A^{-1}(q)M_d^{-1}\left(M_d\ddot{x}_d + K_D\dot{\tilde{x}} + K_P\tilde{x} - M_d\dot{J}_A(q,\dot{q}) - h(I)\right) \tag{4.21}$$

and includes again the interaction force calculated from the electric current. In the interaction with the patient, the robot behaves as a mass-damper-spring mechanical system described by the following relation

$$M_d\ddot{\tilde{x}} + K_D\dot{\tilde{x}} + K_P\tilde{x} = h(I) \tag{4.22}$$

Current-based impedance control can decouple and linearize robot dynamics, also in absence of a force sensor at the end effector; consequently, patient-robot interaction can be regarded as the parallel of two mechanical impedances (one is human, the latter is robot) and at the equilibrium robot elastic term directly balances force exerted by patient. The current based impedance controller is summarized in Fig. 63.

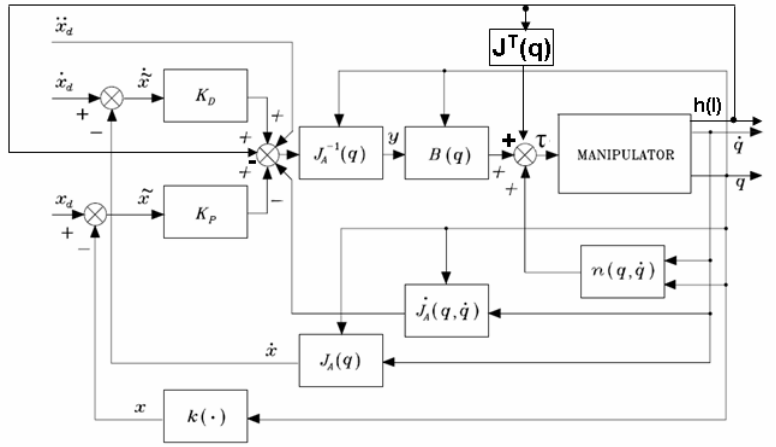

Fig. 63: block scheme of the current based impedance control with $n(q,\dot{q})=C(q,\dot{q})\dot{q}+F_v\dot{q}+F_S(q,\dot{q})+g(q)$

Tesi di dottorato in Ingegneria Biomedica, di Antonino Salerno,
discussa presso l'Università Campus Bio-Medico di Roma in data 20/03/2012.
La disseminazione e la riproduzione di questo documento sono consentite per scopi di didattica e ricerca,
a condizione che ne venga citata la fonte

4.5 Experimental validation of current-based impedance control

4.5.1 Identification of CBM-Motus force/current relation

The idea behind current-based impedance control is to measure interaction force by means of current monitoring in place of direct force monitoring. This entails the need of identifying a relation between electric current and interaction force in the whole robot workspace, by distinguishing current values during free motion (i.e. without interaction) from current values in constrained motion (i.e. during interaction).

The experimental trials of force/current characterization rely on the following assumption: current variation from its typical value in free motion is due to a force applied to the end effector and is an indirect measure of it. Hence, force/current characterization consists of two basic steps: (i) synchronized acquisition of forces and currents in free motion and constrained motion; (ii) correlation analysis of registered current and force data.

The experimental setup consisted of two different data acquisition systems, opportunely synchronized. They were dedicated to measure forces and currents, respectively. The force acquisition system was made up of a six-axis JR3 20E12A-I25 100N5 force/torque sensor with a full scale of 100.00 N, a resolution of 0.01 N and a mass of 0.30 kg. It was mounted on the double prismatic joint of CBM-Motus handle and was connected to a National Instruments Data Acquisition card (NI USB 6009). NI LabVIEW SignalExpress R and MATLAB software packages were used for data acquisition and processing. A low-pass first order Butterworth filter with cutoff frequency of 30 Hz was used for filtering force data, acquired by NI analog to digital converter with a sampling frequency of 1 kHz.

Tesi di dottorato in Ingegneria Biomedica, di Antonino Salerno,
discussa presso l'Università Campus Bio-Medico di Roma in data 20/03/2012.
La disseminazione e la riproduzione di questo documento sono consentite per scopi di didattica e ricerca,
a condizione che ne venga citata la fonte

On the other hand, current values were acquired by means of the CBM-Motus Digital Servo Amplifiers (Ndrive CP20), with a servo loop update rate of 8 kHz. Robot control was programmed in C language with a sample time of 10 ms and communication with Ndrive CP20 via FireWire connection.
Synchronization between the two acquisition systems was obtained by connecting via USB the analog output of the Ndrive servo amplifier to the National Instruments DAQ card, thus generating an acquisition trigger signal. An overview of the experimental setup is shown in Fig. 64.

The robot was programmed to perform 500 point-to-point movements along different directions of the workspace, as shown in Fig. 65(a), in conditions of free motion and constrained motion. In case of constrained motion, the robot was required to perform a point-to-point motion with a known mass applied to the end effector, by means of a pulley-string system shown in Fig. 65(b). Four different experimental conditions were analyzed, corresponding to four different values of applied mass (0.2 kg, 0.4 kg, 1.0 kg, 2.0 kg), in addition to the case of null mass.

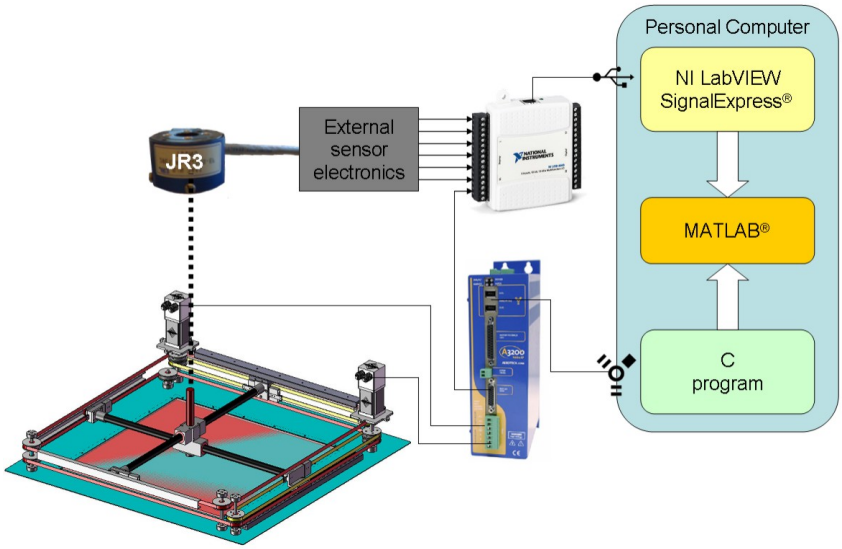

Fig. 64: Experimental setup for force and current recordings.

Tesi di dottorato in Ingegneria Biomedica, di Antonino Salerno,
discussa presso l'Università Campus Bio-Medico di Roma in data 20/03/2012.
La disseminazione e la riproduzione di questo documento sono consentite per scopi di didattica e ricerca,
a condizione che ne venga citata la fonte

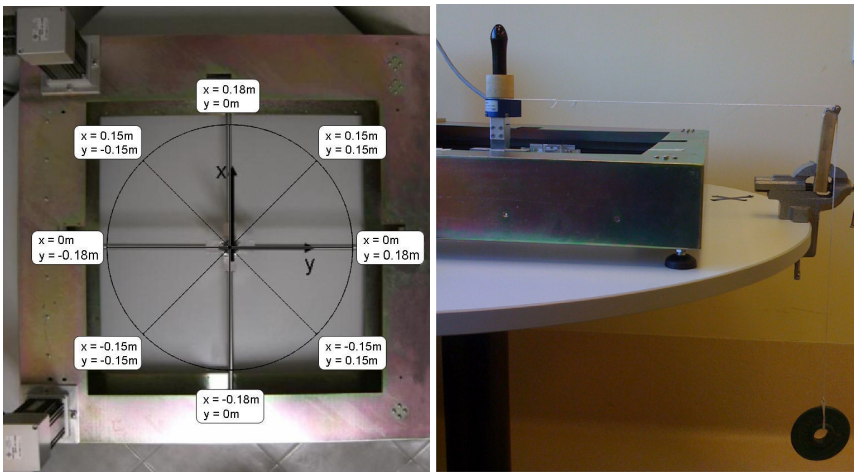

(a) (b)

Fig. 65: (a) Motion directions of the CBM-Motus workspace used for the linear regression analysis; (b) Pulley-string system for force/current characterization.

Because of the unnegligible and anisotropic friction distribution in the robot workspace, four separate linear regression analyses were required for directions towards positive and negative x and y axes (i.e. x^+, y^+, x^-, y^-). Each experimental point represents the mean value of a set of 10 trials for each mass value; x and y axes are referred to joint 1 and 2, respectively.

Results of the four linear regression analyses are reported in Fig. 66.

Tesi di dottorato in Ingegneria Biomedica, di Antonino Salerno,
discussa presso l'Università Campus Bio-Medico di Roma in data 20/03/2012.
La disseminazione e la riproduzione di questo documento sono consentite per scopi di didattica e ricerca,
a condizione che ne venga citata la fonte

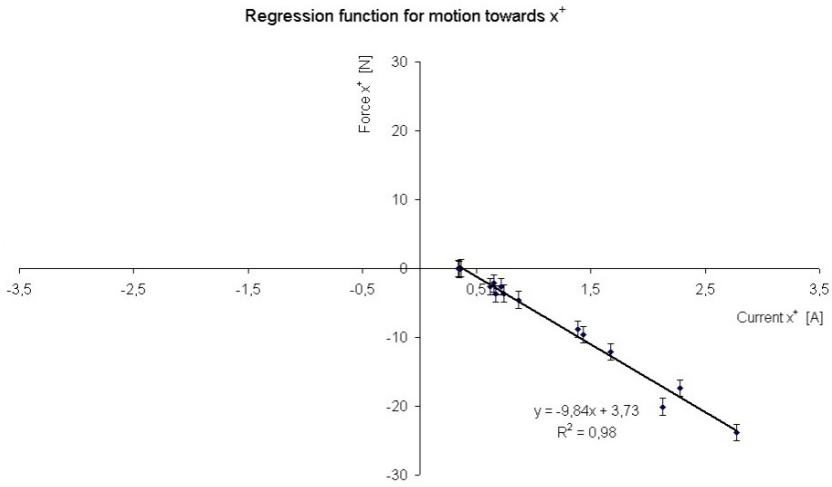

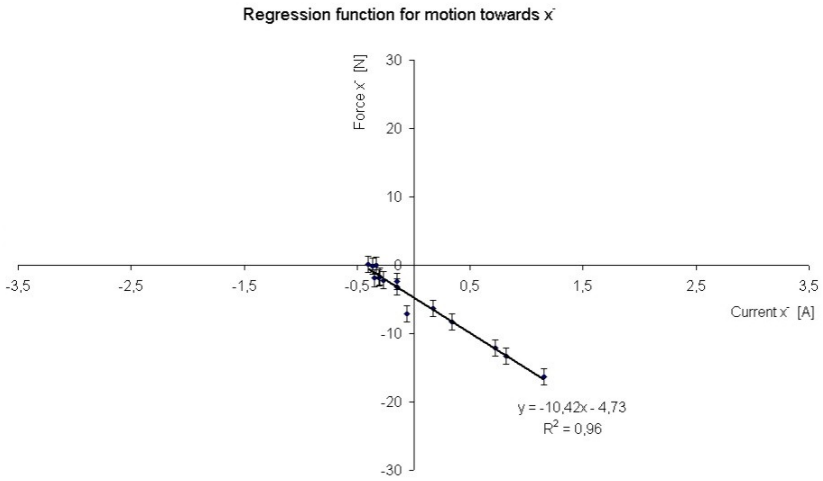

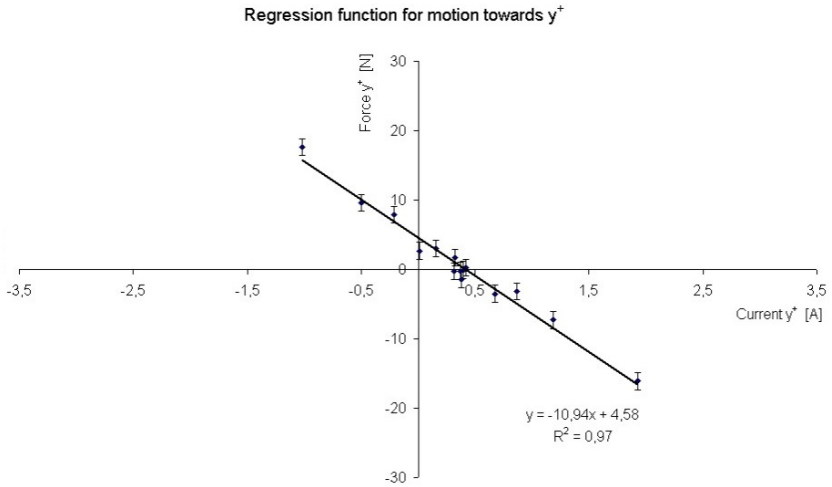

Tesi di dottorato in Ingegneria Biomedica, di Antonino Salerno,
discussa presso l'Università Campus Bio-Medico di Roma in data 20/03/2012.
La disseminazione e la riproduzione di questo documento sono consentite per scopi di didattica e ricerca,
a condizione che ne venga citata la fonte

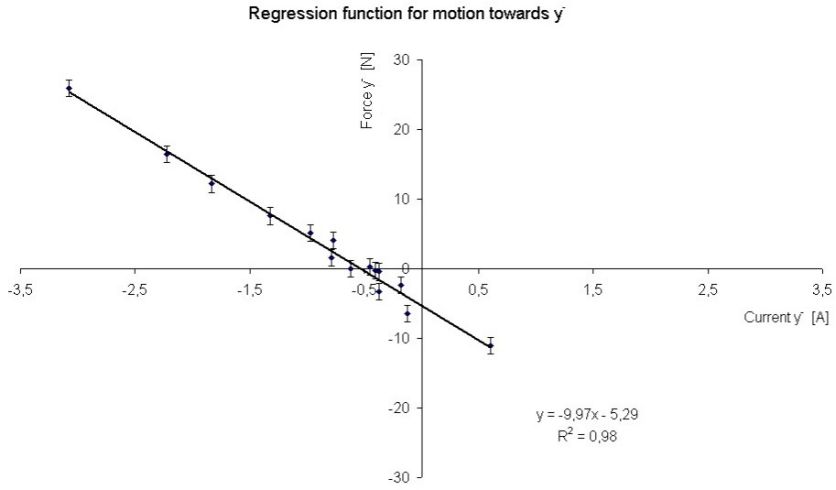

Fig. 66: Regression functions for motion directions towards positive and negative x and y axes. R is the Pearson correlation coefficient for each linear function.

The analytical expressions of the four linear regression functions for each robot configuration are the following:

$$\begin{aligned} h_{x^+} &= -9.84\,I(q) + 3.73; & h_{x^-} &= -10.42\,I(q) - 4.73; \\ h_{y^+} &= -10.94\,I(q) + 4.58; & h_{y^-} &= -9.97\,I(q) - 5.29; \end{aligned} \tag{4.23}$$

where forces are expressed in newton and currents in ampere. It is worth noticing that they are valid when motion occurs along both axes and the other dynamic terms are compensated. Solving eqs. (4.23) with respect to current in absence of interaction force ($h_{x^\pm} = h_{y^\pm} = 0$) provides current mean values in the free space for each direction.

On the other hand, when only one axis is commanded to move while the other one is commanded to maintain actual position, force/current relation for the unmoved axis changes as follows

$$h_{x^\pm} = -10.13\,I(q); \qquad h_{y^\pm} = -10.46\,I(q); \tag{4.24}$$

Tesi di dottorato in Ingegneria Biomedica, di Antonino Salerno,
discussa presso l'Università Campus Bio-Medico di Roma in data 20/03/2012.
La disseminazione e la riproduzione di questo documento sono consentite per scopi di didattica e ricerca,
a condizione che ne venga citata la fonte

For it, current in the free space is null, whereas for the moved axis, relations (4.23) are still valid.

4.5.2 Experimental results

The experimental session was aimed at proving the efficacy of friction compensation and servo-amplifier current monitoring on the improvement of control performance. To this purpose, firstly, experimental trials in the free space were carried out with and without friction compensation. Robot was commanded to track a minimum-jerk trajectory, i.e. a quintic polynomial function from (0; 0) to (0.10; 0.10) m; an inverse dynamics control given by (4.15) - (4.17) in absence of interaction was used in the two cases of friction compensation and non-compensation. Consider that the two control laws expressed by eqs. (4.15) - (4.17) and (4.19) - (4.21) are equivalent in free motion, i.e. in absence of interaction.
Fig. 67 and Fig. 68 show desired and actual end-effector trajectories, position error in norm, recorded electric currents and interaction force when the robot is moving in the free space in the cases of friction compensation and non-compensation, respectively. As expected by comparing Fig. 67 and Fig. 68, the values of static and dynamic friction identified with the procedure in Sect. 4.3 can notably reduce the position error from a mean value of 0.0145 m to a mean value of 0.0017 m, which is comparable with other robotic machines for upper-limb rehabilitation such as the MIT-Manus [55].

Tesi di dottorato in Ingegneria Biomedica, di Antonino Salerno,
discussa presso l'Università Campus Bio-Medico di Roma in data 20/03/2012.
La disseminazione e la riproduzione di questo documento sono consentite per scopi di didattica e ricerca,
a condizione che ne venga citata la fonte

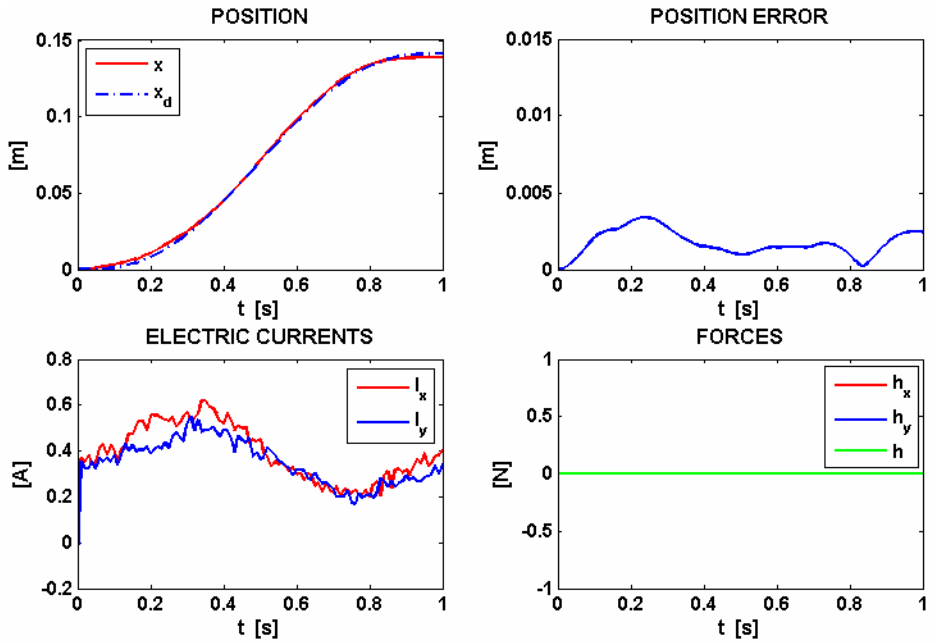

Fig. 67: Experimental results for motion tracking with friction compensation: desired and actual end-effector trajectories (top left), position error in norm (top right), recorded electric currents (bottom left), force values (bottom right). Control gains are K_P = diag{100; 100} and K_D = diag{10; 10}.

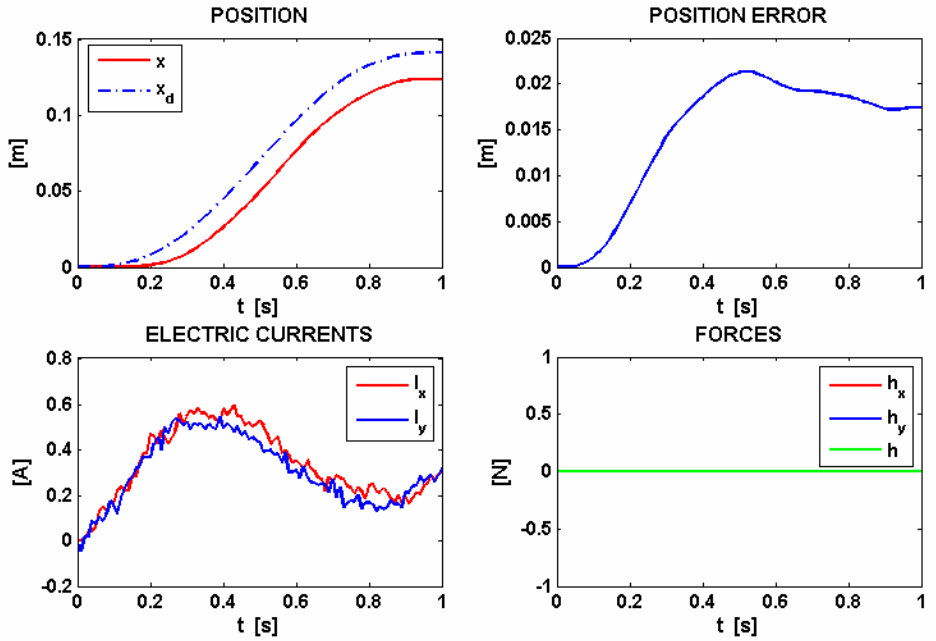

Fig. 68: Experimental results for motion tracking without friction compensation: desired and actual end-effector trajectories (top left), position error in norm (top right), recorded electric

Tesi di dottorato in Ingegneria Biomedica, di Antonino Salerno,
discussa presso l'Università Campus Bio-Medico di Roma in data 20/03/2012.
La disseminazione e la riproduzione di questo documento sono consentite per scopi di didattica e ricerca,
a condizione che ne venga citata la fonte

currents (bottom left), force values extracted from currents (bottom right). Control gains are K_P = diag{100; 100} and K_D = diag{10; 10}.

Secondly, force/current relations in eqs. (4.23) were used to implement and test current-based impedance control in (4.19) - (4.21). The experimental session was aimed at validating the control approach and measuring its performance with respect to impedance control purely based on position feedback, expressed by eqs. (4.15) - (4.17). In both cases, friction was compensated in addition to robot inertia.

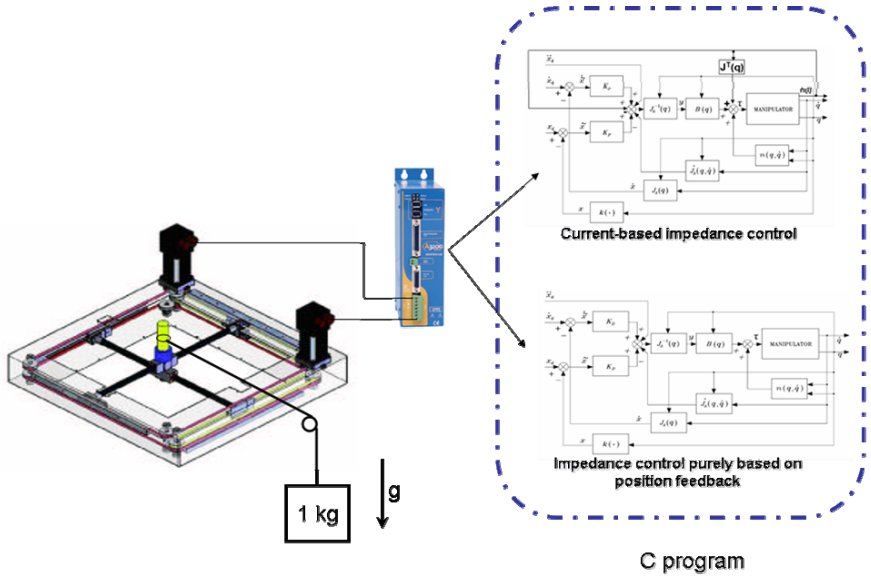

Fig. 69: Sketch of the interaction trials with an external force applied at the end-effector and the compared control laws.

Fig. 69 shows a schematic representation of the experimental trials in the constrained space and the compared control schemes. One kg load was applied to the robot end-effector by means a pulley-string system and system performance has been compared by employing both implemented control laws (i.e. current-based impedance control and impedance control purely based on position feedback).

For constrained tasks, the same trajectory as for the free motion was planned while a weight was applied to the end effector. Different mass values were tested

Tesi di dottorato in Ingegneria Biomedica, di Antonino Salerno,
discussa presso l'Università Campus Bio-Medico di Roma in data 20/03/2012.
La disseminazione e la riproduzione di questo documento sono consentite per scopi di didattica e ricerca,
a condizione che ne venga citata la fonte

with the two control laws by varying control gains and measuring the corresponding end-effector position and motor currents.
Figures Fig. 70 - Fig. 73 report desired and actual end-effector trajectories, position error in norm and recorded electric currents for the two control laws, when a weight of 1 kg is applied and two different sets of control gains are chosen (i.e. K_P = diag{40; 40}, K_D = diag{4; 4} and K_P = diag{100; 100}, K_D = diag{10; 10}). Control gains were empirically chosen in order to set two different levels of robot compliance within system stability limits. Also, force values extracted by the electric currents are shown in Fig. 70 - Fig. 73 (bottom right). It can be noticed that the computed force value is constant as long as the robot end effector holds the position imposed by the applied weight.

A threshold check is made on the electric current, so that when during interaction it goes below 0.57 A for x axis and 0.62 A for y axis (as an effect of the torque control command), interaction force is maintained constant with the position. When current is beyond the threshold, force values vary according to relations (4.23). The threshold values correspond to the maximum current values for each axis in free space motion.

Figures Fig. 70 - Fig. 73 show that, in order to get the same compliant behaviour with the two control laws (about h = 20 N), it is necessary to set different gains: K_P = diag{40; 40} for impedance control purely based on position feedback (Fig. 71) and K_P = diag{100; 100} for current-based impedance control (Fig. 72).

Tesi di dottorato in Ingegneria Biomedica, di Antonino Salerno,
discussa presso l'Università Campus Bio-Medico di Roma in data 20/03/2012.
La disseminazione e la riproduzione di questo documento sono consentite per scopi di didattica e ricerca,
a condizione che ne venga citata la fonte

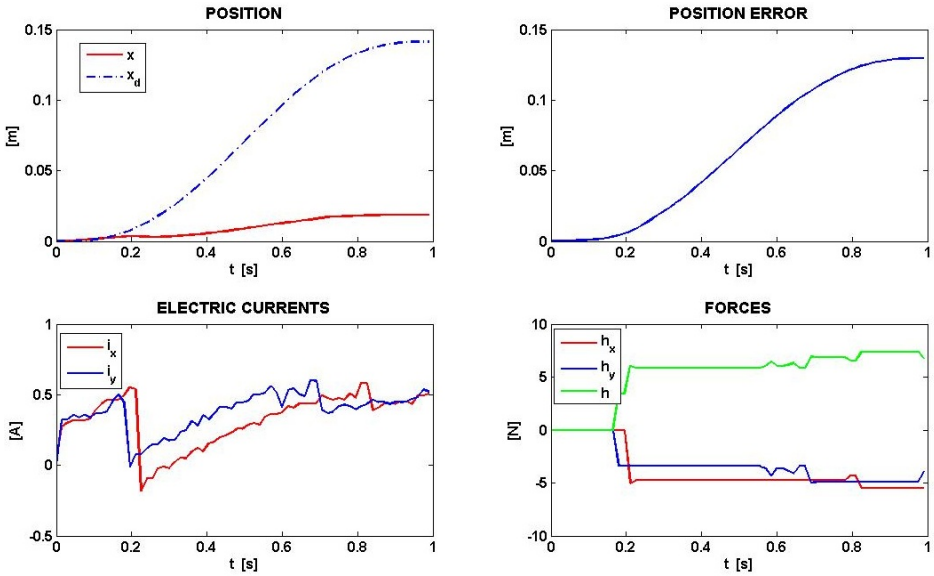

Fig. 70: Experimental results for the current-based impedance control during a constrained task with 1 kg applied at the end effector: desired and actual end-effector trajectories (top left), position error in norm (top right), recorded electric currents (bottom left), force values extracted from currents (bottom right). Control gains are K_P = diag{40; 40} and K_D = diag{4; 4}.

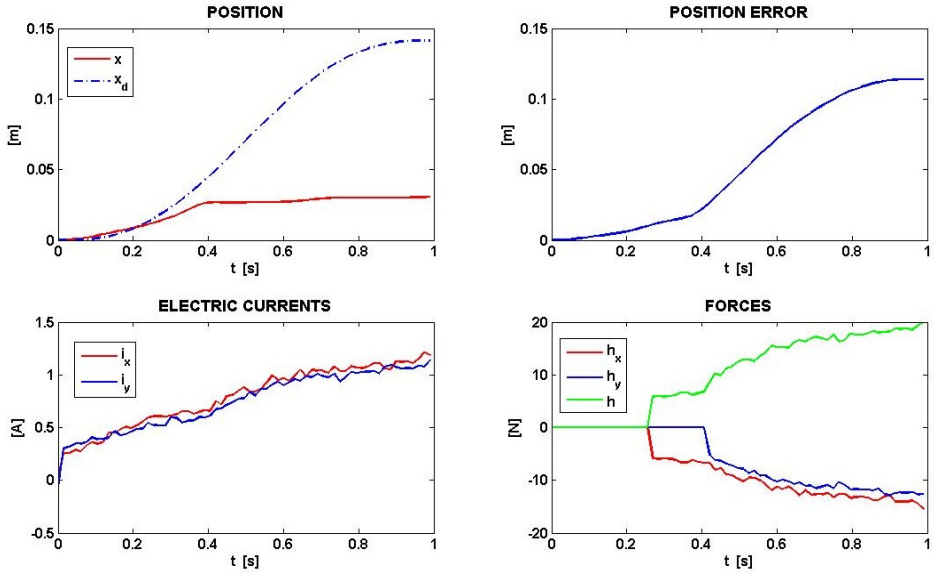

Fig. 71: Experimental results for the impedance control purely based on position feedback during a constrained task with 1 kg applied at the end effector: desired and actual end-effector trajectories (top left), position error in norm (top right), recorded electric currents (bottom left), force values extracted from currents (bottom right). Control gains are K_P = diag{40; 40} and K_D = diag{4; 4}.

Tesi di dottorato in Ingegneria Biomedica, di Antonino Salerno,
discussa presso l'Università Campus Bio-Medico di Roma in data 20/03/2012.
La disseminazione e la riproduzione di questo documento sono consentite per scopi di didattica e ricerca,
a condizione che ne venga citata la fonte

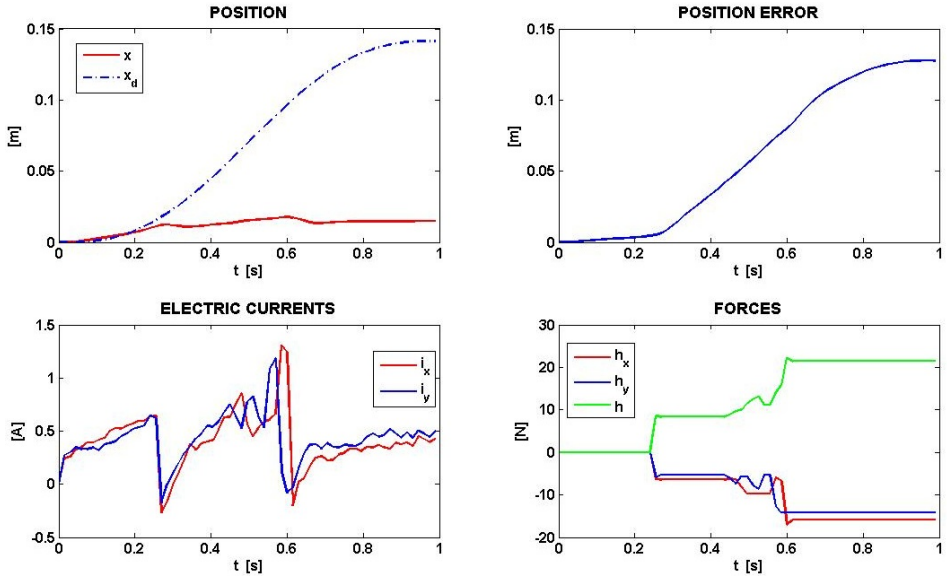

Fig. 72: Experimental results for the current-based impedance control during a constrained task with 1 kg applied at the end effector: desired and actual end-effector trajectories (top left), position error in norm (top right), recorded electric currents (bottom left), force values extracted from currents (bottom right). Control gains are K_P = diag{100; 100} and K_D = diag{10; 10}.

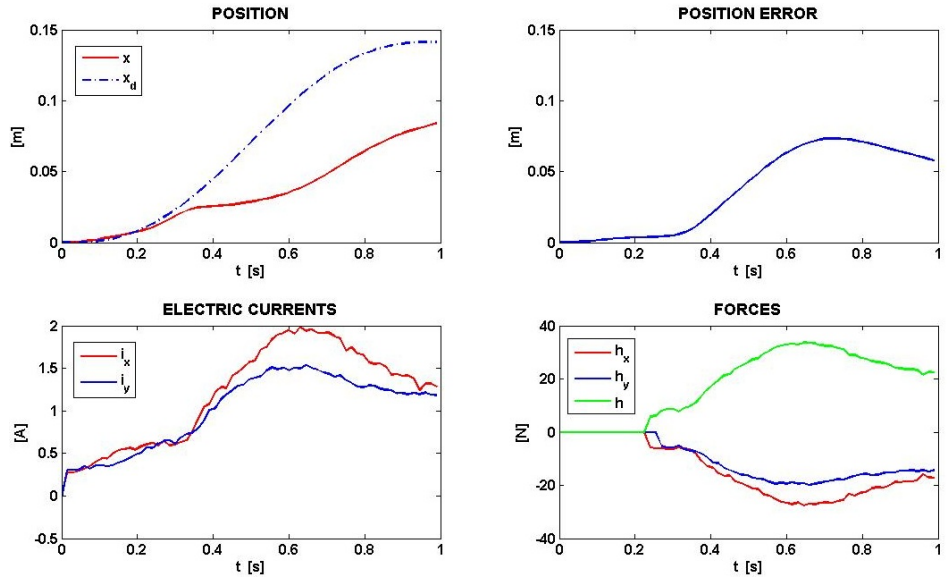

Fig. 73: Experimental results for the impedance control purely based on position feedback during a constrained task with 1 kg applied at the end effector: desired and actual end-effector trajectories (top left), position error in norm (top right), recorded electric currents (bottom left), force values extracted from currents (bottom right). Control gains are K_P = diag{100; 100} and K_D = diag{10; 10}.

Tesi di dottorato in Ingegneria Biomedica, di Antonino Salerno,
discussa presso l'Università Campus Bio-Medico di Roma in data 20/03/2012.
La disseminazione e la riproduzione di questo documento sono consentite per scopi di didattica e ricerca,
a condizione che ne venga citata la fonte

The drawback is that, in absence of constraint, accuracy is much reduced when a current feedback is not provided. Therefore, with the same gain values, current-based impedance control always outperforms impedance control based only on position feedback, thanks to indirect force feedback provided by electric current. In particular, for current-based impedance control it is possible to optimize robot behaviour in free as well as in constrained space through the same set of control gains K_P = diag{100; 100}, thus ensuring a high level of adaptability to the external constraint (h = 21.41 N) and, at the same time, a good level of accuracy in free motion (0.004 m is the maximum value of cartesian position error).

Further, it is possible to make the system selective with respect to motion direction thanks to control linearization and decoupling action. On the other hand, impedance control purely based on position feedback needs of lower gains K_P = diag{40; 40} in order to achieve the same value of interaction force with an unavoidable increase of position error in free space (0.018 m is the maximum value).

It is worth noticing that extracting force values by servo-amplifier current measures could cause a slight reduction of system reactivity; the reason is that interaction force is perceived when a significant change in current level is induced. This means that perception of the interaction force can be delayed of one sample time at maximum, corresponding to 10 ms in the performed experiments. However, as experimentally verified in our tests, this is not critical in applications of robot-aided rehabilitation where motion velocity is very low (under 0.2 - 0.4 m/s).

Finally, software safety measures have been taken in order to minimize the risk of injury to subjects during the experimental trials, potentially caused by an electrically actuated machine capable of independent motion. Specifically, the software continuously monitors torques, velocities, and displacements and disables the system in case preestablished limits are exceeded.

Tesi di dottorato in Ingegneria Biomedica, di Antonino Salerno,
discussa presso l'Università Campus Bio-Medico di Roma in data 20/03/2012.
La disseminazione e la riproduzione di questo documento sono consentite per scopi di didattica e ricerca,
a condizione che ne venga citata la fonte

Chapter 5

Reach-and-Grasp Optimization Algorithm Inspired to Human Arm-Hand Control

Biologically inspired robotic systems can find an important application area in biomedical robotics, where studying and replicating human behavior can provide new insights into motor recovery, functional substitution and human-robot interaction. This chapter focuses on bio-inspired grasping strategies for an anthropomorphic robotic hand. From the study of the human hand anatomy and the observation of its behaviour during grasping, new knowledge on the hand kinematics is extracted and an algorithm for robotic hand grasping is proposed. In order to reduce the complexity of the control algorithm and ensure grasp stability,

Tesi di dottorato in Ingegneria Biomedica, di Antonino Salerno,
discussa presso l'Università Campus Bio-Medico di Roma in data 20/03/2012.
La disseminazione e la riproduzione di questo documento sono consentite per scopi di didattica e ricerca,
a condizione che ne venga citata la fonte

the optimal hand grasp posture is searched. The proposed algorithm is based on the minimization of an objective function expressed by the sum of the distances of the hand joints from the object surface for diagonal volar grasping. Algorithm effectiveness has preliminarily been tested by means of simulation trials. Finally, experimental trials on a real arm-hand robotic system have been carried out in order to validate the approach and measure algorithm performance.

The chapter is structured as follows: in Section 5.2 the algorithm for determining the optimal grasp configuration is presented; in Section 5.3, the experimental setup is described, while the experimental results are reported in Section 5.4. Finally, the algorithm extension to transverse volar grasp is proposed in Section 5.5 in comparison with studies on humans using the same grasp typology.

5.1 Introduction

The ability to perform grasping task is of paramount importance in most industrial applications, as well as in biomedical applications, such as rehabilitation and prosthetics. The difficulty of realizing natural, reliable and optimal grasp has prompted researchers to explore different methods for solving the problem. Studying and replicating human grasping strategies is one of the feasible approaches, which is pursued in this chapter.

Studies on human grasping show that the task can be decomposed into three main phases: reaching, pre-shaping and grasping. During reaching, the hand approaches the object to be grasped. The most appropriate finger configuration to ensure a stable grasp is defined during pre-shaping. Thus, the full-blown grasp follows. In [231], three factors that mainly affect the grasping action were identified: object, hand and task. The object physical characteristics, like shape and weight, affect the hand configuration since the pre-shaping phase [232]. As said before, during preshaping, the hand starts assuming the configuration that best fits the object

Tesi di dottorato in Ingegneria Biomedica, di Antonino Salerno,
discussa presso l'Università Campus Bio-Medico di Roma in data 20/03/2012.
La disseminazione e la riproduzione di questo documento sono consentite per scopi di didattica e ricerca,
a condizione che ne venga citata la fonte

characteristics and the task to be performed. Thus, finger placement can be considered as a function of the object shape. In [233], studies on human beings proved that hand shaping was affected by the end-goal, in addition to object geometry. Different grasping taxonomies, developed on the basis of the object characteristics and of the task, were reported in the literature [234]-[236]. According to the task, two principal classes of grasps could be distinguished: power grasp, which involves the whole hand, and precision grasp, where only fingers are involved. In particular, two types of power grasp were deeply analyzed in [237]: transverse volar grasp, where the thumb is abducted, and diagonal grasp, where the thumb is adducted lying along the longest axis of the object surface.

In this chapter, the attention is focused on power grasp of cylindrical objects. In particular, an algorithm is proposed for determining the optimal hand configuration that fits object characteristics and ensures a stable grasp. The approach draws inspiration from studies on human behaviour, is reformulated for a robotic hand and is experimentally tested on robotic arm-hand system during reach-and-grasp tasks of cylindrical objects.

Many approaches can be found in the literature to the purpose of searching an optimization criterion for selecting the optimal grasp configuration for a given object.

In [238] a review was proposed of various techniques for identifying the optimal grasp within the space of "feasible grasps", given a set of task constraints, like object shape, type of task, hand degrees of mobility, maximum force to be applied, etc. The main difficulty of this approach is the choice of the parameters to be used as constraints and to be included in the objective function [239],[240].

A different approach consists of determining the hand-object contact points that guarantee a firm grip. The problem of contact point identification was often solved by replicating the human behavior in a master-slave configuration. Usually, the human hand wore a sensorized glove which allowed continuously monitoring the hand joint position. The acquired data, in addition to object

Tesi di dottorato in Ingegneria Biomedica, di Antonino Salerno,
discussa presso l'Università Campus Bio-Medico di Roma in data 20/03/2012.
La disseminazione e la riproduzione di questo documento sono consentite per scopi di didattica e ricerca,
a condizione che ne venga citata la fonte

characteristics could be used to train a neural network (NN). After training, a neural system able to provide joint positions and forces that a robotic hand should apply for a stable grasp was obtained [241].

Contact points can also be determined by means of grasp quality measures, which are used to evaluate grasp performance. In [242] two groups of grasp quality measurements were considered: the first one took into account the object properties and was linked to the position of the contact points; the second one was associated with the hand configuration, e.g. in terms of finger joint position. The authors proposed a method for satisfying both grasp quality measurements, by firstly finding the best contact points between the robotic hand and the object and, secondly, taking into account the hand configuration or the limitations on the joint position. In [243], after heuristically generating a set of feasible grasp candidates, grasp quality measures, computed with an ad hoc method, are used to choose the best grasp.

Finally, methods for finding an optimal grasp configuration based on grasping force determination can be mentioned. They rely on the concepts of wrench matrix and friction cone [244][245], which are the basis for the determination of the optimal grasp forces in order to guarantee a stable grasp.

The method proposed in this chapter resorts to recent findings on human optimal grasp for a cylindrical object [246], by assuming that object shape and size are known. The main target is to replicate human ability to realize grasps with extreme precision, by choosing in a complex repertoire of manual grips. Differently from other approaches in the literature, the proposed method is not based on the grasping force determination. It consists of an optimization algorithm able to provide hand position, after reaching, and finger joint configuration, after preshaping, in order to achieve a stable grasp. The algorithm is then tested on an arm-hand robotic platform described in Section 5.3, consisting of the MIT–Manus robotic arm [247] and the DLR-HIT-Hand II [248].

Tesi di dottorato in Ingegneria Biomedica, di Antonino Salerno,
discussa presso l'Università Campus Bio-Medico di Roma in data 20/03/2012.
La disseminazione e la riproduzione di questo documento sono consentite per scopi di didattica e ricerca,
a condizione che ne venga citata la fonte

5.2 Algorithm for the optimal grasp configuration

In this section, an approach for determining a human-like hand grasp configuration is developed by resorting to findings on human behavior in [246] and re-adapting them to an arm-hand robotic system. In [246] it is shown that the optimal configuration for grasping a cylindrical object is the one that minimizes the sum of the distances between the hand joints and the object surface. Based on that, the position of the carpometacarpal (CMC) joint (Fig. 74) that guarantees a stable grasp configuration is obtained by minimizing the following objective function:

$$f = \sum_{i=1}^{4} \sum_{j=1}^{3} dist_j^i(y, \alpha) \tag{5.1}$$

where:

- index i indicates the i-th finger; it ranges from 1 (the index finger) to 4 (the little finger);
- j is the joint index, ranging from 1 (the metacarpophalangeal, MCP, joint) to 3 (the distal interphalangeal, DIP, joint);
- $dist_j^i(y, \alpha)$ is the distance of the j-th joint of the i-th finger from the object surface (red dotted line in Fig. 74). This distance is a function of y, i.e. the CMC y-coordinate in the reference frame of Fig. 74, and α, that is the inclination angle of the object rotation axis with respect to the z-axis of the reference frame;
- r_{obj} is the object radius;
- y_{MCP_i} is the y-coordinate of the MCP joint of the i-th finger in the optimal configuration. Its value depends on the initial configuration ($y_{MCP_i}^{start}$ is the y-

Tesi di dottorato in Ingegneria Biomedica, di Antonino Salerno,
discussa presso l'Università Campus Bio-Medico di Roma in data 20/03/2012.
La disseminazione e la riproduzione di questo documento sono consentite per scopi di didattica e ricerca,
a condizione che ne venga citata la fonte

coordinate of the MCP joint in the start configuration) and on the inclination angle α given by the optimization procedure. In particular:

$$y_{MCP_i} = y + \left(y^{\ start}_{MCP_i} - y^{\ start}_{MCP_4}\right) + \left(z^{\ start}_{MCP_i} - z^{\ start}_{MCP_4}\right) * \tan\alpha \tag{5.2}$$

For each joint (i.e. MCP, PIP and DIP), distances from the object surface can be expressed as:

$$dist^i_{MCP} = \sqrt{y^2_{MCP_i} + (r_{obj} + t_0)}\,, \tag{5.3}$$

$$dist^i_{PIP} = \sqrt{\left(a_1 - \sqrt{\left(r_{obj} + dist^i_{MCP}\right)^2 - \left(r_{obj} + t_1\right)^2}\right)^2 + \left(r_{obj} + t_1\right)^2}\,, \tag{5.4}$$

$$dist^i_{DIP} = \sqrt{\left(a_2 - \sqrt{\left(r_{obj} + dist^i_{PIP}\right)^2 - \left(r_{obj} + t_2\right)^2}\right)^2 + \left(r_{obj} + t_2\right)^2}\,, \tag{5.5}$$

being a_i finger link lengths and t_i finger thickness.

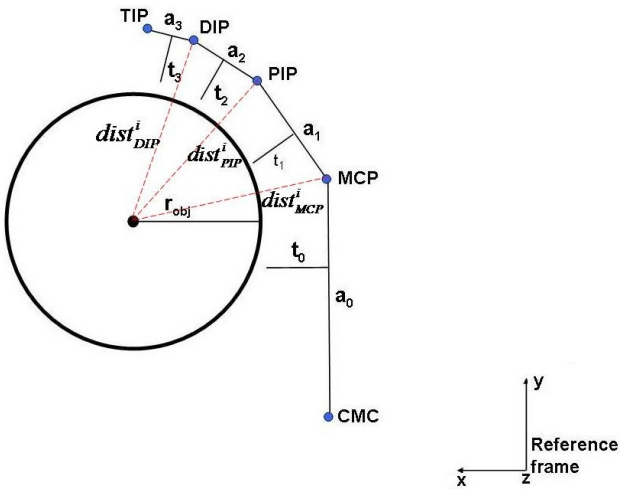

Fig. 74: Schematic representation of virtual scenario in which algorithm has been developed.

Equations (5.3) - (5.5) are valid under the following two hypotheses:

1. the x-coordinate is the same for all MCP joints;

Tesi di dottorato in Ingegneria Biomedica, di Antonino Salerno,
discussa presso l'Università Campus Bio-Medico di Roma in data 20/03/2012.
La disseminazione e la riproduzione di questo documento sono consentite per scopi di didattica e ricerca,
a condizione che ne venga citata la fonte

2. the planes in which the fingers lie are perpendicular to the object rotation axis, i.e. fingers are parallel each other.

Whereas condition 2 is not verified, as it happens in nature (Fig. 75), equations (5.3) - (5.5) have to be modified. In particular, when fingers lie on planes inclined with respect to the plane perpendicular to the object rotation axis (plane xy in Fig. 74), joint projections in this plane need to be considered. These values are determined by replacing the link length a_i, in the distance equations (5.3) - (5.5), with link length projections l_k computed by considering the vector normal to the xy-plane of Fig. 74.

Fig. 75: Human grasp of a cylindrical object. The fingers are inclined among each others.

The length of the k-th finger link in the projection plane is given by:

$$l_k = a_k^2 - \left\| a_k \bullet \left(n_p \times n_o \right) \right\|^2 \bullet \left(n_p \times n_o \right)^2 + \left\| a_k \bullet \left(n_p \times n_o \right) \right\|^2 \tag{5.6}$$

where n_p is the normal vector to the plane perpendicular to the object rotation axis and n_o is the normal vector to the inclined plane where the finger lies. In this way it is possible to work in the projection plane, going back to the simplified case in which all fingers lie in the plane perpendicular to the object rotation axis.

Once the joint coordinates and the joint angles in the projection plane are determined, it is necessary to bring back these results to the original planes where

Tesi di dottorato in Ingegneria Biomedica, di Antonino Salerno,
discussa presso l'Università Campus Bio-Medico di Roma in data 20/03/2012.
La disseminazione e la riproduzione di questo documento sono consentite per scopi di didattica e ricerca,
a condizione che ne venga citata la fonte

the fingers lie. Joint Cartesian coordinates in the original plane are given by the intersection of that plane with the straight-line perpendicular to the original plane and passing through the joint in the projection plane. Starting from joint Cartesian coordinates, the joint angles are determined by means of inverse kinematics.
Through equations (5.1) to (5.5), which return the CMC y-coordinate and the distances of the joints from the object surface, in addition to some geometrical considerations, all the joint coordinates are computed and a human-like optimal grasp configuration is obtained.

5.3 Experimental setup

The ultimate purpose of this Section is to test the algorithm described in Section 5.2 on a real arm-hand robotic system. The experimental platform (Fig. 76) used in this work is composed of the MIT-Manus planar robot, which acts like the arm and realizes the reaching task, and the DLR-HIT-Hand II mounted at the MIT-Manus end effector and responsible for preshaping and grasping.

A set of three cylindrical objects with three different size (diameter of 0.045 m, 0.047 m and 0.032 m, respectively) were selected. They were used for (i) extracting the optimal hand configurations adapted to each object located in a known position of the working plane, by offline running the optimization algorithm in Sect. 5.2; (ii) carrying out the experimental tests of reach-and-grasp by means of the arm-hand robotic system.

In the following, technical details on the robotic arm and hand are reported, by also pointing out the constraints due to their mechanical structure.

Tesi di dottorato in Ingegneria Biomedica, di Antonino Salerno,
discussa presso l'Università Campus Bio-Medico di Roma in data 20/03/2012.
La disseminazione e la riproduzione di questo documento sono consentite per scopi di didattica e ricerca,
a condizione che ne venga citata la fonte

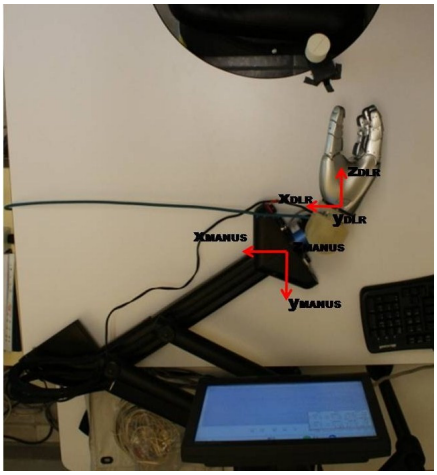

Fig. 76: Experimental setup. The DLR-HIT-Hand II and MIT Manus reference frames are shown.

The MIT-Manus system is a planar robotic arm (typically used for upper-limb rehabilitation) with two rotational degrees of freedom, one for the elbow and one for the shoulder angular motion. It reproduces the planar motion of shoulder and elbow rotational joints of the upper limb in a workspace of 0.40x0.40 m. It is equipped with two optical encoders and a six-axis JR3 force/torque sensor. The Denavit-Hartenberg parameters are shown in Table VII.

TABLE VII
MIT MANUS DENAVIT-HARTENBERG PARAMETERS

Joint	d [m]	ϑ [rad]	a [m]	α [rad]
0	0	0	0	0
1	0	0	0.551	$-\pi/2$
2	0	0	0.407	$-\pi/2$

The five-fingered dexterous robotic hand DLR-HIT-Hand II (Fig. 77) has an independent palm and five identical modular fingers. Each finger has four DoFs (adduction/abduction, MCP, PIP and DIP), three actuated and one passive. The last two joints (PIP and DIP) are 1:1 coupled, meaning that the corresponding flexion/extension angles are equal. The thumb The thumb is mechanically constrained to assume a fixed opposition of 35.51° in the xy-plane with an

Tesi di dottorato in Ingegneria Biomedica, di Antonino Salerno,
discussa presso l'Università Campus Bio-Medico di Roma in data 20/03/2012.
La disseminazione e la riproduzione di questo documento sono consentite per scopi di didattica e ricerca,
a condizione che ne venga citata la fonte

inclination, with respect to z-axis, of 44.13°; this only enables transverse volar grasps with a fixed thumb inclination.

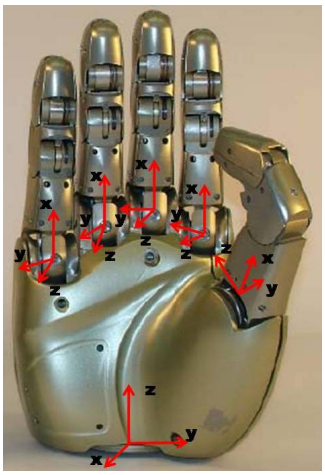

Fig. 77: DLR-HIT-Hand II with joint reference frames.

All the active DoFs are actuated by flat brushless DC motors. Actuators and electronics are embedded in fingers and palm mechanical structure. Furthermore, each finger has three Hall-effect sensors for measuring joint positions, two force/torque sensors and one thermistor as temperature sensor.

Hand geometric data and Denavit-Hartenberg parameters are listed in Table VIII and IX, respectively.

TABLE VIII
DLR-HIT-HAND II GEOMETRIC PARAMETERS

a_01	$CMC\text{-}MCP_{index}$ link length	117×10^{-3} m
a_01	$CMC\text{-}MCP_{middle}$ link length	122×10^{-3} m
a_01	$CMC\text{-}MCP_{ring}$ link length	117×10^{-3} m
a_01	$CMC\text{-}MCP_{little}$ link length	105×10^{-3} m
a_1	Proximal link length	55×10^{-3} m
a_2	Medial link length	25×10^{-3} m
a_3	Distal link length	25×10^{-3} m
t_0	Palm thickness	64×10^{-3} m
t_1	Proximal link thickness	33.37×10^{-3} m
t_2	Medial link thickness	26.74×10^{-3} m
t_3	Distal link thickness	24.61×10^{-3} m

TABLE IX
DENAVIT-HARTENBERG PARAMETERS FOR EACH FINGER OF DLR HIT HAND II

Tesi di dottorato in Ingegneria Biomedica, di Antonino Salerno,
discussa presso l'Università Campus Bio-Medico di Roma in data 20/03/2012.
La disseminazione e la riproduzione di questo documento sono consentite per scopi di didattica e ricerca,
a condizione che ne venga citata la fonte

Joint	d [m]	ϑ [rad]	a [m]	α [rad]
0	0	0	0	0
1	0	0	0	$-\pi/2$
2	0	0	0.055	0
3	0	$-\pi/2$	0.025	0
4	0.025	π	0	$-\pi/2$

An outline of the working scenario where the optimization algorithm was tested is reported in Fig. 78.

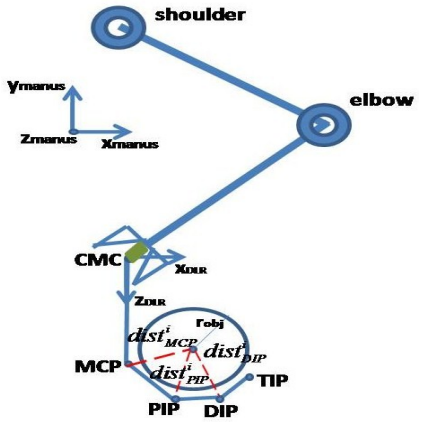

Fig. 78: Top view of the working scenario schematic representation.

Fig. 78 shows (a) a schematic representation of the two-link MIT-Manus robot, with its reference frame ($x_{manus}, y_{manus}, z_{manus}$); (b) the DLR-HIT-Hand II reference frame ($x_{DLR}, y_{DLR}, z_{DLR}$); (c) the hand configuration, coming out from the optimization algorithm, and the object to grasp. The green block between the arm handle and the hand CMC joint is a flange. The distance between finger joints and object rotation axis are outlined with dotted red lines.

The object to be grasped was a cylinder whose shape, weight and position were known. The initial configuration of the hand joints, as well as the optimal configuration from the algorithm were given in the MIT-Manus reference frame.

Tesi di dottorato in Ingegneria Biomedica, di Antonino Salerno,
discussa presso l'Università Campus Bio-Medico di Roma in data 20/03/2012.
La disseminazione e la riproduzione di questo documento sono consentite per scopi di didattica e ricerca,
a condizione che ne venga citata la fonte

Being the MIT-Manus planar, arm and hand height from the table could not be varied. Consequently, the object was properly located in order to allow closing the middle finger at half of the object height. This assumption was coherent with studies on human beings in [249].

Given object position, the optimal CMC Cartesian position and the final hand configuration for grasping the object was obtained by minimizing Eq. (5.1) through the Matlab function *fminsearch (f, [initial condition])*.

During the reaching movement, the hand was moved by the arm towards the optimal CMC position. Thus, the hand was controlled in order to reach the final MCP, PIP, DIP joint angles, also provided by the optimization algorithm.

During reaching, the hand did not change orientation, being arm motion planar: z_{DLR}-axis was always parallel to y_{MANUS}. This assumption is supported by neuroscientific theories [250]. A fifth order polynomial function was used to plan the MIT-Manus linear motion from initial position ($x = -0.1m$, $y = 0.1m$) up to final position ($x = -0.1m$, $y = -0.1m$). Then, a proportional-derivative (PD) torque control in the Cartesian space was used to control arm position (and consequently CMC position) in the plane.

As regards preshaping, final MCP, PIP and DIP joint positions, provided by the optimization algorithm, were taken as reference for the DLR-HIT-Hand motion controller. A third degree polynomial function was used to plan joint motion up to the final reference value and a PD torque control in the joint space enabled reaching the desired final angles. It is worth noticing that, in the DLR-HIT-Hand II, the DIP and PIP joints are coupled with $\vartheta_{PIP} = \vartheta_{DIP}$, thus providing a constraint to the final position of PIP and TIP, that was often slightly different with respect to the desired one.

In addition, conditions 1 and 2 in Sect. 5.2 were not completely satisfied. Firstly, x-coordinate of hand MCP joints (in the hand frame) were different from each other. Secondly, fingers were inclined each other, as in the human hand. The

Tesi di dottorato in Ingegneria Biomedica, di Antonino Salerno,
discussa presso l'Università Campus Bio-Medico di Roma in data 20/03/2012.
La disseminazione e la riproduzione di questo documento sono consentite per scopi di didattica e ricerca,
a condizione che ne venga citata la fonte

middle finger was perpendicular to the object rotation axis. The angle between index and middle finger was 5°; on the other hand, the angle of ring finger and little finger with respect to middle finger was 9°. Therefore, equations (5.3) - (5.5) were modified taking into account the different x-coordinates and replacing the original finger link length with the projected ones, as explained in Section 5.2.

5.4 Experimental results

The described algorithm was firstly tested in a simulated environment with the same characteristics of the real one, where MIT-Manus and DLR-HIT-Hand II kinematics and dynamics were modeled. The obtained results, shown in Fig. 79, were encouraging, thus showing that fingers could properly grasp the object, as expected. The red dot is the CMC joint. Green dots are the index finger MCP, DIP, PIP and TIP joints, while blue dots are the middle finger joints, and magenta dots represent the ring finger joints. Finally, the black dots mark the little finger MCP, PIP, DIP joints and tip.

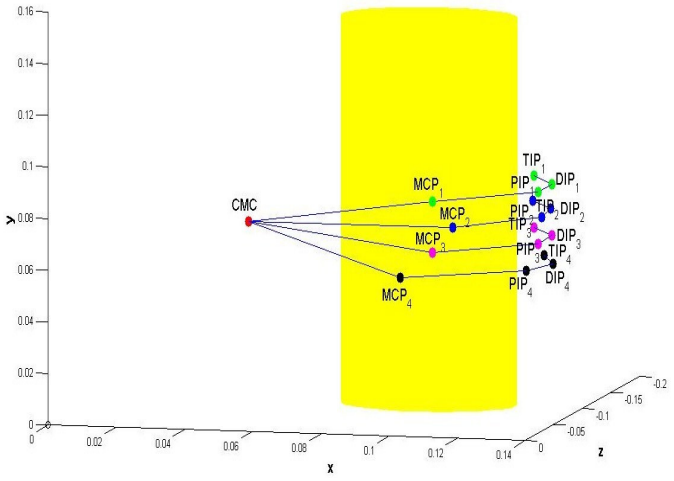

Fig. 79: Plot of joint and object positions in a simulated environment.

Tesi di dottorato in Ingegneria Biomedica, di Antonino Salerno,
discussa presso l'Università Campus Bio-Medico di Roma in data 20/03/2012.
La disseminazione e la riproduzione di questo documento sono consentite per scopi di didattica e ricerca,
a condizione che ne venga citata la fonte

Thus, experimental tests were carried out in the working scenario described in Sect. 5.3 and shown in Fig. 76. In Fig. 80 a representative plot of the robotic hand final configuration, obtained in the experimental tests, is shown. The black dot is the CMC joint, the red dots are the MCP positions for each finger, the pink ones are the PIP joints, while the DIP joints are represented by green dots.

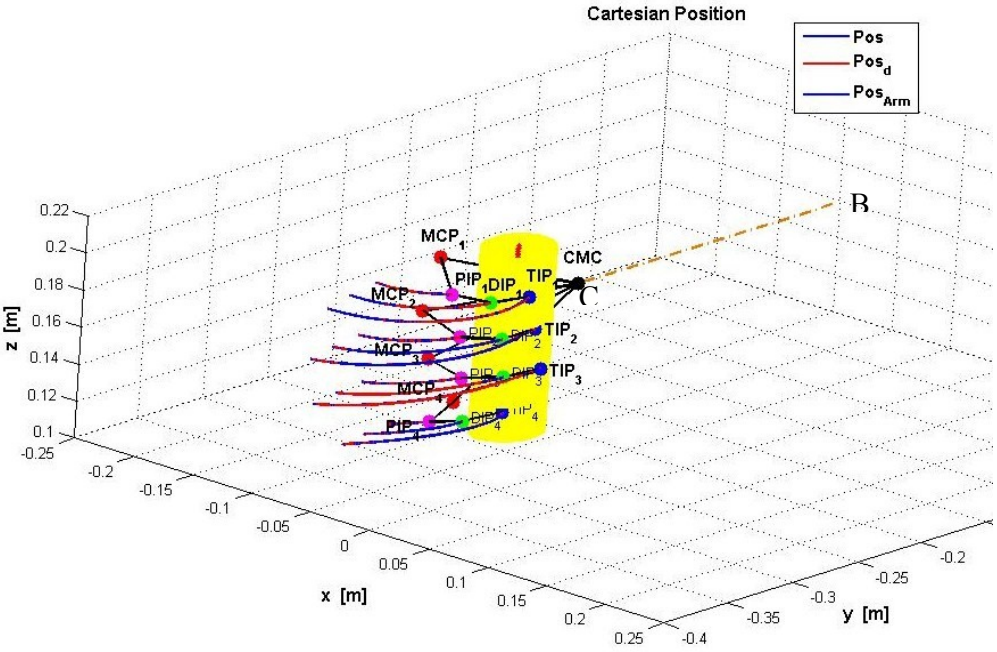

Fig. 80: Grasp configuration of the real hand-arm robotic system.

In Fig. 80, the path described by PIP, DIP and TIP during the grasping action is also represented: the desired path is in red and the actual path is in blue.

A typical reach-and-grasp experimental trial lasted 4.2 s. During reaching, the MIT-Manus moved in 2 s along a straight line from the initial position B=(-0.1, 0.1) m to the final point C=(-0.1, -0.1) m. The corresponding CMC position coming out from the optimization algorithm, was (x=-0.055m, y=0.1602). It accounts for the offset between arm end effector and hand CMC due to the flange. The reaching movement was followed by 1 s of settlement. Thus, grasping was performed by the hand in 1.2 s. Three snapshots of the arm-hand robotic system

Tesi di dottorato in Ingegneria Biomedica, di Antonino Salerno,
discussa presso l'Università Campus Bio-Medico di Roma in data 20/03/2012.
La disseminazione e la riproduzione di questo documento sono consentite per scopi di didattica e ricerca,
a condizione che ne venga citata la fonte

during the experimental trials are shown in Fig. 81. They show, respectively, the initial position during the reaching phase and the power grasp following preshaping. The cylindrical object to grasp had radius 0.0224 m and was located in (-0.051, -0.257) m in the MIT-Manus reference frame.

(a) (b) (c)

Fig. 81: (a) starting point of the reaching phase; (b) end point of the reaching phase; (c) grasping action completed

The control gains used for MIT-Manus PD control in the Cartesian space and DLR-HIT-Hand II PD control in the joint space are, respectively:

$$K_{P_{MANUS}} = diag\{800,800\}\ N/m,$$
$$K_{D_{MANUS}} = diag\{80,80\}\ Ns/m,$$
$$\left.\begin{aligned} K_{P_{HAND}} &= 0.3 Nm/rad \\ K_{D_{HAND}} &= 0.02 Nms/rad \end{aligned}\right] \quad \text{MCP joint},$$
$$\left.\begin{aligned} K_{P_{HAND}} &= 0.4 Nm/rad \\ K_{D_{HAND}} &= 0.027 Nms/rad \end{aligned}\right] \quad \text{PIP joint},$$

Fig. 82 reports arm Cartesian position and position error in norm during reaching. On the other hand, experimental results of grasping phase are drawn in Fig. 83; it shows the position error in norm of MCP and PIP joints during preshaping.

Tesi di dottorato in Ingegneria Biomedica, di Antonino Salerno,
discussa presso l'Università Campus Bio-Medico di Roma in data 20/03/2012.
La disseminazione e la riproduzione di questo documento sono consentite per scopi di didattica e ricerca,
a condizione che ne venga citata la fonte

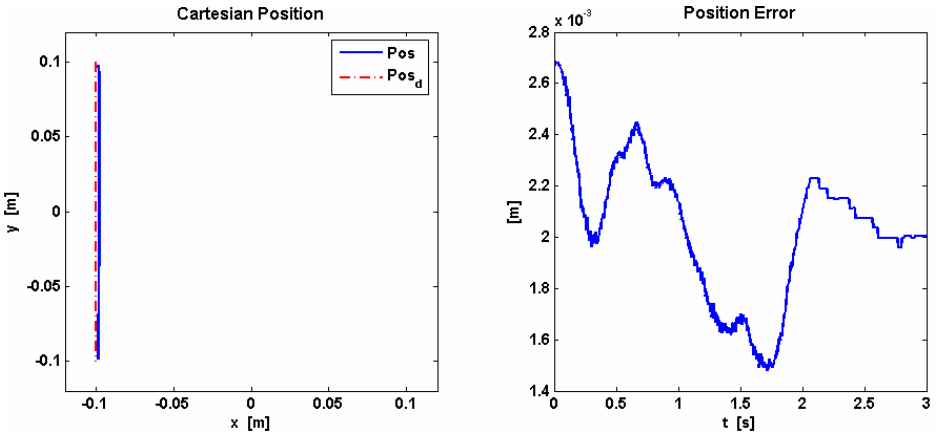

Fig. 82: Plots of the arm Cartesian position and position error in norm.

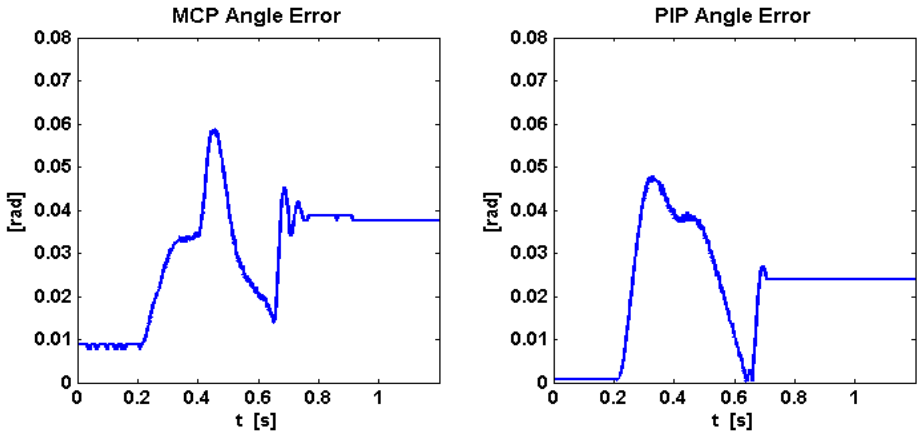

Fig. 83: Plots of the MCP and PIP joint angle trajectory tracking error.

The experiment was repeated for cylinders of different radii. In particular three cases were tested:

A) $r_{obj} = 0.0224m$;

B) $r_{obj} = 0.0236m$;

C) $r_{obj} = 0.0158m$.

In Table X the experimental results, in terms of optimal joint angle values given by the algorithm and effective angles actually reached by the DLR-HIT-Hand are shown.

The convention used in Table IV, for each row, is:

Tesi di dottorato in Ingegneria Biomedica, di Antonino Salerno,
discussa presso l'Università Campus Bio-Medico di Roma in data 20/03/2012.
La disseminazione e la riproduzione di questo documento sono consentite per scopi di didattica e ricerca,
a condizione che ne venga citata la fonte

$$\vartheta_{joint} = \left[\vartheta_{joint}^{index} \quad \vartheta_{joint}^{middle} \quad \vartheta_{joint}^{ring} \quad \vartheta_{joint}^{little} \right],$$

where subscript *joint* can be MCP or PIP.

TABLE X: EXPERIMENTAL RESULTS

Case analyzed	Optimal joint angle (degrees)	Effective joint angle (degrees)
A	ϑ_{MCP} =[61.4 74.6 67.4 44.1]	ϑ_{MCP} =[55 65 65 30]
	ϑ_{PIP} =[49.8 38.9 45.5 55.1]	ϑ_{PIP} =[55 48 50 60]
B	ϑ_{MCP} =[45 47 44 45]	ϑ_{MCP} =[45 57 48 30]
	ϑ_{PIP} =[47.8 37.4 43.6 52.9]	ϑ_{PIP} =[45 47 44 45]
C	ϑ_{MCP} =[66.7 81.2 73.4 47.2]	ϑ_{MCP} =[60 84 70 36]
	ϑ_{PIP} =[63.4 49.9 58.1 69.8]	ϑ_{PIP} =[60 60 60 70]

It is worth observing that position errors between the algorithm optimal joint angles and actual finger joint angles in some cases reach values around 10°. The cause is the hand mechanical structure that do not allow completely reaching the desired joint configurations extracted by the optimization algorithm. As already mentioned in the sections above, two main drawbacks emerged in the experimental session that degraded performance of the reach-and-grasp algorithm:

- the thumb was mechanically constrained to a fixed opposition of 35.51° in the xy-plane with an inclination, respect to z-axis, of 44.13°. This does not allow performing every type of grasp.
- PIP and DIP joints are 1:1 coupled, while in humans, the ratio between them seems to be around 2/3 [251]-[252]. The main consequence is that for some objects (especially for large radii), the final TIP position calculated by the algorithm falls within the object, beyond the object surface.

Tesi di dottorato in Ingegneria Biomedica, di Antonino Salerno,
discussa presso l'Università Campus Bio-Medico di Roma in data 20/03/2012.
La disseminazione e la riproduzione di questo documento sono consentite per scopi di didattica e ricerca,
a condizione che ne venga citata la fonte

5.5 Extension of the algorithm to transversal volar grasp

This section describes how the algorithm presented in previous sections and referred to diagonal volar grasp in Fig. 75 can be applied to transverse volar grasp in Fig. 84 that introduces the thumb behaviour in the grasping action.

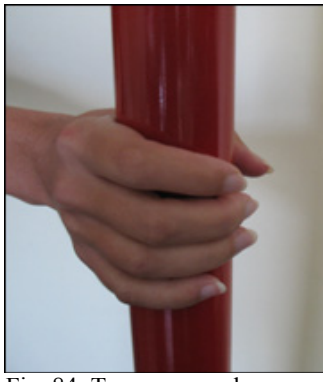

Fig. 84: Transverse volar grasp

By analyzing the robotic literature, it is interesting to note a sizeable lack of information about the thumb behaviour, despite its fundamental role during the grasping action. Inadequate information about the thumb are mainly related to the analysis of functional aspects. Different techniques can be used for measuring the Range Of Motion (ROM) of the fingers [253], e.g. goniometers [254], ultrasound [255], virtual glove, marker-based motion capture [256]. The main advantage of the latter technique with respect to using a data-glove is the possibility of adapting the marker position to hands of different size, thus enabling the generalization of results independently of subject hand size.

Thus, an optoelectronic motion analysis system has been used for collecting information about the thumb and fingers behaviour during grasping. The obtained results have been used for going through the optimization algorithm for determining the optimal grasp configuration for a robotic hand described previously and extending it to 5 fingers.

Tesi di dottorato in Ingegneria Biomedica, di Antonino Salerno,
discussa presso l'Università Campus Bio-Medico di Roma in data 20/03/2012.
La disseminazione e la riproduzione di questo documento sono consentite per scopi di didattica e ricerca,
a condizione che ne venga citata la fonte

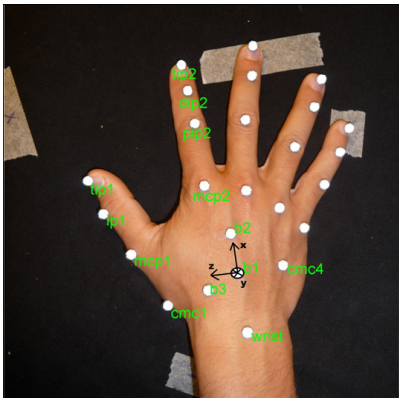

Fig. 85: Marker configuration with reference frame in black

Seven human subjects, 31.7 years old in the average (8.75 Standard Deviation), five men and two women, all right handed, volunteered to participate in this study. Following a predetermined protocol, subjects have been asked to grasp a cylindrical object of 6 cm diameter with a diagonal volar grasp (Fig. 75) and, subsequently, with a transverse volar grasp (Fig. 84) for 10 times each. A Vicon 8-camera motion analisys system has been used to capture data from all the trials; 25 reflective markers of 6 mm diameter were placed on their right hand (Fig. 85). In order to understand if a common behaviour among subjects can be observed during the grasping action, a set of performance parameters have been extracted from the data collected with the Vicon system. They are listed in the following:

- The aperture angle of the hand: it is calculated as the angle between the link connecting the MCP joint of the thumb and the wrist and the link connecting the MCP joint of the index finger and the wrist.
- The radius of curvature of every finger; it is the radius of the obsculator circles tangent, at each joint, the spline passing throughout the finger joints.
- The adduction/abduction angle between the fingers: it is the angle between two adjacent fingers and it is subtended by the distance between the PIP joints of the two fingers.

Tesi di dottorato in Ingegneria Biomedica, di Antonino Salerno,
discussa presso l'Università Campus Bio-Medico di Roma in data 20/03/2012.
La disseminazione e la riproduzione di questo documento sono consentite per scopi di didattica e ricerca,
a condizione che ne venga citata la fonte

- The thumb opposition angle.

In order to compute the thumb opposition angle, two components have been calculated:

- the angle between the projection of the link connecting the MCP joint of the index finger and the CMC1 joint (see Fig. 85) of the thumb onto the xy-plane and the x-axis (see Fig. 74 for the coordinate system);
- the angle between the projection of the link connecting the CMC1 and the MCP1 thumb joints onto the z-axis and the link itself.

In Table XI mean and standard deviation of hand aperture angle during the 10 trials are listed for the diagonal and the transverse volar grasp. From the values it is possible to note a quite invariant behaviour among subjects for the same type of grasp. This consideration gives a general rule about the thumb configuration during the two types of grasp that can be applied to the grasping algorithm explained in section 5.2.

	Diagonal volar grasp		Transverse volar grasp	
Subject #	Mean	SDV	Mean	SDV
1	49.54°	1.39°	51.60°	0.56°
2	48.68°	1.61°	58.27°	1.54°
3	50.39°	1.22°	53.13°	0.42°
4	56.83°	1.91°	52.39°	4.90°
5	56.77°	2.13°	58.67°	1.11°
6	51.56°	1.30°	59.06°	0.38°
7	53.57°	0.68°	59.43°	1.48°

Table XI: Hand aperture angle in transverse and diagonal volar grasp.

The results regarding the radius of curvature will be discussed in following in order to compare the performance of the optimization algorithm for robotic hands with trials on human.

As regards the thumb, the important finding retrieved by the experimental data on human subjects is that the hand aperture angle is quite invariant from subject to subject when a transverse volar grasp is performed. Therefore, assuming that it is known, the MCP joint position can be found with respect to the CMC joint, thus enabling the extension of the optimization algorithm also to the thumb. This

Tesi di dottorato in Ingegneria Biomedica, di Antonino Salerno,
discussa presso l'Università Campus Bio-Medico di Roma in data 20/03/2012.
La disseminazione e la riproduzione di questo documento sono consentite per scopi di didattica e ricerca,
a condizione che ne venga citata la fonte

means that the position of the other thumb joints of the robotic hand can be obtained by minimizing the distances from the thumb joints and the object surface by means of eqs. (5.1) - (5.5). Therefore minimizing the sum of the distance of all joints of each finger is possible to find the optimal grasp configuration according to the object features. Adopting these assumptions several reach and grasp trials have been carried out with objects of different diameter.

The experimental setup and working scenario was the same shown in sect. 5.3 and for brevity only the results for a cylinder with diameter equal to 0.045 m are highlighted for the arm-hand system consistent of MIT-Manus and DLR-HIT Hand II. For the robotic system the same set of gain was chosen to perform reaching and grasping trials.

The obtain results are shown in Fig. 86, where the joints trajectories are reported in the cartesian space.

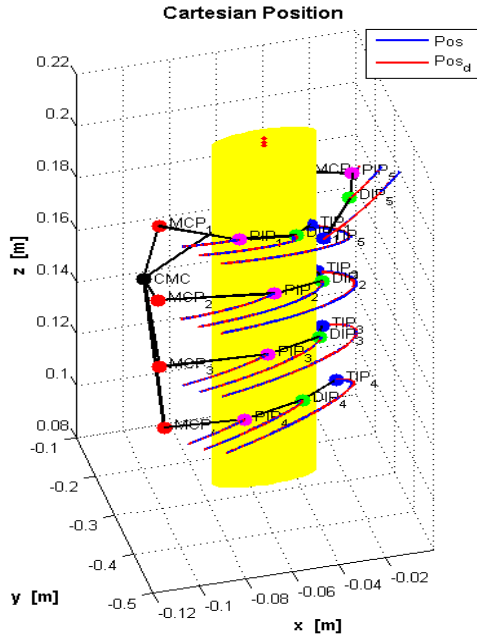

Fig. 86: Hand joints trajectory in the cartesian space for the DLR-HIT-Hand II grasping a cylindrical object with radius 0.020 m.

Tesi di dottorato in Ingegneria Biomedica, di Antonino Salerno,
discussa presso l'Università Campus Bio-Medico di Roma in data 20/03/2012.
La disseminazione e la riproduzione di questo documento sono consentite per scopi di didattica e ricerca,
a condizione che ne venga citata la fonte

The values obtained from the optimization algorithm (i.e. CMC position and flexion and adduction angles for all fingers) have been given in input to the real arm-hand robotic system.

The MIT-Manus moves the hand in such a way that its CMC joint reaches the position defined by the algorithm. Thus, the hand closes the fingers to reach the desired angles for each joint. For the arm, a point-to-point movement has been performed in 3.0 s for each trial, starting from the initial position P_i = [-0.1 0.1]^{T}m to final position P_f = [-0.0975 -0.1245]^{T}m. The final position, reported only for grasping an object with radius of 0.0225 m for sake of brevity, takes into account the CMC position supplied by the algorithm CMC = [-0.0975 -0.179 0.15]^T m as well as the offset between arm end effector and hand CMC due to the flange that connects the DLR-HIT-Hand II to the MIT-Manus robotic arm.

The robotic arm has been controlled for 5.0 s in each trial: (i) three seconds are taken to achieve the final position; (ii) in the last two seconds, the robot holds its posture to enable the grasping phase, lasting 1.2 s. The cylindrical object has been located in (-0.051; -0.257) m in the MIT-Manus reference frame. Once the CMC optimal position has been reached, the hand fingers are moved towards the optimal joint configuration (similarly to Fig. 81).

Table XII reports actual Cartesian coordinates for each joint of the robotic hand performing the transverse diagonal task and compare them with the Cartesian coordinates produced by the optimization algorithm. On the other hand, Table XIII provides the values of the radius of curvature for the robotic hand in the grasping configuration and the comparison with the values calculated for human case and for the output of the optimization algorithm for an object radius of 0.0225 m.

Tesi di dottorato in Ingegneria Biomedica, di Antonino Salerno,
discussa presso l'Università Campus Bio-Medico di Roma in data 20/03/2012.
La disseminazione e la riproduzione di questo documento sono consentite per scopi di didattica e ricerca,
a condizione che ne venga citata la fonte

		"Cartesian position"	
Finger	Joint	Algorithm	Robotic hand
index	MCP	$[0 \;\; 0.045 \;\; 0.088]^T$ m	$[-0.0025 \;\; 0.0368 \;\; 0.1078]^T$ m
	PIP	$[0.0485 \;\; 0.0468 \;\; 0.1040]^T$ m	$[0.0264 \;\; 0.0343 \;\; 0.1545]^T$ m
	DIP	$[0.0672 \;\; 0.0454 \;\; 0.0877]^T$ m	$[0.0513 \;\; 0.0321 \;\; 0.1526]^T$ m
	TIP	$[0.0770 \;\; 0.0434 \;\; 0.0648]^T$ m	$[0.0612 \;\; 0.0312 \;\; 0.1297]^T$ m
middle	MCP	$[0.0012 \;\; 0.0100 \;\; 0.0977]^T$ m	$[-0.0037 \;\; 0.0100 \;\; 0.1178]^T$ m
	PIP	$[0.0541 \;\; 0.0100 \;\; 0.1126]^T$ m	$[0.0437 \;\; 0.0100 \;\; 0.1457]^T$ m
	DIP	$[0.0716 \;\; 0.0100 \;\; 0.0947]^T$ m	$[0.0655 \;\; 0.0100 \;\; 0.1335]^T$ m
	TIP	$[0.0789 \;\; 0.0100 \;\; 0.0708]^T$ m	$[0.0659 \;\; 0.0100 \;\; 0.1085]^T$ m
ring	MCP	$[0 \;\; -0.0250 \;\; 0.0925]^T$ m	$[-0.0025 \;\; -0.0168 \;\; 0.1126]^T$ m
	PIP	$[0.0515 \;\; -0.0268 \;\; 0.1093]^T$ m	$[0.0409 \;\; -0.0130 \;\; 0.1462]^T$ m
	DIP	$[0.0695 \;\; -0.0253 \;\; 0.0922]^T$ m	$[0.0641 \;\; -0.0110 \;\; 0.1371]^T$ m
	TIP	$[0.0784 \;\; -0.0233 \;\; 0.0690]^T$ m	$[0.0685 \;\; -0.0106 \;\; 0.1125]^T$ m
little	MCP	$[-0.0035 \;\; -0.0600 \;\; 0.0735]^T$ m	$[0.0010 \;\; -0.0434 \;\; 0.0936]^T$ m
	PIP	$[0.0365 \;\; -0.0635 \;\; 0.0905]^T$ m	$[0.0313 \;\; -0.0380 \;\; 0.1391]^T$ m
	DIP	$[0.0584 \;\; -0.0615 \;\; 0.0794]^T$ m	$[0.0559 \;\; -0.0337 \;\; 0.1409]^T$ m
	TIP	$[0.0643 \;\; -0.0574 \;\; 0.0558]^T$ m	$[0.0724 \;\; -0.0308 \;\; 0.1223]^T$ m
thumb	MCP	$[0.0647 \;\; 0.0444 \;\; 0.0586]^T$ m	$[0.0622 \;\; 0.0444 \;\; 0.0787]^T$ m
	PIP	$[0.1631 \;\; 0.0720 \;\; 0.0924]^T$ m	$[0.0791 \;\; 0.0496 \;\; 0.1308]^T$ m
	DIP	$[0.1460 \;\; 0.0784 \;\; 0.1047]^T$ m	$[0.0767 \;\; 0.0447 \;\; 0.1552]^T$ m
	TIP	$[0.1248 \;\; 0.0733 \;\; 0.1012]^T$ m	$[0.0648 \;\; 0.0339 \;\; 0.1744]^T$ m

Table XII: Joints cartesian coordinates coming from the optimization algorithm and measured on the robotic hand, in the case of object radius = 0.0225 m in hand reference frame

		"Values of radius of curvature		
Finger	Joint	Human being	Algorithm	Robotic hand
index	MCP	$9.55 * 10^{16} m$	$6.96 * 10^{14} m$	$3.85 * 10^{14} m$
	PIP	$0.028m$	$0.024m$	$0.025m$
	DIP	$0.033m$	$0.029m$	$0.019m$
	TIP	$1.01 * 10^{17} m$	$2.36 * 10^{14} m$	$4.24 * 10^{14} m$
middle	MCP	$7.48 * 10^{16} m$	$5.75 * 10^{15} mm$	$5.9 * 10^{14} m$
	PIP	$0.037m$	$0.024m$	$0.022m$
	DIP	$0.032m$	$0.028m$	$0.016m$
	TIP	$8.9 * 10^{16} m$	$2.2 * 10^{15} m$	$6.5 * 10^{14} m$
ring	MCP	$7.16 * 10^{16} m$	$7.7 * 10^{15} m$	$8.58 * 10^{13} m$
	PIP	$0.037m$	$0.023m$	$0.24m$
	DIP	$0.038m$	$0.03m$	$0.018m$
	TIP	$9.94 * 10^{16} m$	$1.49 * 10^{15} m$	$6.98 * 10^{13} m$
little	MCP	$6.58 * 10^{16} m$	$9.9 * 10^{13} m$	$7.95 * 10^{15} m$
	PIP	$0.043m$	$0.033m$	$0.027m$
	DIP	$0.032m$	$0.014m$	$0.020m$
	TIP	$1.14 * 10^{17} m$	$1.11 * 10^{14} m$	$1.68 * 10^{14} m$
thumb	TM	$3.22 * 10^{16} m$	$7.01 * 10^{14} m$	$2.8 * 10^{14} m$
	MCP	$0.051m$	$0.018m$	$0.043m$
	IP	$0.028m$	0.025	$0.032m$
	TIP	$9.66 * 10^{16} m$	$8.45 * 10^{13} m$	$1.41 * 10^{14} m$

Table XIII: values of the radius of curvature for the human subjects, the output of the optimization algorithm and the robotic hand in case of object radius = 0.0225 m

The main observation concerns the difference in the Cartesian coordinates for the algorithm and the robotic hand and, consequently, for the finger joints. It is due to the mechanical structure of the robotic hand that constraints the motion of the thumb and the DIP joints in a way that is different with respect to the human

Tesi di dottorato in Ingegneria Biomedica, di Antonino Salerno,
discussa presso l'Università Campus Bio-Medico di Roma in data 20/03/2012.
La disseminazione e la riproduzione di questo documento sono consentite per scopi di didattica e ricerca,
a condizione che ne venga citata la fonte

hand. In particular, the robotic thumb is mechanically constrained to a fixed opposition of 35.51° in the xy-plane with an inclination of 44.13° with respect to z-axis; instead, from the analysis of the data obtained with the Vicon system on the human subjects, the angle in the xy-plane is on average 33° and the angle with respect to z-axis is around 37°. Also the aperture angle is different: about 37° for the robotic hand, 56° on average for the human hand.

Since the algorithm is based on data obtained from the observation of human behaviour, obviously there is a difference in the experimental results, due to the different mechanical structure of the hand performing the task. Nevertheless, interestingly, the values obtained for the radius of curvature of the joints of the DLR-HIT-HAND II are very similar to those computed using the data obtained from the algorithm and from the observation of human beings (see Table XII). Additionally it worth noticing that the radius of curvature values for MCP joints of the long finger and TM joint of the thumb are not of interest due to the definition of this quantity. In fact, the radius of curvature is the radius of the obsculator circle tangent, at each joint, the spline passing throughout the finger joints with initial point placed on CMC. Thus calculating the radius of curvature at MCP joint means to search this physical quantity for a linear path and this tends to infinitive.

Taking into account the mechanical constrains of the DLR-HIT\HAND II and the matching with human grasp of spherical objects, the optimization algorithm could be applied to tridigital grasp of spherical objects. To this purpose, the human grasp mechanism during grasping tasks of spherical objects is investigated at Campus Bio-Medico University. The distance between the center of the sphere and each fingers joint is computed by means of BTS motion capture system. Based on these experimental results, the algorithm adaptation to tridigital grasping of spherical objects for the robotic hand will be evaluated taking also into account the fingers orientation.

Tesi di dottorato in Ingegneria Biomedica, di Antonino Salerno,
discussa presso l'Università Campus Bio-Medico di Roma in data 20/03/2012.
La disseminazione e la riproduzione di questo documento sono consentite per scopi di didattica e ricerca,
a condizione che ne venga citata la fonte

Chapter 6

Conclusions

In this chapter the conclusions and ideas for futures works are reported. The first part of this thesis was focused on the implementation of control systems for rehabilitative (end-effector) machines of the upper limb. In the second part special attention is paid on the development of a optimization criterion for retrieving the contact points and the optimal hand posture for reach and grasp taks performed by a robotic arm-hand system.

The contents organization of this chapter reflects the overall structure of the thesis. In section 6.1 the conclusions on development of new control systems (submovements-based and current-based controls) for robot aided therapy are reported; Section 6.2 concludes the activity on the development of the

Tesi di dottorato in Ingegneria Biomedica, di Antonino Salerno,
discussa presso l'Università Campus Bio-Medico di Roma in data 20/03/2012.
La disseminazione e la riproduzione di questo documento sono consentite per scopi di didattica e ricerca,
a condizione che ne venga citata la fonte

optimization algorithm for reach and grasp tasks described in chapter 5. Finally section 6.3 illustrates the possible future works for all the explained themes.

6.1 Conclusions on developed control systems for robot-aided rehabilitation

In the field of rehabilitation robotics two complementary approaches have been proposed. The first relies on findings on motion generation of the human motor control, whereas the second one is mainly based on impedance control exploiting the motor currents monitoring to reconstuct the force applied on the robot end-effector and modelling of system dynamics including generally neglected terms such as frictions.

In the chapter 3 a new robot control approach was presented, which relies on recent findings in neuroscience on intermittent nature of neural control in movement and sensorymotor coordination. Firstly a feasibility study has been carried out on the possibility to generate submovements with predetermined features.

The experimental results showed that: (i) In motion control, positioning accuracy was related to submovements amplitude and number. In particular, amplitude increase caused a degradation of position error, whereas an increase of the number of motion units determined error improvement and, correspondingly, velocity reduction. Further, a dependence on motion units order and symmetry in a single sequence was also observed, thus demonstrating that a global smoother bell-shaped velocity profile improved performance in positioning tasks. (ii) In interaction control, experimental results showed that peak force and occurrence of peak force could be regulated by properly ordering submovements in a sequence during the impact. Furthermore, the number of motion units notably affected the

Tesi di dottorato in Ingegneria Biomedica, di Antonino Salerno,
discussa presso l'Università Campus Bio-Medico di Roma in data 20/03/2012.
La disseminazione e la riproduzione di questo documento sono consentite per scopi di didattica e ricerca,
a condizione che ne venga citata la fonte

average level of exerted force. An increase of the interaction force with the number of submovements was observed, comparable to the increase generated by PD control with higher stiffness gains in the traditional approach. Once demonstrated the capabilities of the approach a robot control based on dynamic submovements motion generator has been developed and implemented.

The core of the robot control is a dynamic sequence generator module, in charge of on-line generating sequences of elementary motion units, named submovements, that are opportunely scaled in number and amplitude in accordance with task requirements. The novel sequence generator was implemented exploiting the dynamic behaviour of four oscillators opportunely dephased and modulated in amplitude. A modulation function able to modify submovement features was experimentally identified on a 2-dof robot arm. The theoretical formulation of the proposed control approach was presented and the validation on a 2-dof robot arm was carried out by means of experimental trials of motion in free space and simulation tests of interaction with an external elastic environment.

The results showed that in the free space the use of the dynamic sequence generator achieves position regulation with different accuracy as traditionally does with offline gains change in a tradition PD control. In addition, accuracy can improve with respect to a traditional PD control with the same gains. In particular, the submovement-based dynamic generator improves system accuracy up to 5mm and robot presents a more isotropic behaviour. In the interaction control, the submovement-based approach was able to achieve a force regulation action comparable to the effect of control gain change in a traditional PD control. This results cannot be achieved by employing a standard PD controller during the reaching task execution, but an offline tuning of the control gains is needed.

As regards the second topic of the research on rehabilitation robotics, the work has been focussed on an interaction control for rehabilitation machines with

Tesi di dottorato in Ingegneria Biomedica, di Antonino Salerno,
discussa presso l'Università Campus Bio-Medico di Roma in data 20/03/2012.
La disseminazione e la riproduzione di questo documento sono consentite per scopi di didattica e ricerca,
a condizione che ne venga citata la fonte

unnegligible friction and low capabilities of finely tuning visco-elastic properties. An impedance control based on inverse dynamics and electric current feedback was proposed in order to compensate for friction and improve system performance in the interaction with the patient without increasing moving masses and wires due to force sensor.

The control approach was applied to the CBM-Motus rehabilitation machine. It was kinematically and dynamically modeled, and a characterization of static and dynamic friction was carried out. The friction identification procedure was validated by means of experimental trials of motion tracking; the interaction control law was tested in experimental trials of constrained motion and experimentally compared to a traditional impedance control based on position feedback.

The work demonstrated that current-based impedance control can solve issues related to degradation of robot performance due to friction, thanks to inverse dynamics compensation, and outperforms impedance control purely based on position control, thanks to indirect force measure through electric currents. The compared analysis of control performance pointed out that current feedback can decouple the system, similarly to a force feedback, and simplify gain tuning, by allowing the same set of PD gains (e.g. K_P = diag{100; 100} and K_D = diag{10; 10}) to be used in free as well as constrained space with a good level of accuracy (0.004 m is the peak of position error) and force regulation (h = 21.41 N is the peak of interaction force) for the addressed application. Intrinsically being an inverse dynamics control, current-based impedance control has the same level of applicability of a traditional impedance control. Therefore, it has the same main limiting factor of requiring estimating robot dynamic parameters, which is demanding especially for complex structures. This entails a meaningful increase of control computational burden with the number of robot degrees of freedom but, conversely, it allows successfully controlling simple as well as very complex

Tesi di dottorato in Ingegneria Biomedica, di Antonino Salerno,
discussa presso l'Università Campus Bio-Medico di Roma in data 20/03/2012.
La disseminazione e la riproduzione di questo documento sono consentite per scopi di didattica e ricerca,
a condizione che ne venga citata la fonte

robotic structures, also in presence of tendon-driven transmission and coupling in the joints [203].

Main novelties of the proposed control with respect to the traditional impedance control are (i) friction compensation, often neglected, and (ii) current monitoring, used to detect interaction with the patient. Both issues require to continuously carry out estimation procedures of static and dynamic friction and current threshold, because of their variability with environmental conditions. In our case, this was efficiently achieved by developing an initial robot calibration procedure, running every time the machine is turned on, that is able to automatically implement friction identification procedure described in Sect. 4.3 and current threshold identification, mentioned in Sect. 4.5.

The proposed interaction control strongly relies on the identification of force-current relationship and is applied in this work to the robotic machine developed by the authors, which has a simple planar structure. However, it can be extended to more complex robotic structure with electric actuation by means of a multivariate regression analysis. Special care is required for redundant robots, where redundancy needs to be addressed by an inverse kinematic algorithm before applying the force-current characterization procedure.

Apart from the need of a preliminary linear regression analysis to define force/torque relation, the use of electric currents to detect interaction offers the important benefits of (1) higher reliability than force sensors, notoriously characterized by significant noise; noise is much lower in current readings with no need for low-pass filtering; (2) robustness, being the probability of damages to force sensors higher than that for electric actuators.

This is an important achievement in rehabilitation robotics, since it answers a more general aim of enhancing robot dependability in human-robot interaction.

Tesi di dottorato in Ingegneria Biomedica, di Antonino Salerno,
discussa presso l'Università Campus Bio-Medico di Roma in data 20/03/2012.
La disseminazione e la riproduzione di questo documento sono consentite per scopi di didattica e ricerca,
a condizione che ne venga citata la fonte

6.2 Conclusions on developed control system for grasping activities

A biologically inspired approach for finding the optimal grasp configuration has been presented in chapter 5. It focuses on the prediction of the final position of the reaching movement and the optimal finger configuration for a power grasp, provided information on object size and location. The algorithm accounts for data on human subjects partly retrieved in the literature and partly obtained by the direct observation of human behavior during diagonal and transverse volar grasps. The proposed approach on one hand provides new insights into the comprehension of the human grasping strategy and, on the other hand, provides a general rule for grasping cylindrical objects with an anthropomorphic robotic hand. It has been preliminary tested in simulation and validated through experimental trials with a real arm-hand robotic system, composed of the MIT-Manus robot arm and the DLR-HIT-Hand II. Experimental results on the described robotic platform have proved its feasibility and reliability but have also shown limitations in the grasping tasks due to constraints imposed by the mechanical structure, not completely addressing the similarity with the human structure. Indeed, the robotic hand involved in the sperimentation presented two main drawbacks: (i) the robotic thumb is mechanically placed to a fixed opposition of 35.51° in the xy plane and 44.13° with respect to z-axis of the chosen reference frame; (ii) for each finger PIP and DIP joints are 1:1 coupled. This entails that for objects with large radii, the TIP final position falls inside the object surface.

Tesi di dottorato in Ingegneria Biomedica, di Antonino Salerno,
discussa presso l'Università Campus Bio-Medico di Roma in data 20/03/2012.
La disseminazione e la riproduzione di questo documento sono consentite per scopi di didattica e ricerca,
a condizione che ne venga citata la fonte

6.3 Future works

The submovements-based control approach has been presented and validated in condition of structured environment.
Future efforts will be addressed to the experimental validation of the submovement-based control in the interaction with patients. Additionally the extension to the 3-D space motion will be considered in order to offer a wider workspace where trains the patient with point-to-point motions. Additionally, comparative tests among different tasks in interaction and motion control will be carried out in order to validate the control approach in different working contexts.

As regards current-based impedance control described in chapter 4, future efforts will be addressed to further validate the control with an extensive comparative analysis with other sensorless approaches proposed in the literature and finalize system behaviour for an extensive use in clinical practice with neurological patients (such as chronic post-stroke, inpatients, brain injured people). An application of the CBM-Motus robotic system to tele-rehabilitation is finally envisaged.
Moreover the current-based and submovements-based could be contemporaneously applied to the same robotic system able to provide 3D motor tasks with electric actuation.

The activities on the design and development of an algorithm for the optimal grasp configuration were mainly focussed on cilindrical objects, but future work will be devoted to extend this approach to other types of objects, also taking into account mechanical constraints coming from the available robotic hand, and to deepen studies on the thumb configuration in grasping tasks, still being neglected in the current literature. An application of the algorithm for the optimal grasp configuration to prosthetic hands is envisaged as prosecution of the work.

Tesi di dottorato in Ingegneria Biomedica, di Antonino Salerno,
discussa presso l'Università Campus Bio-Medico di Roma in data 20/03/2012.
La disseminazione e la riproduzione di questo documento sono consentite per scopi di didattica e ricerca,
a condizione che ne venga citata la fonte

Currently studies on humans are investigating the extension of the optimization gasp algorithm to tridigital grasp of spherical objects. The experimentation is carried out at Campus Bio-Medico University, by using the BTS motion capture system in order to evaluate the distance of each anatomical finger joint from the centre of spherical objects. It is expected that the grasp algorithm explained in chapter 5 could be extended to tridigital gasp of spherical objects with minor revisions related to the finger orientation. The feasibility of the algorithm extension to tridigital grasp will be investigated in future researches.

Tesi di dottorato in Ingegneria Biomedica, di Antonino Salerno,
discussa presso l'Università Campus Bio-Medico di Roma in data 20/03/2012.
La disseminazione e la riproduzione di questo documento sono consentite per scopi di didattica e ricerca,
a condizione che ne venga citata la fonte

List of publications

Journal papers

Franciso J. Badesa, Ricardo Morales, Nicolas Garcia-Aracil, Carlos Perez-Vidal, Jose M. Sabater, Eugenia Papaleo, **Antonino Salerno**, Loredana Zollo, Eugenio Guglielmelli, "Development of an Intelligent Multimodal Assistive Robot", Robotics & Automation Magazine, **submitted**.

L. Zollo, **A. Salerno**, M. Vespignani, D. Accoto, M. Passalacqua, E. Guglielmelli, "Control of a Planar Robotic Machine for Neuro-Rehabilitation of the Upper Limb", *Advanced Robotics*, **submitted**.

F. Cordella, L. Zollo, **A. Salerno**, E. Guglielmelli, B. Siciliano, "Development and Experimental Validation of a Grasp Optimization Algorithm for a Robotic Hand Inspired to Human Behaviour", *IEEE\ASME Transaction on Mechatronics*, Focused Section on Bio-Inspired Mechatronics, **submitted**.

I. Gaudiello, D. Caligiore, G. Schiavone, **A. Salerno**, F. Sergi, L. Zollo, E. Guglielmelli, D. Parisi, G. Baldassarre, R. Nicoletti and A. M. Borghi, "Effect on space representation of using a tool and a button", *Cognitive Processing*. Special Issue pp. 153-154, September 2009.

Conference papers

F. Cordella, L. Zollo, **A. Salerno**, E. Guglielmelli, and B. Siciliano, "Validation of a power grasping algorithm for an anthropomorphic robotic hand on the basis of human grasping action", 13th International Symposium on Advances in Robot Kinematics (ARK 2012), June 2012, Innsbruck, Austria, **accepted**.

Antonino Salerno, Loredana Zollo, Eugenio Guglielmelli, "Dynamic Sequence Generator for the Control of a Robot Manipulator", GNB2012, June 26th-29th 2012, Rome, Italy, **submitted**.

Antonino Salerno, Loredana Zollo, Eugenio Guglielmelli, "Dynamic Submovement Composition for Motion and Interaction Control of a Robot Manipulator", IEEE International Conference on Biomedical Robotics and Biomechatronics (BIOROB 2012), June 24th-28th, 2012 Roma, Italy, **accepted**.

Tesi di dottorato in Ingegneria Biomedica, di Antonino Salerno,
discussa presso l'Università Campus Bio-Medico di Roma in data 20/03/2012.
La disseminazione e la riproduzione di questo documento sono consentite per scopi di didattica e ricerca,
a condizione che ne venga citata la fonte

F. Cordella, L. Zollo, **A. Salerno**, E. Guglielmelli, B. Siciliano, "Experimental Validation of a Reach-and-Grasp Optimization Algorithm Inspired to Human Arm-Hand Control", *33rd Annual International Conference of the IEEE Engineering in Medicine and Biology Society* (EMBC 2011), Boston, August 30th-September 3rd, 2011.

Luca Rossini, **Antonino Salerno**, Loredana Zollo, Eugenio Guglielmelli, "Human Movement Decomposition into Submovements for Robot Control in Neuro-Rehabilitation", 14th *European Congress on Clinical Neurophysiology*, Rome, 21-25 June 2011.

L. Zollo, **A. Salerno**, L. Rossini, E. Guglielmelli, "Submovement Composition for Motion and Interaction Control of a Robot Manipulator", *IEEE International Conference on Biomedical Robotics and Biomechatronics* (BIOROB), September 26-29, 2010, Tokyo, Japan.

L. Rossini, **A. Salerno**, L. Zollo, E. Guglielmelli, "Neuroinspired Controller for Motion and Interaction Control of a Robot Manipulator", Secondo Congresso Nazionale di Bioingegneria - Torino, 8-10 Luglio 2010.

A. Salerno, L. Zollo, M. Vespignani, D. Accoto, E. Guglielmelli, "Current based impedance control of a robot with unnegligible friction", in Atti del convegno nazionale NEURORIABILITAZIONE ROBOTICA DELL'ARTO SUPERIORE, 14 e 15 dicembre 2009, Genova.

I. Gaudiello, D. Caligiore, G. Schiavone, **A. Salerno**, F. Sergi, L. Zollo, E. Guglielmelli, D. Parisi, G. Baldassarre, R. Nicoletti, A. M. Borghi, "Effects on space representation of using a tool and a button", *4th International Conference on Spatial Cognition*, Rome 2009.

Workshop

Loredana Zollo, **Antonino Salerno**, Eugenia Papaleo, Eugenio Guglielmelli, Carlos Pérez, Nicolás García, Eduardo Fernández, "Multimodal interfaces to improve therApeutic outcomes in robot-Assisted rehabiliTation", European Robotics Forum Workshop, Västeras/Sweden, April 6-8, 2011.

Tesi di dottorato in Ingegneria Biomedica, di Antonino Salerno,
discussa presso l'Università Campus Bio-Medico di Roma in data 20/03/2012.
La disseminazione e la riproduzione di questo documento sono consentite per scopi di didattica e ricerca,
a condizione che ne venga citata la fonte

Bibliography

[1] Statistics Canada. Morality, Summary List of Causes 2008. Released October 18, 2011.
[2] Tracking Heart Disease and Stroke in Canada. Released June 2009.
[3] Véronique L. Roger, Alan S. Go, Donald M. Lloyd-Jones, Emelia J. Benjamin, Jarett D. Berry, William B. Borden, Dawn M. Bravata, Shifan Dai, Earl S. Ford, Caroline S. Fox, Heather J. Fullerton, Cathleen Gillespie, Susan M. Hailpern, John A. Heit, Virginia J. Howard, Brett M. Kissela, Steven J. Kittner, Daniel T. Lackland, Judith H. Lichtman, Lynda D. Lisabeth, Diane M. Makuc, Gregory M. Marcus, Ariane Marelli, David B. Matchar, Claudia S. Moy, Dariush Mozaffarian, Michael E. Mussolino, Graham Nichol, Nina P. Paynter, Elsayed Z. Soliman, Paul D. Sorlie, Nona Sotoodehnia, Tanya N. Turan, Salim S. Virani, Nathan D. Wong, Daniel Woo and Melanie B. Turner. "Heart Disease and Stroke Statistics--2012 Update: A Report From the American Heart Association". *Circulation: Journal of the American Heart Association*. Published online December 15, 2011.
[4] Kelly-Hayes M, Beiser A, Kase CS, Scaramucci A, D'Agostino RB, Wolf PA. The influence of gender and age on disability following ischemic stroke: the Framingham study. J Stroke Cerebrovasc Dis. 2003;12:119 –126.
[5] JE Harris and JJ Eng. Paretic upper-limb strength best explains arm activity in people with stroke. Phys Ther, 87(1):88–97, 2007.
[6] MM Mirbagheri, L Alibiglou, M Thajchayapong, and WZ Rymer. Muscle and reflex changes with varying joint angle in hemiparetic stroke. J Neuroengineering Rehabil, 5:6, 2008.
[7] JW Lance. What is spasticity? Lancet, 335(8689):606, 1990.
[8] JPA Dewald and RF Beer. Abnormal joint torque patterns in the paretic upper limb of subjects with hemiparesis. Muscle Nerve, 24(1):273–283, 2001.
[9] Kempermann G., Van Praag H., Gage F.H. Activity-dependent regulation of neuronal plasticity and self repair. Prog Brain Res, vol. 127, pp. 35-48, 2000.
[10] J Liepert, H Bauder, H R Wolfgang, W H Miltner, E Taub, and C Weiller. Treatment induced cortical reorganization after stroke in humans. Stroke, 31(6):1210–1216, 2000.
[11] Rakic, P. "Neurogenesis in adult primate neocortex: an evaluation of the evidence". Nature Reviews Neuroscience 3 (1): 65–71. doi:10.1038/nrn700
[12] P Lum, D Reinkesmeyer, R Mahoney, W Z Rymer, and C Burgar. Robotic devices for movement therapy after stroke: Current status and challenges to clinical acceptance. Topics in Stroke Rehabilitation, 8(4):40–53, 2002.
[13] H M Feys, W J De Weerdt, and B E Selz. Effect of a therapeutic intervention for the hemiplegic upper limb in the acute phase after stroke: A single-blind, randomized, controlled multicenter trial. Stroke, 29(4):785–792, 1998.
[14] Marshall RS, Perera GM, Lazar RM, Krakauer JW, Constantine RC, DeLaPaz RL. Evolution of cortical activation during recovery from corticospinal tract infarction. Stroke. 2000;31(3):656–61. [PMID: 10700500]
[15] Cramer SC, Nelles G , Benson RR, Kaplan JD, Parker RA, Kwong KK, Kennedy DN, Finklestein SP, Rosen BR. A functional MRI study of subjects recovered from hemiparetic stroke. Stroke. 1997;28(12):2518–27. [PMID: 9412643]
[16] Cramer SC, Moore CI, Finklestein SP, Rosen BR. A pilot study of somatotopic mapping after cortical infarct. Stroke. 2000;31(3):668–71. [PMID: 10700502]
[17] Cramer SC, Nelles G , Schaechter JD, Kaplan JD, Finklestein SP, Rosen BR. A functional MRI study of three motor tasks in the evaluation of stroke recovery. Neurorehabil Neural Repair. 2001;15(1):1–8. [PMID: 11527274]

Tesi di dottorato in Ingegneria Biomedica, di Antonino Salerno,
discussa presso l'Università Campus Bio-Medico di Roma in data 20/03/2012.
La disseminazione e la riproduzione di questo documento sono consentite per scopi di didattica e ricerca,
a condizione che ne venga citata la fonte

[18] Miyai I, Suzuki T, Mikami A, Kubota K, Volpe BT. Patients with capsular infarct and Wallerian degeneration show persistent regional premotor cortex activation on functional magnetic resonance imaging. J Stroke Cerebrovasc Dis. 2002;10(5):210–16.
[19] Neville Hogan,; Hermano I. Krebs; Brandon Rohrer; Jerome J. Palazzolo; Laura Dipietro; Susan E. Fasoli; Joel Stein; Richard Hughes; Walter R. Frontera; Daniel Lynch; Bruce T. Volpe. Motions or muscles? Some behavioral factors underlying robotic assistance of motor recovery. Journal of Rehabilitation Research & Development, Volume 43, Number 5, Pages 605–618, 2006.
[20] S. SCHULZ, C. PYLATIUK and G. BRETTHAUER, " A New Ultralight Anthropomorphic Hand", Proceedings of the 2001 IEEE International Conference on Robotics & Automation Seoul, Corea, May 2001.
[21] L. Biagiotti, F. Lotti, C. Melchiorri, G. Vassura, "How far is the Human Hand? A review on Anthropomorphic Endeffectors", DIES Internal Report, University of Bologna, 2004.
[22] Bicchi A. Hands for dexterous manipulation and robust grasping: a difficult road toward simplicity. *Robotics and Automation, IEEE Transactions on*, vol. *16*, pp. 652-662, 2000.
[23] Tomovic, R. & Boni, G. An adaptive artificial hand. *Automatic Control, IRE Transactions on*, vol. *7*, pp. 3-10, 1962.
[24] Okada, T. Computer Control of Multijointed Finger System for Precise Object Handling.. *IEEE TRANS. SYS., MAN, AND CYBER.*, vol. *12*, pp. 289-298, 1982.
[25] Salisbury, K. & Roth, B. Kinematics and force analysis of articulated mechanical hands. *Journal of Mechanisms, Transmissions and Actuation in Design*, vol. *105*, pp. 35-41, 1983.
[26] Jacobsen, S., Iversen, E., Knutti, D., Johnson, R. & Biggers, K. Design of the Utah/MIT Dextrous Hand. *Robotics and Automation. Proceedings. 1986 IEEE International Conference on*, 1986.
[27] Bekey, G., Tomovic, R. & Zeljkovic, I. Control architecture for the Belgrade/USC hand. *Book of Dextrous robot hands*, pp. 136-149, 1990.
[28] Townsend, W. The BarrettHand Grasper-Programmably Flexible Part Handling and Assembly. *Industrial Robot: An International Journal*, vol. *27*, pp. 181-188, 2000.
[29] Lotti, F., Tiezzi, P., Vassura, G., Biagiotti, L. & Melchiorri, C. UBH 3: an anthropomorphic hand with simplified endo-skeletal structure and soft continuous fingerpads. *Robotics and Automation, 2004. Proceedings. ICRA'04. 2004 IEEE International Conference on*, *2004*.
[30] Lotti, F., Tiezzi, P., Vassura, G., Biagiotti, L., Palli, G. & Melchiorri, C. Development of UB Hand 3: Early Results. *Robotics and Automation, 2005. Proceedings of the 2005 IEEE International Conference on*, pp. 4488-4493, 2005.
[31] Melchiorri, C. & Vassura, G. Mechanical And Control Features Of The University Of Bologna Hand Version 2. *Intelligent Robots and Systems, 1992., Proceedings of the 1992 lEEE/RSJ International Conference on*, 1992.
[32] Ali, M., Kyriakopoulos, K. & Stephanou, H. The kinematics of the Anthrobot-2 dextrous hand. *Robotics and Automation, 1993. Proceedings., 1993 IEEE International Conference on*, pp. 705-710, 1993.
[33] Crisman, J., Kanojia, C. & Zeid, I. Graspar: a flexible, easily controllable robotic hand. *Robotics & Automation Magazine, IEEE*, vol. *3*, pp. 32-38, 1996.
[34] Butterfass, J., Grebenstein, M., Liu, H. & Hirzinger, G. DLR-Hand II: next generation of a dextrous robot hand. *Robotics and Automation, 2001. Proceedings 2001 ICRA. IEEE International Conference on*, *1*, pp. 109-114, 2001.
[35] Butterfass, J., Hirzinger, G., Knoch, S. & Liu, H. DLR's Multisensory Articulated Hand Part I: Hard and Software Architecture. *Proc. of the 1998 IEEE Int. Conf. on Robotics and Automation*, *3*, vol. 2081-2086, 1998.
[36] Borst, C., Fischer, M., Haidacher, S., Liu, H. & Hirzinger, G. DLR hand II: experiments and experience with an anthropomorphic hand. *Robotics and Automation, 2003. Proceedings. ICRA'03. IEEE International Conference on*, *1*, pp. 702-707, 2003.

Tesi di dottorato in Ingegneria Biomedica, di Antonino Salerno,
discussa presso l'Università Campus Bio-Medico di Roma in data 20/03/2012.
La disseminazione e la riproduzione di questo documento sono consentite per scopi di didattica e ricerca,
a condizione che ne venga citata la fonte

[37] Gazeau, J., Zehloul, S., Arsicault, M. & Lallemand, J. The LMS hand: force and position controls in the aim of the fine manipulation of objects. *Robotics and Automation, 2001. Proceedings 2001 ICRA. IEEE International Conference on*, *3*, 2001.

[38] Caffaz, A. & Cannata, G. The design and development of the DIST-Hand dextrous gripper. *Robotics and Automation, 1998. Proceedings. 1998 IEEE International Conference on*, *3*, 1998.

[39] Lovchik, C., Diftler, M., Branch, R., Center, N. & Houston, T. The Robonaut hand: a dexterous robot hand for space. *Robotics and Automation, 1999. Proceedings. 1999 IEEE International Conference on*, *2*, 1999.

[40] Fukaya, N., Toyama, S., Asfour, T. & Dillmann, R. Design of the TUAT/Karlsruhe humanoid hand. *Intelligent Robots and Systems, 2000.(IROS 2000). Proceedings. 2000 IEEE/RSJ International Conference on*, *3*, 2000.

[41] Kawasaki, H., Shimomura, H. & Shimizu, Y. Educational--industrial complex development of an anthropomorphic robot hand 'Gifu hand'. *Advanced Robotics*, vol. *15*, pp. 357-363, 2001.

[42] Light, C. & Chappell, P. Development of a lightweight and adaptable multiple-axis hand prosthesis. *Medical Engineering and Physics*, vol. *22*, pp. 679-684, 2000.

[43] Kawasaki, H., Komatsu, T. & Uchiyama, K. Dexterous anthropomorphic robot hand with distributed tactile sensor: Gifu hand II. *Mechatronics, IEEE/ASME Transactions on*, vol. *7*, pp. 296-303, 2002.

[44] Cabas, R. & Balaguer, C. Design and development of a light weight embodied robotic hand activated with only one actuator. *Intelligent Robots and Systems, 2005.(IROS 2005). IEEE/RSJ International Conference on*, pp. 2369-2374, 2005.

[45] Fite, K., Withrow, T., Wait, K. & Goldfarb, M. A Gas-Actuated Anthropomorphic Transhumeral Prosthesis. *Robotics and Automation, IEEE International Conference on*, pp. 3748-3754, 2007.

[46] Carrozza, M.C.; Dario, P.; Vecchi, F.; Roccella, S.; Zecca, M.; Sebastiani, F.; " The Cyberhand: on the design of a cybernetic prosthetic hand intended to be interfaced to the peripheral nervous system", IEEE/RSJ International Conference on Intelligent Robots and Systems, 2003.

[47] Y. Matsuoka, P. Afshar, and M. Oh, "On the design of robotic hands for brain machine interface," Neurosurg. Focus, vol. 20, no. 5, pp. 1–9, 2006.

[48] L.E. Kahn, M. Averbuch, W.Z. Rymer, D.J. Reinkensmeyer, "Comparison of robot-assisted reaching to free reaching in promoting recovery from chronic stroke", in Integration of assistive technology in the information age, Mokhtari M Ed., IOS Press, Amsterdam (the Netherlands), pp. 39-44, 2001.

[49] C.G. Burgar, P.S. Lum, P.C. Shor, M. Van der Loos, "Development of robots for rehabilitation therapy: the Palo Alto VA/Stanford experience", J. Rehabil. Res. Dev., vol. 37, pp. 663-73, 2000.

[50] Lum PS, Burgar CG, Shor PC, Majmundar M, Van der Loos M. "Robot-assisted movement training compared with conventional therapy techniques for the rehabilitation of upper-limb motor function after stroke". Archives of Physical Medicine and Rehabilitation. 2002, 83: pp. 952-959.

[51] Harwin, W.S., Loureiro, R.C.V., Amirabdollahian, F., Taylor, L.M., Johnson, G., Stokes, E., Coote, S., Topping, M., Collin, C., Tamparis, S., Kontoulis, J., Munih, M., Hawkins, P., Driessen, B; "The GENTLES/S project: A new method of delivering neuro-rehabilitation", Assistive Technology- Added value to the quality of life, IOS Press. 10: 36-41 (2001).

[52] S Coote, EK Stokes, BT Murphy, WS Harwin, "The effect of GENTLE/s robot mediated therapy on upper extremity function post stroke", Proc. of 8th International Conference on Rehabilitation Robotics, Published by HWRS-ERC Human-friendly Welfare Robot System Engineering Research Center KAIST 2003, Republic of Korea, pp.59-61.

Tesi di dottorato in Ingegneria Biomedica, di Antonino Salerno,
discussa presso l'Università Campus Bio-Medico di Roma in data 20/03/2012.
La disseminazione e la riproduzione di questo documento sono consentite per scopi di didattica e ricerca,
a condizione che ne venga citata la fonte

[53] T. M. Sukal, M. D. Ellis, J. P. A. Dewald, " Shoulder abduction-induced reductions in reaching work area following hemiparetic stroke: neuroscientific implications", Exp Brain Res (2007) 183:215–223. DOI 10.1007/s00221-007-1029-6

[54] Toth A, Fazekas G, Arz G, Jurak M, Horvath M. Passive robotic movement therapy of the spastic hemiparetic arm with REHAROB: report of the first clinical test and the follow-up system improvement. IEEE 9th International Conference on Rehabilitation Robotics. Chicago, IL, USA, pp. 127-130, 2005.

[55] Krebs HI, Hogan N, Aisen ML, Volpe BT. Robot-aided neurorehabilitation. IEEE Transactions on Rehabilitation Engineering. 1998, 6: pp. 75-87.

[56] Volpe BT, Krebs HI, Hogan N, Edelstein L, Diels C, Aisen M. A novel approach to stroke rehabilitation: robot-aided sensorimotor stimulation. Neurology. 2000, 54: pp. 1938-1944.

[57] Reinkensmeyer DJ, Kahn LE, Averbuch M, McKenna-Cole A, Schmit BD, Rymer WZ. Understanding and treating arm movement impairment after chronic brain injury: progress with the ARM guide. Journal of Rehabilitation Research and Development. 2000, 37: pp. 653-662.

[58] David Mayhew, Benjamin Bachrach, W. Zev Rymer, and Randall F. Beer, "Development of the MACARM – a Novel Cable Robot for Upper Limb Neurorehabilitation", IEEE 9th International Conference on Rehabilitation Robotics June 28 - July 1, 2005, Chicago.

[59] Stienen AHA, Hekman EEG, Van der Helm FCT, Prange GB, Jannink MJA, Aalsma AMM, Van der Kooij H. Freebal: dedicated gravity compensation for the upper extremities. IEEE 10th International Conference on Rehabilitation Robotics. Noordwijk, The Netherlands, pp. 804-808, 2007.

[60] Claudio Fanin, Paolo Gallina, Aldo Rossi, Umberto Zanatta, Stefano Masiero, "NeRebot: a wire-based robot for neurorehabilitation", The 8th International Conference on Rehabilitation Robotics, 2003.

[61] G. Rosati, P. Gallina, A. Rossi, and S. Masiero Wire-based robots for upper-limb rehabilitation International Journal of Assistive Robotics and Mechatronics, 7(2):3–10, 2006.

[62] S. Micera , M. C. Carrozza, E. Guglielmelli, G. Cappiello, F. Zaccone, C. Freschi, R. Colombo, A. Mazzone, C. Delconte, F. Pisano, G. Minuco and P. Dario, "A Simple Robotic System for Neurorehabilitation", Autonomous Robots, vol. 19, n. 3, pp. 271-284, 2005.

[63] L. Zollo, D. Accoto, F. Torchiani, D. Formica, E. Guglielmelli, "Design of a Planar Robotic Machine for Neuro-rehabilitation", ICRA 2008 – International Conference on Robotics and Automation, Pasadena, CA, 2008.

[64] D. Accoto, F. Torchiani, E. Guglielmelli, L. Zollo, E. Cecchini, M. Orsini, "Dispositivo per la terapia motoria robot-mediata dell'arto superiore", patent RM2008A000242, 2008/05/06.

[65] Tariq Rahman, Whitney Sample, Rahamim Seliktar, Mena T. Scavina, Alisa L. Clark, Kacy Moran, and Michael A. Alexander, Design and Testing of a Functional Arm Orthosis in Patients With Neuromuscular Diseases, IEEE TRANSACTIONS ON NEURAL SYSTEMS AND REHABILITATION ENGINEERING, VOL. 15, NO. 2, pp. 244-251, 2007.

[66] Sanchez RJ, Liu J, Rao S, Shah P, Smith R, Rahman T, Cramer SC, Bobrow JE, Reinkensmeyer DJ. Automating arm movement training following severe stroke: functional exercises with quantitative feedback in a gravity-reduced environment. IEEE Transactions on Neural Systems and Rehabilitation Engineering. 2006, 14: pp. 378-389.

[67] Nef T, Riener R. ARMin-design of a novel arm rehabilitation robot. IEEE 9th International Conference on Rehabilitation Robotics. Chicago, IL, USA, pp. 57-60, 2005.

[68] Tobias Nef, Matjaz Mihelj, Gery Colombo, Robert Riener, ARMin – Robot for Rehabilitation of the Upper Extremities, Proceedings of the 2006 IEEE International Conference on Robotics and Automation Orlando, Florida - May 2006.

[69] Tobias Nef, Matjaz Mihelj, Robert Riener, ARMin: a robot for patient-cooperative arm therapy, Medical and Biological Engineering and Computing, Vol. 45, 2007, p.p. 887-900, 2007.

Tesi di dottorato in Ingegneria Biomedica, di Antonino Salerno,
discussa presso l'Università Campus Bio-Medico di Roma in data 20/03/2012.
La disseminazione e la riproduzione di questo documento sono consentite per scopi di didattica e ricerca,
a condizione che ne venga citata la fonte

[70] Carignan C, Liszka M, Roderick S. Design of an arm exoskeleton with scapula motion for shoulder rehabilitation. Proceedings on the 12th International Conference on Advanced Robotics. Seattle, WA, USA, pp. 524-531, 2005.
[71] Sugar TG, He J, Koeneman EJ, Koeneman JB, Herman R, Huang H, Schultz RS, Herring DE, Wanberg J, Balasubramanian S, Swenson P, Ward JA. Design and control of RUPERT: a device for robotic upper extremity repetitive therapy. IEEE Transactions on Neural Systems and Rehabilitation Engineering. 2007, 15: pp. 336-346.
[72] Stienen AHA, Hekman EEG, Prange GB, Jannink MJA, Aalsma AMM, van der Helm FCT, van der Kooij H. Dampace: design of an exoskeleton for force-coordination training in upper-extremity rehabilitation. Journal of Medical Devices. 2009, 3: pp. 031003–1-031003–10.
[73] Balasubramanian S, Klein J, Burdet E. Robot-assisted rehabilitation of hand function. Current Opinion in Neurology. 2010, 23: pp. 661-670. (DOI:10.1097/WCO.0b013e32833e99a4)
[74] Hermano Igo Krebs, Bruce T. Volpe, Dustin Williams, James Celestino, Steven K. Charles, Daniel Lynch, and Neville Hogan, Robot-Aided Neurorehabilitation: A Robot for Wrist Rehabilitation, IEEE TRANSACTIONS ON NEURAL SYSTEMS AND REHABILITATION ENGINEERING, VOL. 15, NO. 3, pp. 327-335, 2007.
[75] O'Malley MK, Sledd A, Gupta A, Patoglu V, Huegel J, Burgar C. The RiceWrist: a distal upper extremity rehabilitation robot for stroke therapy. Proceedings of the IMECE International Mechanical Engineering Congress and Exposition. Chicago, IL, USA, 2006.
[76] Gupta A, O'Malley MK. Design of a haptic arm exoskeleton for training and rehabilitation. IEEE Transactions on Mechatronics. 2006, 11: pp. 280-289.
[77] Takahashi CD, Der-Yeghiaian L, Le VH, Cramer SC. A robotic device for hand motor therapy after stroke. 9th International Conference on Rehabilitation Robotics. Chicago, IL, USA, pp. 17-20, 2005.
[78] DiCicco M, Lucas L, Matsuoka Y. Comparison of control strategies for an EMG controlled orthotic exoskeleton for the hand. Proceedings of the IEEE International Conference on Robotics and Automation. New Orleans, LA, USA, pp. 1622-1627, 2004.
[79] Fiorilla AE, Tsagarakis N, Nori F, Sandini G. Design of a 2-finger hand exoskeleton for finger stiffness measurements. Applied Bionics and Biomechanics. 2008, 00: pp. 1-13.
[80] Lucas L, DiCicco M, Matsuoka Y. An EMG-controlled hand exoskeleton for natural pinching. Journal of Robotics and Mechatronics. 2004, 16: pp. 482-488.
[81] Makaran JB, Dittmer DK, Buchal RO, MacArthur DB. The SMART wrist-hand orthosis (WHO) for quadriplegic patients. Journal of Prosthetics & Orthotics. 1993, 5: pp. 27-30.
[82] Winter SH, Bouzit M. Testing and usability evaluation of the MRAGES force feedback glove. International Workshop on Virtual Rehabilitation. New York, NY, USA, pp. 82-87, 2006.
[83] Dovat L, Lambercy O, Gassert R, Maeder T, Milner T, Leong TC, Burdet E. HandCARE: a cableactuated rehabilitation system to train hand function after stroke. IEEE Transactions on Neural Systems and Rehabilitation Engineering. 2008, 16: pp. 582-591.
[84] Hesse S, Kuhlmann H, Wilk J, Tomelleri C, Kirker S. A new electromechanical trainer for sensorimotor rehabilitation of paralysed fingers: a case series in chronic and acute stroke patients. Journal of NeuroEngineering and Rehabilitaion. 2008, 5: pp. 1-21.
[85] Kollreider A, Ram D, Scherer R, Grieshofer P. Robotic hand/finger rehabilitation for apoplexy patients. European Symposium Technical Aids for Rehabilitation-TAR. Berlin, Germany, pp. 41-42, 2007.
[86] Lambercy O, Dovat L, Gassert R, Burdet E, Chee Leong T, Milner T. A haptic knob for rehabilitation of hand function. IEEE Transactions on Neural Systems and Rehabilitation Engineering. 2007, 15: pp. 356-366.
[87] available on http://www.tyromotion.com/en/products/amadeo
[88] Masia L, Krebs HI, Cappa P, Hogan N. Design and characterization of hand module for whole-arm rehabilitation following stroke. IEEE Transactions on Mechatronics. 2007, 12: pp. 399-407.

Tesi di dottorato in Ingegneria Biomedica, di Antonino Salerno,
discussa presso l'Università Campus Bio-Medico di Roma in data 20/03/2012.
La disseminazione e la riproduzione di questo documento sono consentite per scopi di didattica e ricerca,
a condizione che ne venga citata la fonte

[89] Yeong CF, Melendez-Calderon A, Gassert R, Burdet E. ReachMAN: a personal robot to train reaching and manipulation. IEEE International Conference Intelligent Robots and Systems. St. Louis, MO, USA, pp. 4080-4085, 2009.
[90] Rashedi E, Mirbagheri A, Taheri B, Farahmand F, Vossoughi GR, Parnianpour M. Design and development of a hand robotic rehabilitation device for post stroke patients. IEEE Annual International Conference Engineering in Medicine and Biology Society. Minneapolis, MN, USA, pp. 5026-5029, 2009.
[91] Bouzit M, Burdea G, Popescu G, Boian R. The Rutgers Master II-new design force-feedback glove. IEEE Transactions on Mechatronics. 2002, 7: pp. 256-263.
[92] Birch B, Haslam E, Heerah I, Dechev N, Park EJ. Design of a continuous passive and active motion device for hand rehabilitation. IEEE Annual International Conference Engineering in Medicine and Biology Society. Vancouver, Canada, pp. 4306-4309, 2008.
[93] Connelly L, Yicheng J, Toro ML, Stoykov ME, Kenyon RV, Kamper DG. A pneumatic glove and immersive virtual reality environment for hand rehabilitative training after stroke. IEEE Transactions on Neural Systems and Rehabilitation Engineering. 2010, 18: pp. 551-559.
[94] Ito S, Ishigure Y, Ueki S, Mizumoto J, Nishimoto Y, Abe M, Kawasaki H. A hand rehabilitation support system with improvements based on clinical practices. Preprints of the 9th International Symposium on Robot Control. Gifu, Japan, 2009.
[95] Koeneman EJ, Schultz RS, Wolf SL, Herring DE, Koeneman JB. A pneumatic muscle hand therapy device. IEEE 26th Annual International Conference Engineering in Medicine and Biology Society. San Francisco, CA, USA, pp. 2711-2713, 2004.
[96] Rosati G, Cenci S, Boschetti G, Zanotto D, Masiero S. Design of a single-DOF active hand orthosis for neurorehabilitation. IEEE International Conference on Rehabilitation Robotics. Kyoto, Japan, pp. 161-166, 2009.
[97] Yamaura H, Matsushita K, Kato R, Yokoi H. Development of hand rehabilitation system for paralysis patient-universal design using wire-driven mechanism. IEEE Annual International Conference Engineering in Medicine and Biology Society. Minneapolis, MN, USA, pp. 7122-7125, 2009.
[98] Kline T, Kamper D, Schmit B. Control system for pneumatically controlled glove to assist in grasp activities. Proceedings of the IEEE International Conference on Rehabilitation Robotics. Chicago, IL, USA, pp. 78-81, 2005.
[99] Mulas M, Folgheraiter M, Gini G. An EMG-controlled exoskeleton for hand rehabilitation. Proceedings of the IEEE International Conference on Rehabilitation Robotics. Chicago, IL, USA, pp. 371-374, 2005.
[100] http://www.vrlogic.com/html/immersion/cybergrasp.html.
[101] Ren Y, Park HS, Zhang LQ. Developing a whole-arm exoskeleton robot with hand opening and closing mechanism for upper limb stroke rehabilitation. IEEE 11th International Conference on Rehabilitation Robotics. Kyoto, Japan, pp. 761-765, 2009.
[102] Yeong CF, Melendez-Calderon A, Gassert R, Burdet E. ReachMAN: a personal robot to train reaching and manipulation. IEEE International Conference Intelligent Robots and Systems. St. Louis, MO, USA, pp. 4080-4085, 2009.
[103] Podobnik J, Munih M, Cinkelj J. HARMiS-Hand and arm rehabilitation system. Proceedings of the 7th ICDVRAT International Conference on Disability, Virtual Reality and Associated Technologies. Maia, Portugal, pp. 237-244, 2008.
[104] Loureiro RCV, Harwin WS. Reach & Grasp therapy: design and control of a 9-DOF robotic neuro-rehabilitation system. Proceedings of the IEEE 10th International Conference on Rehabilitation Robotics. Noordwijk, The Netherlands, pp. 757-763, 2007.
[105] Loureiro RCV, Amirabdollahian F, Topping M, Driessen B, Harwin W. Upper limb robot mediated stroke therapy-GENTLE/s approach. Autonomous Robots. 2004, 15: pp. 35-51.
[106] Johnson MJ, Wisneski KJ, Anderson J, Nathan D, Smith RO. Development of ADLER: the activities of daily living exercise robot. IEEE International Conference on Biomedical Robotics and Biomechatronics. Pisa, Italy, pp. 881-886, 2006.

Tesi di dottorato in Ingegneria Biomedica, di Antonino Salerno,
discussa presso l'Università Campus Bio-Medico di Roma in data 20/03/2012.
La disseminazione e la riproduzione di questo documento sono consentite per scopi di didattica e ricerca,
a condizione che ne venga citata la fonte

[107] Perry JC, Rosen J, Burns S. Upper-limb powered exoskeleton design. IEEE Transactions on Mechatronics. 2007, 12: pp. 408-417.
[108] Letier P, Avraam M, Veillerette S, Horodinca M, De Bartolomei M, Schiele A, Preumont A. SAM: a 7-DOF portable arm exoskeleton with local joint control. IEEE International Conference on Intelligent Robots and Systems. Nice, France, pp. 3501-3506, 2008.
[109] Oblak J, Cikajlo I, Matjačić Z. Universal haptic drive: a robot for arm and wrist rehabilitation. IEEE Transactions on Neural Systems and Rehabilitation Engineering. 2010, 18: pp. 293-302.
[110] Matari MJ, Eriksson J, Feil-Seifer DJ, Winstein CJ, "Socially assistive robotics for post-stroke rehabilitation.", J Neuroeng Rehabil. 2007, 4:5.
[111] Lum PS, Reinkensmeyer DJ, Lehman SL: Robotic assist devices for bimanual physical therapy: preliminary experiments. IEEE Transactions on Rehabilitation Engineering 1993, 1(3):185-191.
[112] Lum PS, Lehman SL, Reinkensmeyer DJ: The bimanual lifting rehabilitator: a device for rehabilitating bimanual control in stroke patients. IEEE Transactions on Rehabilitation Engineering 1995, 3(2):166-174.
[113] Aisen ML, Krebs HI, Hogan N, McDowell F, Volpe BT: The effect of robot-assisted therapy and rehabilitative training on motor recovery following stroke. Archives of Neurology 1997, 54(4):443-446.
[114] Cai LL, Fong AJ, Otoshi CK, Liang Y, Burdick JW, Roy RR, Edgerton VR: Implications of assist-as-needed robotic step training after a complete spinal cord injury on intrinsic strategies of motor learning. Journal of Neuroscience 2006, 26(41):10564-8.
[115] Colombo R, Pisano F, Micera S, Mazzone A, Delconte C, Carrozza M, Dario P, Minuco G: Robotic techniques for upper limb evaluation and rehabilitation of stroke patients. IEEE Transactions on Neural Systems and Rehabilitation Engineering 2005, 13(3):311-324.
[116] Ekkelenkamp R, Veltink P, Stramigioli S, Kooij H van der: Evaluation of a Virtual Model Control for the selective support of gait functions using an exoskeleton. Proceedings of the IEEE 10th International Conference on Rehabilitation Robotics, ICORR 2007:693-699.
[117] Peshkin M, Brown DA, Santos-Munné JJ, Makhlin A, Lewis E, Colgate JE, Patton J, Schwandt D: KineAssist: A robotic overground gait and balance training device. Proceedings of the 2005 IEEE 9th International Conference on Rehabilitation Robotics 2005:241-246.
[118] Lotze M, Braun C, Birbaumer N, Anders S, Cohen LG: Motor learning elicited by voluntary drive. Brain 2003, 126(4):866-872.
[119] Perez MA, Lungholt BK, Nyborg K, Nielsen JB: Motor skill training induces changes in the excitability of the leg cortical area in healthy humans. Exp Brain Res. 2004, 159(2):197-205.
[120] Kahn LE, Zygman ML, Rymer WZ, Reinkensmeyer DJ: Robotassisted reaching exercise promotes arm movement recovery in chronic hemiparetic stroke: A randomized controlled pilot study. Journal of Neuroengineering and Rehabilitation 2006, 3(12).
[121] Krebs HI, Palazzolo JJ, Dipietro L, Ferraro M, Krol J, Rannekleiv K, Volpe BT, Hogan N: Rehabilitation robotics: performance based progressive robot-assisted therapy. Autonomous Robots 2003, 15:7-20.
[122] Hogan N, Krebs HI: Interactive robots for neuro-rehabilitation. Restorative Neurology and Neuroscience 2004, 22(3–5):349-358.
[123] Agrawal SK, Banala SK, Fattah A: A gravity balancing passive exoskeleton for the human leg. Proceedings of Robotics: Science and Systems 2006.
[124] Matjacic Z, Hesse S, Sinkjaer T: BalanceReTrainer: A new standing-balance training apparatus and methods applied to a chronic hemiparetic subject with a neglect syndrome. NeuroRehabilitation 2003, 18(3):251-259.
[125] Montagner A, Frisoli A, Borelli L, Procopio C, Bergamasco M, Carboncini MC, Rossi B: A pilot clinical study on robotic assisted rehabilitation in VR with an arm exoskeleton device. Virtual Rehabilitation 2007:57-64.

Tesi di dottorato in Ingegneria Biomedica, di Antonino Salerno,
discussa presso l'Università Campus Bio-Medico di Roma in data 20/03/2012.
La disseminazione e la riproduzione di questo documento sono consentite per scopi di didattica e ricerca,
a condizione che ne venga citata la fonte

[126] Dipietro L, Ferraro M, Palazzolo JJ, Krebs HI, Volpe BT, Hogan N: Customized interactive robotic treatment for stroke: EMG triggered therapy. IEEE Transactions on Neural Systems and Rehabilitation Engineering 2005, 13(3):325-334.

[127] Riener R, Lunenburger L, Jezernik S, Anderschitz JM, Colombo G, Dietz V: Patient-cooperative strategies for robot-aided treadmill training: first experimental results. IEEE Trans Neural Syst Rehabil Eng. 2005, 13(3):380-394.

[128] Kahn LE, Rymer WZ, Reinkensmeyer DJ: Adaptive assistance for guided force training in chronic stroke. Proceedings of the 26th Annual International Conference of the IEEE Engineering in Medicine and Biology Society Meeting, IEMBS 2004:2272-2725.

[129] Veg A, Popovic DB: Walkaround: Mobile balance support for therapy of walking. IEEE Transactions on Neural Systems and Rehabilitation Engineering 2008, 16(3):264-269.

[130] Jackson A, Culmer P, Makower S, Levesley M, Richardson R, Cozens A, Williams MM, Bhakta B: Initial patient testing of iPAM – a robotic system for stroke rehabilitation. IEEE 10th International Conference on Rehabilitation Robotics, ICORR 2007:250-256.

[131] Mihelj M, Nef T, Riener R: A novel paradigm for patient-cooperative control of upper-limb rehabilitation robots. Advanced Robotics 2007, 21(8):843-867.

[132] Surdilovic D, Zhang J, Bernhardt R: STRING-MAN: Wire-robot technology for safe, flexible and human-friendly gait rehabilitation. IEEE 10th International Conference on Rehabilitation Robotics, ICORR 2007:446-453.

[133] Steger R, Kim SH, Kazerooni H: Control scheme and networked control architecture for the Berkeley lower extremity exoskeleton (BLEEX). Proceedings 2006 IEEE International Conference on Robotics and Automation, ICRA 2006:3469-3476.

[134] Frey M, Colombo G, Vaglio M, Bucher R, Jorg M, Riener R: A novel mechatronic body weight support system. IEEE Transactions on Neural Systems and Rehabilitation Engineering 2006, 14(3):311-321.

[135] Wolbrecht ET, Chan V, Le V, Cramer SC, Reinkensmeyer DJ, Bobrow JE: Real-time computer modeling of weakness following stroke optimizes robotic assistance for movement therapy. 3rd International IEEE/EMBS Conference on Neural Engineering, CNE 2007:152-158.

[136] Emken JL, Benitez R, Reinkensmeyer DJ: Human-robot cooperative movement training: learning a novel sensory motor transformation during walking with robotic assistance-asneeded. J Neuroeng Rehabil. 2007, 4:8.

[137] Emken JL, Bobrow JE, Reinkensmeyer DJ: Robotic movement training as an optimization problem: Designing a controller that assists only as needed. IEEE 9th International Conference on Rehabilitation Robotics, ICORR 2005:307-312.

[138] Reinkensmeyer DJ, Liu J, Emken JL, Bobrow JE: The nervous system appears to minimize a weighted sum of kinematic error, force, and change in force when adapting to viscous environments during reaching and steppings. III Symp in Advances in Computational Motor Control 2004

[139] Reinkensmeyer D, Pang C, Nessler J, Painter C: Web-based telerehabilitation for the upper extremity after stroke. IEEE Transactions on Neural Systems and Rehabilitation Engineering 2002, 10(2):102-108.

[140] Rosati G, Bobrow JE, Reinkensmeyer DJ: Compliant control of post-stroke rehabilitation robots: using movement-specific models to improve controller performance. In Proceedings of the ASME International Mechanical Engineering Congress & Exposition IMECE 2008 Boston, MA, USA; 2008.

[141] Guadagnoli M, Lee T: Challenge point: a framework for conceptualizing the effects of various practice conditions in motor learning. J Mot Behav. 2004, 36(2):212-224.

[142] Brewer BR, Klatzky R, Matsuoka Y: Initial therapeutic results of visual feedback manipulation in robotic rehabilitation. International Workshop on Virtual Rehabilitation 2006:160-166.

Tesi di dottorato in Ingegneria Biomedica, di Antonino Salerno,
discussa presso l'Università Campus Bio-Medico di Roma in data 20/03/2012.
La disseminazione e la riproduzione di questo documento sono consentite per scopi di didattica e ricerca,
a condizione che ne venga citata la fonte

[143] Brewer BR, Klatzky R, Matsuoka Y: Visual feedback distortion in a robotic environment for hand rehabilitation. Brain Research Bulletin 2008, 75(6):804-813.

[144] Lum PS, Burgar CG, Shor PC: Evidence for improved muscle activation patterns after retraining of reaching movements with the MIME robotic system in subjects with post-stroke hemiparesis. IEEE Transactions on Neural Systems and Rehabilitation Engineering 2004, 12(2):186-194.

[145] Lum PS, Uswatte G, Taub E, Hardin P, Mark VW: A telerehabilitation approach to delivery of constraint-induced movement therapy. J Rehabil Res Dev. 2006, 43(3):391-400.

[146] Hesse S, Schulte-Tigges G, Konrad M, Bardeleben A, Werner C: Robot-assisted arm trainer for the passive and active practice of bilateral forearm and wrist movements in hemiparetic subjects. Arch Phys Med Rehabil. 2003, 84(6):915-920.

[147] Boian R, Sharma A, Han C, Merians A, Burdea G, Adamovich S, Recce M, Tremaine M, Poizner H: Virtual reality-based post-stroke hand rehabilitation. Proceedings of Medicine Meets Virtual Reality 2002:64-70.

[148] Bi S, Ji L, Wang Z: Robot-aided sensorimotor arm training methods based on neurological rehabilitation principles in stroke and brain injury patients. 27th Annual International Conference of the Engineering in Medicine and Biology Society, IEEE-EMBS 2005:5025-5027.

[149] Shaw SE, Morris DM, Uswatte G, McKay S, Meythaler JM, Taub E: Constraint-induced movement therapy for recovery of upper-limb function following traumatic brain injury. J Rehabil Res Dev. 2005, 42(6):769-778.

[150] Johnson MJ, Loos HFM Van der, Burgar CG, Shor P, Leifer LJ: Design and evaluation of Driver's SEAT: A car steering simulation environment for upper limb stroke therapy. Robotica 2003, 21:13-23.

[151] Simon AM, Gillespie RB, Ferris DP: Symmetry-based resistance as a novel means of lower limb rehabilitation. Journal of Biomechanics 2007, 40(6):1286-1292.

[152] Patton JL, Stoykov ME, Kovic M, Mussa-Ivaldi FA: Evaluation of robotic training forces that either enhance or reduce error in chronic hemiparetic stroke survivors. Experimental Brain Research 2006, 168(3):368-383.

[153] Patton JL, Kovic M, Mussa-Ivaldi FA: Custom-designed haptic training for restoring reaching ability to individuals with poststroke hemiparesis. J Rehabil Res Dev 2006, 43(5):643-56.

[154] Reisman DS, Wityk R, Silver K, Bastian AJ: Locomotor adaptation on a split-belt treadmill can improve walking symmetry post-stroke. Brain 2007, 130(7):1861-1872.

[155] Wei Y, Bajaj P, Scheidt R, Patton J: Visual error augmentation for enhancing motor learning and rehabilitative relearning. 9th International Conference on Rehabilitation Robotics, ICORR 2005, 505-510.

[156] Kousidou S, Tsagarakis NG, Smith C, Caldwell DG: Task-orientated biofeedback system for the rehabilitation of the upper limb. IEEE 10th International Conference on Rehabilitation Robotics, 13–15 June ICORR 2007:376-384.

[157] Patton JL, Dawe G, Scharver C, Mussa-Ivaldi FA, Kenyon R: Robotics and virtual reality: the development of a life-sized 3-D system for the rehabilitation of motor function. 26th Annual International Conference of the IEEE Engineering in Medicine and Biology Society, IEMBS 2004:4840-4843.

[158] Adamovich SV, Merians AS, Boian R, Tremaine M, Burdea GS, Recce M, Poizner H: A virtual reality based exercise system for hand rehabilitation post-stroke: transfer to function. 26th Annual International Conference of the IEEE Engineering in Medicine and Biology Society, IEMBS 2004:4936-4939.

[159] Broeren J, Georgsson M, Rydmark M, Sunnerhagen KS: Virtual reality in stroke rehabilitation with the assistance of haptics and telemedicine. Proceedings of the 4th International Conference on Disability, Virtual Reality and Associated Technologies 2002:71-76.

Tesi di dottorato in Ingegneria Biomedica, di Antonino Salerno,
discussa presso l'Università Campus Bio-Medico di Roma in data 20/03/2012.
La disseminazione e la riproduzione di questo documento sono consentite per scopi di didattica e ricerca,
a condizione che ne venga citata la fonte

[160] Kazerooni, H., Houpt, P. K., and Shecridan, T. B., "Robust Compliant Motion for Manipulators. Part 1. The Fundamental Concepts of Compliant Motion. Part 2. Design Methods", IEEE J. Robot.Autom., vol. 2, pp. 83-105, 1986.

[161] N. Hogan, "Impedance Control: An Approach to Manipulation, Part I, II, II", ASME J. Dyn. Syst. Meas. Control, vol. 107, pp. 124, 1985.

[162] Gross, J., Timmermann, L., Kujala, J., Dirks, M., Schmitz, F., Salmelin, R., Schnitzler, A., The neural basis of intermittent motor control in humans, Proc Natl Acad Sci, vol. 99, 2002, pp. 2299–2302.

[163] von Hofsten C., Structuring of early reaching movements: a longitudinal study, Journal of Motor Behavior, vol. 23, 1991, pp. 280-292.

[164] M. Rucci, D. Bullock, and F. Santini, Integrating robotics and neuroscience: brains for robots, bodies for brains, Advanced Robotics, vol. 21, 2007, pp. 1115–1129.

[165] Rohrer,B., Hogan, N., Avoiding Spurious Submovement Decompositions II: A Scattershot Algorithm, Biological Cybernetics, vol. 94, 2006, pp. 409–414.

[166] Collewijn H, Erkelens CJ, Steinman RM, Binocular coordination of human horizontal saccadic eye movements, Journal of Physiology, vol. 404, 1988, pp. 157-182.

[167] Dounskaia, N.,Kinematic invariants during cyclical arm movements, Biological Cybernetics, vol. 96, 2007, pp. 147–163.

[168] Morasso, P., Spatial control of arm movements, Experimental Brain Research, vol. 42, 1981, pp. 223–227.

[169] Laura Dipietro, Hermano I. Krebs, Susan E. Fasolid, Bruce T. Volpe and Neville Hogan, Submovement changes characterize generalization of motor recovery after stroke, Cortex, Volume 45, Issue 3, March 2009, Pages 318-324.

[170] T. Flash, N. Hogan, The coordination of arm movements: An experimentally confirmed mathematical model, The Journal of Neuroscience, vol. 5, 1985, pp. 1688–1703.

[171] Lee, D., Port, N.L., Georgopoulos, A.P., Manual interception of moving targets. II. On-line control of overlapping submovements, Experimental Brain Research, vol. 116, 1997, pp. 421–433

[172] Zollo, L., Rossini, L., Bravi, M., Magrone, G., Sterzi, S., Guglielmelli, E., Quantitative evaluation of upper-limb motor control in robot-aided rehabilitation, Medical and Biological Engineering and Computing, 2011, DOI: 10.1007/s11517-011-0808-1.

[173] Siciliano, B., and Villani, L., 1999, Robot Force Control, Kluwer Academic Publishers, Boston, MA.

[174] Canudas de Wit, C., Siciliano, B., and Bastin, G., (Eds.), 1996, Theory of Robot Control, Springer-Verlag, London, UK.

[175] L. Zollo, B. Siciliano, A. De Luca, E. Guglielmelli, P. Dario, Compliance control for an anthropomorphic robot with elastic joints: Theory and experiments, ASME Journal of Dynamic Systems, Measurement, and Control, vol. 127, 2005, pp. 321–328.

[176] Y. Mochizuki, S. Inokuchi, K. Omura, Generating artificially mastered motions for an upper limb in baseball pitching from several objective functions, IEEE transactions on systems, man, and cybernetics. Part B, Cybernetics, 2000, vol. 30, pp. 373–382.

[177] G. Neumann, W. Maass, Learning Complex Motions by Sequencing Simpler Motion Templates, Proceedings of the 26th International Conference on Machine Learning, Montreal, Canada, 2009.

[178] A.J. Ijspeert, J. Nakanishi, S. Schaal, Learning Attractor Landscapes for Learning Motor Primitives, Advances in Neural Information Processing Systems, 2003, pp. 1523–1530.

[179] Auke Jan Ijspeert, Alessandro Crespi, Dimitri Ryczko, Jean-Marie Cabelguen, From swimming to walking with a salamander robot driven by a spinal cord model, Science, 2007.

[180] L. Zollo, A. Salerno, L. Rossini, E. Guglielmelli, Submovement Composition for Motion and Interaction Control of a Robot Manipulator, Proceedings of IEEE International Conference on Biomedical Robotics and Biomechatronics (BIOROB), September 26-29, 2010, Tokyo, Japan.

Tesi di dottorato in Ingegneria Biomedica, di Antonino Salerno,
discussa presso l'Università Campus Bio-Medico di Roma in data 20/03/2012.
La disseminazione e la riproduzione di questo documento sono consentite per scopi di didattica e ricerca,
a condizione che ne venga citata la fonte

[181] J.D. Murray, Mathematical Biology II: Spatial Models and Biomedical Applications, Springer, 2003.
[182] Jun Morimoto, Gen Endo, Jun Nakanishi, Sang-Ho Hyon, and Gordon Cheng, Modulation of simple sinusoidal patterns by a coupled oscillator model for biped walking, Proceedings of IEEE International Conference on Robotics and Automation (ICRA), 2006
[183] Jonas Buchli, Ludovic Righetti and Auke Jan Ijspeert, Engineering Entrainment and Adaptation in Limit Cycle Systems From biological inspiration to applications in robotics, Biological Cybernetics, Vol. 95 No 6, 2006.
[184] Ludovic Righetti, Jonas Buchli, Auke Jan Ijspeert, Dynamic Hebbian learning in adaptive frequency oscillators, Physica D: Nonlinear Phenomena, Vol. 216, pp. 269281, 2006
[185] Fishbach, A., S. A. Roy, Bastianen, C., Miller, L.E., Houk, J.C., Kinematic properties of on-line error corrections in the monkey, Experimental Brain Research, vol. 164, 2005, pp. 442–57.
[186] Vallbo, A.B., Wessberg, J., Organization of motor output in slow finger movements in man, The Journal of physiology, vol. 469, 1993, pp. 673–91.
[187] Stefan Schaal, Jan Peters, Jun Nakanishi and Auke Ijspeert, " Learning Movement Primitives", Springer Tracts in Advanced Robotics, Volume 15, pp. 561-572, 2005, DOI: 10.1007/11008941_60
[188] B. H. Williams, M. Toussaint, " Modelling motion primitives and their timing in biologically executed movements", Information Processing Systems, 2008.
[189] Flash, T. & Henis, E. Arm trajectory modifications during reactargets. Journal of cognitive neuroscience, vol. 3, pp. 220-230, 1991.
[190] Abend W., Bizzi E., Morasso P. Human arm trajectory formation. Brain: a journal of neurology, vol. 5, pp. 331-348, 1982.
[191] Crossman, E. & Goodeve, P. Feedback control of hand-movement and Fitt's law. The Quarterly Journal of Experimental Psychology Section A, 35, 251-278, 1983.
[192] Milner TE and Ijaz MM. The effect of accuracy constrains on three dimensional movement kinematics. Neuroscience 35: 365–374, 1990.
[193] Milner, T. A model for the generation of movements requiring endpoint precision. Neuroscience, 49, 487-496, 1992.
[194] Berthier, N. Learning to Reach: A Mathematical Model. Developmental Psychology, vol. 32, pp. 811-823, 1996.
[195] Novak, K. E., Miller, L. E., & Houk, J. C. The use of overlapping submovements in the control of rapid hand movements. Experimental Brain Research, 144(3), 351–364, 2002.
[196] Krebs, H., Aisen, M., Volpe, B. & Hogan, N. Quantization of continuous arm movements in humans with brain injury. Proceedings of the National Academy of Sciences, 1999.
[197] von Hofsten, C. Development of visually guided reaching: The approach phase. Journal of Human Movement Studies, vol. 5, pp. 160-178, 1979.
[198] D. Reinkensmeyer, N. Hogan, H.I. Krebs, S.L. Lehman, P.S. Lum, "Rehabilitators, Robots and Guides: New Tools for Neurological Rehabilitation", In: Biomechanics and Neural Control of Posture and Movement, J. Winters and P. E. Crago, Eds. Springer-Verlag, Berlin, pp. 516534, 2000.
[199] E. Gallotta, G. Magrone, A. Romanelli, M. Milazzo, L. Zollo, D. Formica, E. Guglielmelli, S. Sterzi, "Neurorehabilitation of the upper limb using robotic systems", J. Rehabil. Med., suppl. 47, p. 276, 2008.
[200] L. Zollo, M. Passalacqua, D. Formica, E. Guglielmelli, "Performance Analysis of Adaptive Interaction Control Laws for Rehabilitation Robotics", 2nd Biennial IEEE/RAS-EMBS Int. Conf. on Biomedical Robotics and Biomechatronics, Scottsdale, AZ, USA, 2008.
[201] B. Siciliano, L. Villani, Robot Force Control, Kluwer Academic, Boston, 1999.
[202] D.M. Gorinevsky, A.M. Formalsky, A.Y. Schneider, Force Control of Robotics Systems, CRC Press, Boca Raton, 1997.

Tesi di dottorato in Ingegneria Biomedica, di Antonino Salerno,
discussa presso l'Università Campus Bio-Medico di Roma in data 20/03/2012.
La disseminazione e la riproduzione di questo documento sono consentite per scopi di didattica e ricerca,
a condizione che ne venga citata la fonte

[203] L. Zollo, B. Siciliano, C. Laschi, G. Teti, P. Dario, "An Experimental Study on Compliance Control for a Redundant Personal Robot Arm", Rob. Auton. Syst., vol. 44, pp. 101-129, 2003.
[204] D. Formica, L. Zollo, E. Guglielmelli, "Torque-dependent Compliance Control in the Joint Space of an Operational Robotic Machine for Motor Therapy", ASME J. Dyn. Syst. Meas. Control, vol. 128, pp. 152-158, 2006.
[205] L. Zollo, B. Siciliano, A. De Luca, E. Guglielmelli, P. Dario, "Compliance control for an anthropomorphic robot with elastic joints: Theory and experiments", ASME J. Dyn. Syst. Meas. Control, vol. 127, pp. 321-328, 2005.
[206] D.A. Lawrence, "Impedance control stability properties in common implementations", Proc. 1988 Int. Conf. on Robotics and Automation, Philadelphia, PA, USA, pp. 1185-1191, 1988.
[207] C.S. Cai, B. Roth, "On the spatial motion of a rigid body with point contact", Proc. 1987 Int. Conf. on Robotics and Automation, pp. 686-695, 1987.
[208] A. Sharon, N. Hogan, D.E. Hardt, "The Macro/Micro Manipulator: An Improved Architecture for Robot Control", Robotics and Computer-Integrated Manufacturing, 1993, vol. 10, pp. 209-222.
[209] N. Hogan, H.I. Krebs, A. Sharon, J. Charnnarong, "Interactive robotic therapist", Massachusetts Inst. Technol., Cambridge, U.S. Patent #5466213, 1995.
[210] T.H. Massie, J. K. Salisbury, "The PHANTOM Haptic Interface: A Device for Probing Virtual Objects", Proc. of the ASME Winter Annu. Meeting, Symp. on Haptic Interfaces for Virtual Environment and Teleoperator Systems, Chicago, IL, 1994.
[211] C.R. Carignan, H.I. Krebs, "Telerehabilitation robotics: Bright lights, big future?", J Rehabil Res Dev, vol. 43, pp. 695-710, 2006.
[212] J. Furusho, K. Koyanagi, Y. Imada, Y. Fujii, K. Nakanishi, K. Domen, K. Miyakoshi, U. Ryu, S. Takenaka, A. Inoue, "A 3-D rehabilitation system for upper limbs developed in a 5-year NEDO project and its clinical testing", Proc. 2005 Int. Conf. on Rehabilitation Robotics, Chicago, Illinois, pp. 53-56, 2005.
[213] S.J. Ball, I.E. Brown, S.H. Scott, "A planar 3DOF robotic exoskeleton for rehabilitation and assessment", 29th Annu. Int. Conf. of the IEEE Engineering in Medicine and Biology Society, Lyon, France, pp. 4024-4027, 2007.
[214] L. Sciavicco and B. Siciliano, Modelling and Control of Robot Manipulators, Springer-Verlag, London, UK, 2000.
[215] Tae-Yong Kim, Joongwon Woo, Dongwon Shin, Jongwon Kim, "Indirect cutting force measurement in multi-axis simultaneous NC milling processe", International Journal of Machine Tools & Manufacture, vol. 39, pp. 1717-1731, 1999
[216] Xiaoli Li, Han-Xiong Li, Senior Member, IEEE, Xin-Ping Guan, and R. Du, "Fuzzy Estimation of Feed-Cutting Force From Current Measurement-A Case Study on Intelligent Tool Wear Condition Monitoring", IEEE Transactions on Systems, Man, and Cybernetics-PART C: Applications and Reviews, vol. 34, no. 4, November 2004
[217] J. L. Stein, D. Colvin, G. Clever, and C.-H. Wang, "Evaluation of dc servo machine tool feed drives as force sensors", J. Dynamic Syst., Measurement & Control, Trans. ASME, vol. 108, pp. 279-288, 1986
[218] S. Katsura, Y. Matsumoto, K. Ohnishi, "Modeling of Force Sensing and Validation of Disturbance Observer for Force Control", Industrial Electronics, IEEE Transactions on, vol. 54, pp. 530-538, 2007.
[219] T. Murakami, F. Yu, K. Ohnishi, "Torque sensorless control in multidegree-of-freedom manipulator", Industrial Electronics, IEEE Transactions on, vol. 40, pp. 259-265, 1993.
[220] T.S. Payossim Sono, L.L. Menegaldo, "Myoelectric Hand Prosthesis Force Control Through Servo Motor Current Feedback", Arti_cial Organs, vol. 33, Issue 10, pp. 871-876, 2009

Tesi di dottorato in Ingegneria Biomedica, di Antonino Salerno,
discussa presso l'Università Campus Bio-Medico di Roma in data 20/03/2012.
La disseminazione e la riproduzione di questo documento sono consentite per scopi di didattica e ricerca,
a condizione che ne venga citata la fonte

[221] D. Accoto, L. Zollo, E. Guglielmelli, "Design of a Planar Robotic Machine for Tele-Rehabilitation of Elderly Patient", Gerontechnology, vol. 7, p. 65, 2008 (doi:10.4017/gt.2008.07.02.002.00).

[222] B. Armstrong-Helouvry, P. Dupont, C. Canudas De Wit, "A Survey of Models, Analysis Tools and Compensation Methods for the Control of Machine with Friction", Automatica, vol. 30, No. 7, pp. 1083-1138, 1994

[223] C. Canudas de Wit, H. Olsson, K. J. Astrom, P. Lischinnsky, "A New Model for Control of Systems with Friction", IEEE Transaction on Automatic Control, vol. 40, no. 3, March 1995.

[224] Craig T. Johnson and Robert D. Lorenz, "Experimental Identi_cation of Friction and Its Compensation in Precise, Position Controlled Mechanisms", IEEE Transactions on Industry Applications, vol. 28, no. 6, November/December 1992.

[225] Tobias Nef, Peter Lum, "Improving backdrivability in geared rehabilitation robots", Med Biol Eng Comput DOI 10.1007/s11517-009-0437-0, accepted on January 2009

[226] Amir M. Tahmasebi, Babak Taati, Farid Mobasser, and Keyvan Hashtrudi-Zaad, "Dynamic Parameter Identification and Analysis of a PHANToMTM Haptic Device", in Proc. IEEE Int. Conf. Control Appl., Toronto, ON, Canada, Aug. 2005, vol. 2, pp. 1251-1256.

[227] Basilio Bona and Marina Indri, "Friction Compensation in Robotics: an Overview", Proceedings of IEEE Conference on Decision and Control, and the European Control Conference 2005, Seville, Spain, December 12-15, 2005

[228] Dong Sang Yoo, Myung Jin Chung, Zeungnam Bien, "Real-Time Implementation and Evaluation of Dynamic Control Algorithms for Industrial Manipulator", IEEE Transaction on Industrial electronics, vol. 38, no. 1, February 1991

[229] G. Liu, "Decomposition-Based Friction Compensation Using a Parameter Linearization Approach", International Conference on Robotics and Automation, Seoul, Korea, May 21-26, 2001

[230] K. Kiguchi, K. Iwami, M. Yasuda, K. Watanabe, "An exoskeletal robot for human shoulder joint motion assist", IEEE/ASME Trans. Mechatron., vol. 8, pp. 125-135, 2003.

[231] C. L. Mackenzie, T. Iberall, "The grasping hand", *Elsevier-North Holland*, 1994.

[232] Jeannerod M, Arbib MA, RizzolattiG, Sakata H., "Grasping objects: the cortical mechanisms of visuomotor transformation". *Trends Neurosci 1995*, 18:314-320.

[233] C. Ansuini, M. Santello, S. Massacesi, U. Castiello, "Effects of end-goal on hand shaping", *Journal of Neurophysiology* 95:2456-2465, 2006.

[234] T. Feix, R. Pawlik, H. Schmiedmayer, J. Romero, D. Kragic, "A comprehensive grasp taxonomy", in *Robotics, Science and Systems Conference: Workshop on Understanding the Human Hand for Advancing Robotic Manipulation*, poster presentation, 2009.

[235] N. Kamakura, M. Matsuo, H. Ishii, F. Mitsuboshi, Y. Miura, "Patterns of static prehension in normal hands", *The American Journal of Occupational Therapy*, vol. 4, no 7, pp. 437-445, 1980.

[236] J. R. Napier, "The prehensile movements of the human hand", *Journal of Bone & Joint Surgery*, vol. 38-B, no 4, pp. 902-913, 1956.

[237] Buchholz B., Armstrong T. "A kinematic model of the human hand to evaluate its prehensile capabilities". *Journal of Biomechanics*, 25(2) : 149-162, 1992.

[238] Cutkosky M. R. "On grasp choice, grasp models, and the design of hands for manufacturing tasks". *IEEE Transactions on Robotics and Automation*, 5(3): 269-279, 1989.

[239] Kerr J., Roth B. "Analysis of multifingered hands". *International Journal of Robotics Research*, 4(4): 3-17, 1986.

[240] Nakamura Y., Nagai K., Yoshikawa T. "Mechanics of coordinate manipulation by multiple robotic mechanisms". *Proceedings of the IEEE International Conference on Robotics and Automation*, 991-998, 1987.

Tesi di dottorato in Ingegneria Biomedica, di Antonino Salerno,
discussa presso l'Università Campus Bio-Medico di Roma in data 20/03/2012.
La disseminazione e la riproduzione di questo documento sono consentite per scopi di didattica e ricerca,
a condizione che ne venga citata la fonte

[241] M. Folgheraiter, I. Baragiola, G. Gini, "Teaching grasping to a humanoid hand as a generalization of human grasping data", *Knowledge Exploration in Life Science Informatics (KELSI), Lecture notes in AI, Springer Verlag*, 139-150, 2004

[242] Z. Xue, J. M. Zoellner, R. Dillmann, "Grasp planning: find the contact points*", Proceedings of the 2007 IEEE International Conference on Robotics and Biomimetics*, 2007, pp.835-840.

[243] Ch. Borst, M. Fischer, G. Hirzinger, "A fast and robust grasp planner for arbitrary 3D objects, *Proceedings of the 1999 IEEE International Conference on Robotics & Automation*

[244] Li Z., Sastry S. "Task oriented optimal grasping by multifingered robot hands", *IEEE Journal of Robotics and Automation*, 4(1) : 389-394, 1987.

[245] Bicchi A., Kumar V. "Robotic grasping and contact: a review*". In Proc. IEEE Conference on Robotics and Automation*, 348-353. 2000.

[246] W. Lee, X. Zhang, "Development and evaluation of an optimization-based model for power-grip posture prediction", *Journal of Biomechanics*, vol. 38, pp. 1591-1597, 2005.

[247] N. Hogan, H. I. Krebs, J. Charnnarong, P. Srikrishna, A. Sharon, "MIT-Manus: a workstation for manual theraphy and training", *Proceedings of the 1992 IEEE International Workshop on Robot and Human Communication*, 161-165, 1992.

[248] H. Liu et al., "Multisensory five-finger dexterous hand: the DLR-HIT Hand II", *2008 IEEE/RSJ International Conference on Intelligent Robots and Systems*, 3692-3697, 2008

[249] J. Lukos, C. Ansuini, M. Santello, "Choice of contact points during multidigit grasping: effect of predictability of object center of mass location". *The Journal of Neuroscience*, vol. 27 no 14, pp. 3894-3903, 2007.

[250] F. Lacquaniti, J. F. Soechting, "Coordination o farm and wrist motion during a reaching task", Journal of Neuroscience, 2(4): 399-408, 1982.

[251] J. Lin, Y. Wu, T.S. Huang, "Modeling the constraints of the human hand motion", *In Proceedings of the 5th Annual Federated Laboratory Symposium,* 2001.

[252] J. Lee, T. L. Kunii, "Model-based analysis of hand posture", *IEEE Computer Graphics and Applications*, vol. 15, no 5, pp. 77-86, 1995.

[253] G. Stillfried, P. Van Der Smagt, Movement model of a human hand based on magnetic resonance imaging (MRI), ICABB, 2010

[254] M. Jenkins, H.B. Bamberger, L. Black, R. Nowinski, Thumb joint flexion. What is normal ?, Journal of hand surgery, vol. 23, pp. 796-797, 1998.

[255] P. Hahn, H. Krimmer, A. Hradetzky, U. Lanz, Quantitative analysis of the linkage between the interphalangeal joints of the index finger: An in vivo study, The Journal of hand surgery, vol. 20, 1995

[256] C.D. Metcalf, S.V. Notley, P.H. Chappell, J.H. Burridge, V.T. Yule, Validation and application of a computational model for wrist and hand movements using surface markers, IEEE Transaction on biomedical engineering, vol. 55, no. 3, 2008.

[257] K. E. Novak, L. E. Miller, J. C. Houk, "Features of motor performance that drive adaptation in rapid hand movements", Exp Brain Res (2003) 148:388–400.